ORIGIN OF DEFECTS IN DIRECTED SELF-ASSEMBLY OF DIBLOCK COPOLYMERS USING FEATURE MULTIPLICAITON

Paulina Alejandra RINCON DELGADILLO

Supervisor:
Prof. Guido Groeseneken
Prof. Paul F. Nealey

Members of the Examination Committee:
Dr. Roel Gronheid
Prof. Steven de Feyter
Prof. Paula Moldenaers
Prof. Juan de Pablo
Prof. Matthew Tirrell

Dissertation presented in partial fulfillment of the requirements for the degree of Doctor of Engineering Science

May 2014

ISBN 978-94-6018-837-4
D/2014/7515/61

Preface-Acknowledgements

Preface

Directed self-assembly (DSA) of block copolymers is an effective method to pattern dense arrays of features with dimensions in the nano-scale. The implementation of the Liu-Nealey (LiNe) chemo-epitaxy flow on 300 mm wafers has allowed the investigation of materials and processing conditions that define the parameter space in which to optimize DSA for commercially relevant process windows and levels of defectivity. The fabrication of chemically nanopatterned substrates in an all-track process using 193 nm immersion tools provided 14 nm half-pitch line-and-space patterns with a high degree of perfection. Key parameters such as the width of the preferential-wetting guiding stripes and background chemistry of the chemical patterns govern the process latitude and pattern perfection. Advances in full-wafer metrology and identification of sources of defects resulted in a better understanding of the quality of the chemical patterns and therefore the quality of the structure of the assembled block copolymer. This work provides guidelines for the most impactful pathways to follow in the development of materials and processes to minimize the number of defects using DSA of BCP for high volume manufacturing.

Acknowledgements

Through the last six years, I have met many people that have supported and encouraged me and whose personal and scientific contributions have made this PhD way more exciting than I ever thought.

First, I would like to thank my advisor, Professor Paul Nealey, for giving me the opportunity to start the journey. Without previous knowledge of my background, he let me work in his research group and has been since that day a continuous guidance and support. During my graduate studies, I cannot think of another student with such an amazing opportunity as the collaboration with imec. Even from the distance, his feedback and direction made this project a successful one.

I would like to thank the members of the group, who taught me about block copolymers, life in Wisconsin, Chinese food, and more. Dr. Shenxiang Ji and Dr. Lei Wan were the best teachers and friends I could ask for. Dr. Charlie Liu and Dr. Christopher Thode did the best they could to prepare me for going to imec. Sangwon Kim, Guoliang Liu, Lance Williamson, Michelle Wilson, Bernardo Yañez, Liz Tocce, Robert Seidel, Adam Welander, Karl Stuen and the rest of the group for your help before and during the PhD.

Outside of the lab, I have to thank specially Andres Merchan who, with infinite patience, spent countless hours explaining linear algebra to me. Gretchen, Kushal, Suyash, Laurie and Elif provided the moral support required to make it through the first years.

For the second part of my PhD at imec, I would like to thank my daily supervisor Dr. Roel Gronheid. He taught me the basic lithography concepts and how to survive in the cleanroom. Dr. Gronheid gave me the freedom to explore different aspects of directed self-assembly in the fab and the opportunity to present my work around the world.

At imec, I had the opportunity to collaborate with amazing people that made my projects possible. BT Chan, Efrain Altamirano, and Jean-Francoise de Marneffe supported the etching process. Mark Somervell, Ben Rathsack, Kathleen Nafus, Koichi Matsunaga, Shane O'Neal, and Ainhoa Romo gave me continuous support with the tracks. Yi Cao, Guanyang Lin, and YoungJun Her provided me with the materials required to develop the different projects. Todd Younkin provided continuous and valuable feedback during the weekly meetings. Yu-tsung Lee collected many painful images. I cannot name all the other colleagues at imec, but surely I learned a lot from everyone.

Outside the lab, Nuria Vendrell, Jana Loyo, Carmen Diaz, Alessandro Vaglio, Gustaf Winroth, Christos Trompoukis, Menelaos Tsigourakos, Konstantinos Garidis, Oreste Madia showed me how amazing Europe is.

My last year in Chicago has been supported by Diana Morgan, Xuanxuan Chen, Gurdaman Khaira, Grant Garner, Abelardo Ramirez, Jiaxing Ren, Takejiro Inoue and all the new members of the group.

Last, I would like to thank my family, especially my mother, who encouraged me and believed in me always, and my sister, who has been the most wonderful companion. Support from abroad has come non-stop from grandma, my father, my brother, Adriana Julian, and Adriana Castro.

That was a very international list! Many other names came to my mind when I was writing this section, but I need some space for the actual research.

Abstract

In the last five years, directed self-assembly of block copolymers has undergone a transition from the laboratory space to the fab environment, with the objective of becoming a next generation lithographic technique. This method has very attractive attributes from the industrial perspective, such as resolution, cost, and throughput, but the final requirement that will lead DSA to high volume manufacturing is demonstration of low defectivity. The aim of the present work is to answer the question whether defects inherent to the DSA process exist and, if they do, how many, and how can we annihilate them.

In order to answer to these questions, the chemo-epitaxy scheme developed by Liu and Nealey (LiNe) was used as a baseline. This approach allows for the control of the critical parameters in the fabrication of chemical patterns, such as the geometry and the chemistry. Building upon extensive theoretical and experimental work, the implementation of the LiNe flow was done in industrial equipment at imec. The scale-up of this process, described in Chapter 1, conveyed challenges beyond the wafer size, related to materials, tool configuration and process steps that are not considered when working with a 1x1cm silicon chip. As a result, we obtained fully patterned wafers where DSA of BCP resulted in a high degree of perfection using a 4X feature multiplication factor with a BCP with a natural periodicity (L_0) of 25nm. Chapter 2 shows the feasibility to use this process with other materials, such as a BCP of L_0 = 28nm and a 3X multiplication factor. Moreover, the use of programmed defects is discussed as an initial attempt to calibrate the newly developed optical inspection techniques. However, it served as an evaluation of the healing properties of the BCP, as in most cases it could correct imperfections coming from the chemical patterns.

The next phase of this work consisted in the characterization of the chemical patterns. Chapter 3 describes the thorough inspection of each step of the process to evaluate the generation and propagation of defects through the chemical pattern fabrication, as well as their contribution to final defectivity. This work was particularly meaningful as it allowed the identification of defects coming from the external sources. In Chapters 4 and 5, the impact of the chemistry and geometry on DSA of BCP was investigated. To this end, characterization of the dimensions and materials comprising the chemical patterns and their relationship to defect formation is discussed in each chapter, respectively.

Finally, a brief description of the progress in the development of the defect metrology is described in Appendix A. The significance of this work is high, since it is detection of the small defects in the very high resolution patterns that are provided by DSA is non-trivial. This work is still in progress.

Throughout this thesis, we reaffirmed the concepts and theories developed in the lab and, at the same time, developed the methods to do full-wafer characterization that will allow the evaluation of DSA of BCP for industrial implementation. Our results indicate that, with some further optimization of materials and processes, DSA has the potential to meet the defectivity requirements posed by the industry for high volume manufacturing.

Samenvatting

In de afgelopen vijf jaar heeft geleide zelfassemblage (DSA) van block copolymeren (BCP) de overgang van het laboratorium naar industriële ontwikkeling gemaakt, met als doel om het als toekomstige lithografie techniek te gebruiken. Deze methode om patronen te maken heeft vanuit industrieel perspectief enkele zeer aantrekkelijke eigenschappen, zoals hoge resolutie en productiviteit gekoppeld aan lage kost. Een van de openstaande technische vereisten om DSA in productie toe te passen is defectiviteit. Het doel van het werk zoals beschreven in dit proefschrift is om de vraag te beantwoorden of er defecten bestaan die inherent zijn aan het DSA proces, en zo die er zijn, hoeveel dat er zijn en of hun vorming beïnvloed kan worden.

Om deze vragen te beantwoorden werd het chemo-epitaxy proces zoals ontwikkeld door Liu en Nealey (LiNe) als test object gebruikt. Dit proces staat controle toe over de kritische parameters voor vorming van de chemische patronen, met name hun geometrie en hun chemie. Gebruik makend van de uitgebreide theoretische en experimentele achtergrondkennis werd het LiNe proces geïmplementeerd op de industriële toestellen op imec. De opschaling van dit proces, zoals beschreven in Hoofdstuk 1, stelde niet alleen uitdagingen aangaande de wafer afmeting, maar ook aangaande materiaal keuze, toestel configuratie en proces stappen die niet in aanmerking werden genomen voor de experimenten op 1x1cm silicium chips. Als eindresultaat werden patronen over het volledige waferoppervlak verkregen waar door middels van DSA een viervoudige patroondichtheidstoename werd verkregen, gebruik maken van een BCP met een natuurlijke periodiciteit (L_0) van 25nm. Hoofdstuk 2 toont de mogelijkheid om dit proces met andere materialen te gebruiken zoals een BCP met L_0 = 28nm en een drievoudige patroondichtheidstoename. Bovendien wordt hier het gebruik van geprogrammeerde defecten beschreven in een eerste poging om nieuw ontwikkelde optische inspectietechnieken te kalibreren. Het BCP bleek deze imperfecties in het chemische patroon echter in de meeste gevallen te kunnen repareren.

De volgende fase van dit werk bestond uit de karakterisering van de chemische patronen. Hoofdstuk 3 beschrijft de gedetailleerde inspectie van elke stap van het proces om de vorming en evolutie van defecten tijden de fabricage van de chemische patronen te evalueren, alsook hun bijdrage aan de finale defectiviteit. Een belangrijke bijdrage van dit werk was dat het de bijdrage van externe bronnen identificeerde. In Hoofdstukken 4 en 5

werd de impact van geometrie en chemie op DSA van BCP bestudeerd. Hiertoe wordt de karakterisering van respectievelijk de dimensies en de materialen die de chemische patronen beschrijven bestudeerd, alsmede hun bijdrage tot defect formatie.

Tenslotte wordt een korte beschrijving van vooruitgang in de ontwikkeling van de defect metrologie beschreven in Appendix A. Het belang van dit werk is hoog, omdat detectie van kleine defecten in de zeer hoge resolutie patronen die door DSA gemaakt worden niet triviaal is. Dit werk is nog niet afgerond.

Met het werk zoals beschreven in dit proefschrift werden de concepten en theorieën zoals die werden ontwikkeld in het lab herbevestigd. Terzelfdertijd werden methoden ontwikkeld voor karakterisering op volledige wafers, wat evaluatie van DSA van BCP voor industriële toepassingen toelaat. Onze resultaten tonen aan dat met verdere optimalisatie van materialen en processen DSA het potentieel heeft om de defect vereisten voor productie te bereiken zoals vooropgesteld door de industrie.

Abbreviations and symbols

χ: Flory-Huggins parameter

γ: Interfacial energy (mN/m)

σ_i: sigma inner

σ_o: sigma outer

A: Interfacial area

AFM: Atomic force microscopy

ARC: Anti-reflective coating

BCB: Benzocylcobutene

BCP: Block copolymer

CD: Critical dimension

CVD: Chemical vapor deposition

DoI: Defects of interest

DSA: Defect source analysis

DSA: Directed self-assembly

DoF: Depth of focus

E: Energy (mJ/cm^2)

EBR: Edge bead removal

EL: Exposure latitude

EUV: Extreme ultra-violet

f: Volume fraction of each block

FEM: Focus-exposure matrix

GISAXS: Grazing-incidence small-angle x-ray scattering

HVM: High volume manufacturing

IC: Integrated circuits

L_0: Natural periodicity of the block copolymer (nm)

L_s: Pre-pattern pitch (nm)

LER: Line edge roughness

LiNe: Liu-Nealey

LWR: Line width roughness

N: Degree of polymerization

OH: Hydroxyl (functional group)

PAB: Post apply bake

PEB: Post exposure bake

PGMEA: Propylene glycol monomethyl ether acetate

PMMA: Poly(methyl methacrylate)

POR: Process of reference

PS: Poly(styrene)

P(S-*b*-MMA)): Poly(styrene-block-(methyl methacrylate))

P(S-*r*-MMA)): Poly(styrene-random-(methyl methacrylate))

RCWA: Rigorous Coupled Wave Analysis

SEM: Scanning electron microscopy

SiN: Silicon nitride

TEM: Transmission electron microscope

W: Width of the guiding stripe

WCA: Water contact angle

X-PS: Cross-linkable poly(styrene)

Table of Contents

Chapter 1

Introduction

1.1 Background

During the last four decades, the increased complexity of integrated circuit (IC) design has been driven by Moore's law, which states that the number of transistors in an IC doubles every two years.[1] This conveys a reduction in the size of each transistor to accommodate more units in the same (or less) area, mainly to improve device performance and enable cost reduction. Traditionally, smaller feature dimensions were obtained by decreasing the wavelength used in the photolithography process, or by the use of additional means to improve the resolution, such as in the case of 193nm immersion lithography (193i).[2] However, more recently, for the 22nm node, expensive and complex approaches, such as double patterning, have been utilized to achieve the required critical dimensions and pitches (CD). Looking further into the 16nm and 11nm nodes, extreme ultra-violet was until recently considered as the main candidate for patterning. However, technological delays on EUV source power (which is linked to throughput), source stability and EUV mask defectivity, have delayed the introduction of this technology for high volume manufacturing (HVM). Recently, the International Technology Roadmap for Semiconductors has included alternative methods to generate the nanopatterns with the proper dimensions require for future technologies, as shown on Figure 1.[3]

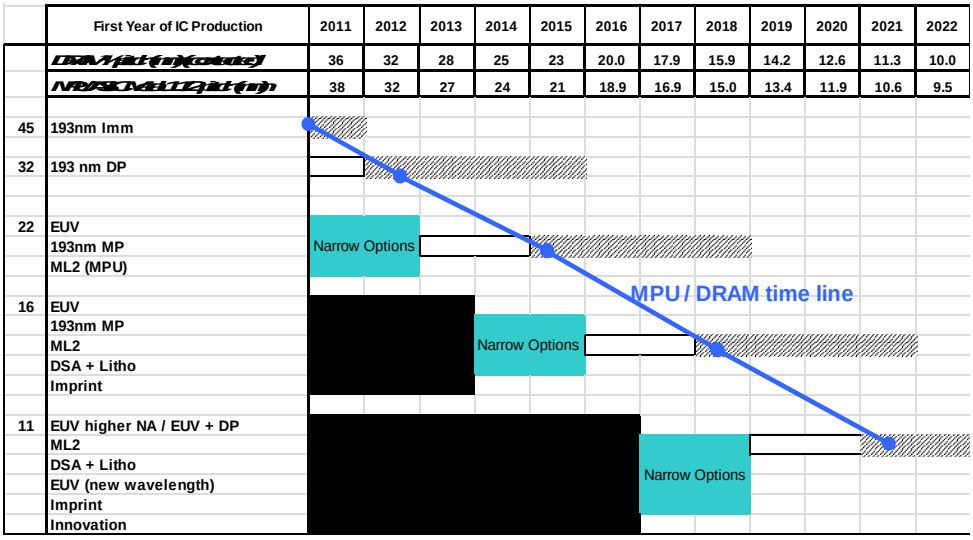

Figure 1. Potential techniques to obtain line/space patterns of pitches below 45nm for DRAM and MPU applications proposed by the ITRS (2012 Update). The colors indicate the time during which research (black), development (blue), qualification/preproduction (white), and improvement (gray) should take place for each proposed solution.

Even though all the listed candidates present diverse challenges, directed self-assembly (DSA) of block copolymers (BCP) has gained significant momentum in the last couple of years as it has been has proven to be an effective method to achieve dense arrays of features with the sizes that are required for the 16 nm node and below, utilizing existing processing tools.[4-7] In addition to the length scales that are proper to this technique (5-50nm), directed self-assembly (DSA) of BCP offers several advantages over other processes in terms of ultimate resolution, cost, and throughput that have placed it as a viable solution for meeting the requirements for MPU/DRAM (Microprocessors/dynamic random-access memory) 16 nm half pitch and below. A major challenge for the implementation of DSA in semiconductor processing will be to achieve the industry requirements in terms of pattern placement accuracy, defectivity, and DSA compatible circuit design.[3] Targeting the defectivity question, part of the research in DSA of BCP has migrated from lab to a fab environment, where the use of automated tools, electronic-grade materials, and the processing/inspection of large areas can provide the defectivity information to optimize material and processing conditions to effectively assess this technique for production.[8-10]

1.2 Self-assembly of block copolymers

Block copolymers (BCP) are macromolecules formed by two or more chemically distinct polymer chains joined together by a covalent bond. Among the characteristics that make them the subject of intense study is their ability to microphase separate and self-assemble into equilibrated ordered structures with spatial periodicity and dimensions at the nanometer scale.[11] The variables governing such behavior are the overall molecular weight, the volume fraction of each component, *f*, and the Flory-Huggins interaction parameter, χ[11]. The molecular weight is usually defined in terms of the degree of polymerization, N (number of repeating monomer units in a polymer chain) and the Flory-Huggins interaction parameter is used to describe the attractive or repulsive forces between a polymer and a solvent or a polymer with another polymer. The first two parameters can be manipulated via controlled polymerization, while the third parameter is material and, to a lesser degree, temperature dependent. The architecture obtained with any block copolymer will indicate the state of minimum free energy of the system, i.e. the result of interfacial and elastic energy contribution of each block. Matsen[12] and Bates[13] calculated and verified experimentally the phase diagram for diblock copolymers, which indicates that they can assemble into four different configurations: spheres, cylinders, gyroid, or lamellae. Also, theoretical and experimental work has shown that for a simple AB copolymer phase separation will only occur when the product of χN has a minimum value of ~10.4. Below this value, the two materials can co-exist as a mixture.

Additionally, the study of self-assembly of BCP in thin films must consider the interaction of the blocks with the free surface and the substrate. Differences in surface energies of the blocks with the boundaries have to be contemplated, since they play a determinant role in the orientation of domains. [14-16] Parallel or perpendicular structures, with respect to the substrate, may be achieved by tuning the surface energy of the substrate and making it preferentially wet by one or both blocks, respectively (Figure 2). To illustrate this, Russell [17] demonstrated the effect of a preferential substrate and the quantization of film thickness (island and hole formation) that takes place when the block with smaller air-polymer interfacial energy tries to occupy the free surface. In addition, Mansky and Han [18] showed that by choosing the composition of random copolymers grafted to the surface, surface affinity with the BCP can be finely tuned and flat films with domains oriented perpendicularly with respect to the substrate are obtained when assembled on a non-preferential brush. The impact of different brush compositions on the orientation of BCP domains is shown in Figure 2B. It is important to note that poly(styrene-*b*-methyl

methacrylate) (P(S-*b*-MMA)) is a widely used BCP system due to the similar surface energies of both blocks in the annealing temperature range used in most studies (160-200°C). As a result, the free surface has nearly a non-preferential character.[19]

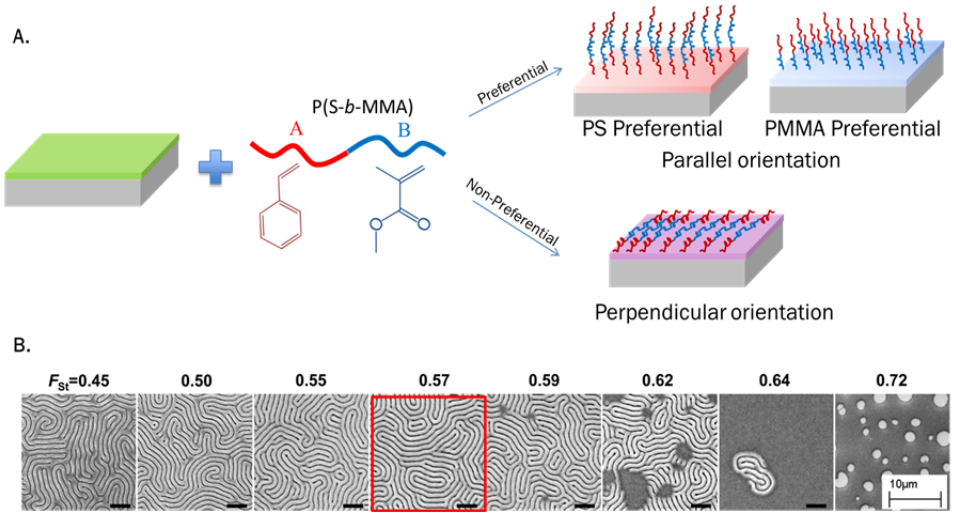

Figure 2. A) Schematic of the effect of a preferential or non-preferential substrate on BCP orientation. B) Top-down scanning electron micrographs of a symmetric PS-b-PMMA BCP assembled on P(S-*r*-MMA random copolymers. The numbers at the top of each image indicated the polystyrene fraction in the brush.[20]

1.3 Directed self-assembly of block copolymers

In order to obtain structures that are useful for applications, control of the orientation and the placement (direction) of the BCP structures is required. For this purpose, several techniques have been developed, such as grapho-epitaxy and chemo-epitaxy. [21, 22] The first one makes use of topographic features to guide the block copolymer material and through the preferential wetting of (usually) one block to the substrate's walls, spatial control of the domains can be achieved. This technique has been explored as a means to direct the assembly of line patterns, as shown on Figure 3 a, b, c, and d, by using perpendicularly oriented lamellae[23] or parallel cylinders,[24, 25] and hole patterns, with multiple cylinders assembled in long trenches (lines/spaces)[26] or individual/multiple cylinders in contact holes or short trenches.[27] Due to the flexibility and simplicity of grapho-epitaxy, a large number of reports can be found in literature.

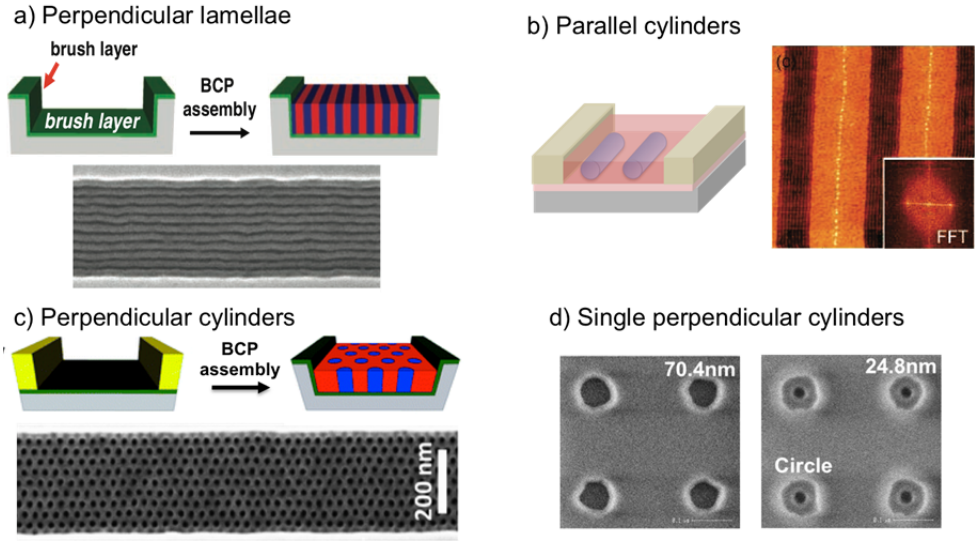

Figure 3. Different grapho-epitaxy schemes and their applications: lines obtained with a) lamellae or b) cylinder forming BCP [23, 25], or holes generated with c) multiple or d) individual cylinders [26, 27].

For the work reported in this thesis another method for directing the BCP patterns is used. This second approach to achieve spatial control over the assembled BCP features is referred to as chemo-epitaxy. This method consists in the generation of regions with surface energy contrast, which attract the block of similar nature, i.e. preferential wetting is the driving force for the assembly.[28, 29] Chemo-epitaxy has been widely explored by Nealey et. al. as a route to obtain perpendicular structures with a high degree of perfection using thermal annealing.[28, 30-36] Figure 4 schematically shows the process followed for the DSA process of a symmetric (lamella forming) BCP, resulting in a line-space pattern.

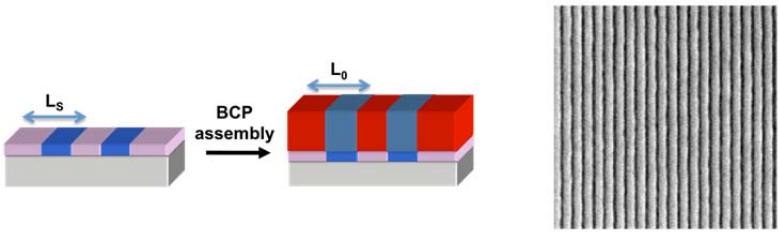

Figure 4. Chemical nanopatterned substrates for DSA of BCP where the pre-pattern pitch is the same as the BCP L_0. The process is driven by referential wetting of the blocks to the different regions and provides aligned BCP structures with a high degree of perfection.

In order to gain detailed knowledge of directed self-assembly of block copolymers, one must first understand that the interplay between thermodynamics and kinetics will determine the properties of the polymer structures, such as shape, orientation, and

direction.[34, 35, 37, 38] This work will focus mainly on the thermodynamic parameters governing DSA and their relation to the total free energy of the system, including the BCP and the boundary conditions provided by its surroundings.[37, 38] A thorough analysis of the kinetics of the assembly process is currently being developed and is not included in this thesis document. When spin-coating a thin film of BCP on a chemically nanopatterned substrate, contributions to the total free energy from the BCP, its interface with the substrate, and its interface at the top of the film must be considered. Edwards et al. showed that when the pitch of the initial pre-pattern (L_s) is similar to the bulk lamellar period of the BCP (L_0), a high degree of perfection in the assembled structures is obtained for both strong and weak interaction between one of the regions and the polystyrene (PS) block (the interaction between the poly(methyl methacrylate) block and the polar stripe is strong in all cases).[37] Incommensurability between L_s and L_0 causes the chains to stretch or compress to accommodate to the pitch of the nanopatterns. This effect conveys a conformational penalty that will increase the free energy of the system. In this case, only a strong interaction between the substrate and the PS block allowed for a mismatch larger than 10% of L_0 before presence of defects or loss of registration with the underlying chemical pattern was observed. The total free energy of the system will, therefore, depend on the materials and the substrate conditions, and will dictate the probability to generate defects.

1.4 Liu-Nealey (LiNe) flow for density multiplication using DSA of BCP

One of the major advances in directed self-assembly of block copolymers was to improve the resolution of current lithography techniques. In previous work, Ruiz reported that chemo-epitaxy can be utilized for density multiplication of hole patterns using cylinder forming BCP.[5] At the same time Cheng *et. al.*[7] and Liu *et. al.*[39] developed techniques to increase the feature density for line/space patterns, by a factor of 3 and 4, using a symmetric P(S-*b*-MMA) BCP, based on 193nm immersion lithography for pre-pattern generation. These demonstrations attracted the interest of the industry and placed it as a potential candidate to become a complementary next generation lithographic technique. However, in order for DSA of BCP to be implemented for high volume manufacturing, a defect density of 0.01 defects/cm^2 needs to be proven.[3]

A versatile test vehicle to assess the potential of DSA of BCP to achieve the defect levels required by the industry is the scheme proposed by Liu and Nealey *et. al*. (LiNe flow), shown in Figure 5. This technique provides an effective method to control the substrate

properties, mainly the chemistry and dimensions of the chemical pre-pattern, and relate them to fundamental thermodynamic parameters, as a means to minimize the total free energy of the system during the assembly, [38, 40] The LiNe flow starts by spin-coating a film of cross-linkable polystyrene (X-PS) on a substrate. After annealing, a photoresist is applied and exposed to generate lines and spaces of specific L*s*. One of the key aspects of this scheme is the trim etch step, shown in Figure 5c). During the trim etch, the critical dimension (CD) of the photoresist is reduced to dimension that can cannot be resolved in the lithography step, and, at the same time, remove the X-PS material between the lines. Then, an organic solvent is used to strip the remaining photoresist and X-PS guiding stripes are obtained. In the next step, a hydroxyl terminated P(S-*r*-MMA) random brush is coated and annealed. The OH- functionality will react with the substrate at the regions between the guiding stripes, referred to as the backfill region, via condensation reaction. Next, the excess material that is not grafted to the surface is rinsed with solvent. During the brush grafting (step e), two aspects are considered in order to achieve a controlled chemistry of the nanopatterns. First, the cross-linked matrix forming the guiding stripes prevents any interpenetration of the brush molecules during the annealing. Second, because the brush deposition is the last step in the fabrication of the chemical patterns, the brush does not experience any further processing that may alter its chemical properties. Upon completion of the chemical pattern fabrication process (step f), a chemical pattern with defined dimensions (interfacial areas) and chemistry (surface energy) can be used to spin-coat a film of BCP and obtain a high degree of perfection of the BCP structures.

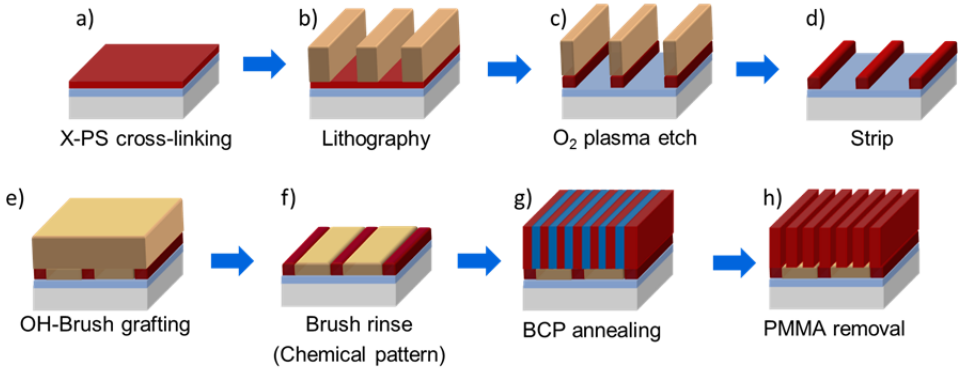

Figure 5. LiNe flow for the fabrication of chemical patterns and feature density multiplication using directed self-assembly of block copolymers.

The geometry of the chemical patterns fabricated with the LiNe flow is defined by the dimensions of the initial pre-pattern pitch (L_s) and the width of the guiding stripe (W), as shown on Figure 6. Previous work by Liu and Ramirez et. al. showed that L_s must be an approximate multiple of the natural periodicity of the BCP (L_0), and that when $W = 0.5L_0$, perpendicular structures throughout the film are obtained.[38, 41] The chemistry of the guiding and backfill regions of the chemical patterns will determine their interfacial energy with the overlying BCP. For example, for density multiplication of P(S-*b*-MMA) using a polystyrene guiding stripe, it has been shown that, for a given annealing time and temperature, the best assembly occurs when a slightly preferential material is used in the background region.[38] Through a careful design of the process and materials, the boundary conditions may be tuned to achieve the minimum defect density at given annealing conditions of the BCP.

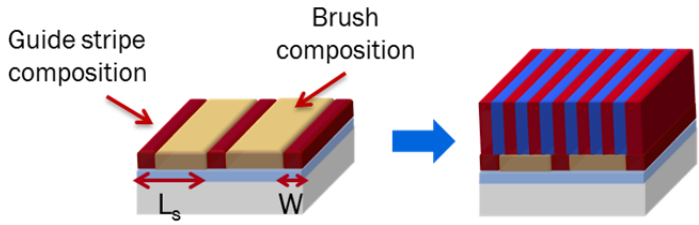

Figure 6. Critical parameters in the fabrication of chemical patterns for feature density multiplication. Control of the composition and dimensions of the chemical patterns allows for the minimization of the interfacial energy between the chemical pattern and the BCP.

1.5 Defectivity

When working in the nanoscale, one of the challenges is the metrology, since non-optical techniques are necessary for visualization of the resulting structures. In most studies, the directed self-assembly process has been analyzed using scanning electron microscopy (SEM) and atomic force microscopy (AFM), which only allow for the inspection of limited areas. For this reason, experimental reports are limited in number and/or inspected regions.[42] Theoretical work, such as molecular simulations, has been an invaluable tool to compliment the experimental work, especially in the calculation of free energies of defect structures. Free energies of defects that are commonly formed in DSA of BCP, such as dislocations and disclinations have been calculated for chemo-epitaxy and grapho-epitaxy schemes.[43, 44] Examples of these defect types are shown in Figure 7. In both cases, for thermodynamically equilibrated structures, the ΔF values are so high (hundreds of k_BT) that the likelihood to find a defect is practically zero. These findings predict that

implementation of DSA for high volume manufacturing is not limited by defectivity, given the optimized boundaries and processing conditions.

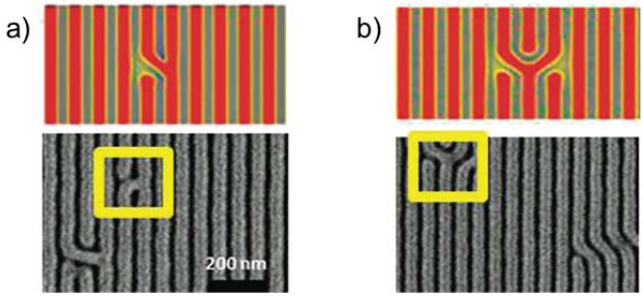

Figure 7. Examples of a) dislocation and b) disclination defects obtained through molecular simulations and experimentally.

1.6 Objectives and Methods

The objective of this work is to analyze the origin of defects and their relationship to various boundary conditions in the directed self-assembly of diblock copolymers on chemically nanopatterned substrates. The LiNe flow, described previously, was implemented in the fab and characterized to be used as a platform for the study and elimination of defects in the DSA process and the elucidation of critical parameters for line/space frequency multiplication. To this end, the present thesis work has been divided in sub-goals, which will be discussed in detail through the different chapters in the following way:

- Chapter 2, scale-up of the LiNe flow on 300mm wafers at imec. The individual steps of the process were implemented and the impact of different processing conditions, such as, sample size, tool configuration, and oxygen content during the annealing steps, was initially assessed. Reproducibility of the laboratory conditions was verified, such as film thickness (X-PS and brush layers), cross-linking efficiency of the X-PS, and perpendicular orientation of the BCP on neutral surfaces, among others. Film thickness and crosslinking efficiency after brush anneal were measured using ellipsometry. The orientation of the BCP structures was verified using optical microscopy/SEM after coating the BCP film and verifying for hole/island structure formation. Once all the individual steps of the process were optimized and the first samples were run using the LiNe flow, top-down SEM images were used to assess the process window for a 4X density multiplication factor using a 100nm pitch pre-pattern and a 25nm L_0 BCP.

- Chapter 3, evaluation of defect remediation through DSA of BCP. Programmed defects were originally included in the mask design to induce defects after DSA and assess the capture rate of defects with the inspection. However, the BCP healed the defects coming from the nanopatterns. Therefore, the sensitivity of the BCP to defects originated from the photo-resist was evaluated using top-down SEM images. At the same time, the process window of a new BCP material with L_0=28nm was obtained using a 3X density multiplication factor. The design of the DSA dedicated reticle includes two large inspection blocks of 84 and 112nm pitch, which were incorporated to study different feature density multiplication factors. Although that project is out of the scope of this thesis, the transition to the 28nm was required to make use of the structures available in the reticle.

- Chapter 4, defect source analysis of directed self-assembly. Each step of the process in the chemical pattern fabrication was inspected using optical techniques. Full wafer maps with the locations of potential defects were used to trace the generation and propagation of defects through the full process. This experiment provided the first evidence of the impact of the quality of the chemical patterns on defect formation, as it also allowed the differentiation of defects due to the assembly process or to external sources. SEM review of the defects at each step of the process showed that dislocations and defect clusters may be generated due to pinholes in the guiding stripes and particles from the backfill brush. Additionally, it became evident that material optimization was necessary to reduce the particle counts after BCP assembly.

- Chapter 5, Impact of the geometry of the chemically nanopatterns on BCP assembly. The impact of the dimensions of the chemical patterns on BCP assembly was investigated, in terms of commensurability (L_S/L_0) and W, by varying the pitch and the CD of the printed photoresist. A focus-exposure matrix (FEM) was used to access a larger number of experimental conditions, as the CD of the resist and, therefore, W, can be varied through the energy steps. SEM images were used to verify the degree of order for each L_S-W condition and a score was assigned to quantify the degree of order of the BCP domains. A phenomenological model was developed to describe the relationship between the interfacial energy and the block copolymer with our experimental observations.

- Chapter 6, Impact of the chemistry of the chemical nanopatterns on BCP assembly. In collaboration with AZ-Electronic Materials, several random brushes

of different compositions were obtained and used to backfill in step e) of the LiNe flow. A comparison with the material used in our process of reference was done to find the best chemistry for the 3X density multiplication in terms of interfacial energy and dislocation formation. FEM wafers were exposed and processed with the different materials. Top-down SEM images were used to verify the presence of defects on relatively large areas (60μm^2/condition). Again, a phenomenological model was used to describe the impact of the composition on DSA of BCP.

Finally we also present preliminary optical inspection results to assess the experimental results. Since these are preliminary result they are included in the Appendix. They show that only by using the proper metrology, fine evaluation of materials and processing conditions is possible.

1.7 References

1. Moore, G., *Cramming More Components onto Integrated Circuits*. 1965, Electronics Magazine.
2. Kato, A., *Chronology of Lithography Milestones* 2007, http://www.lithoguru.com/scientist/litho_history/Kato_Litho_History.pdf.
3. International Technology Roadmap for Semiconductors, 2012, *Lithography*.
4. Liu, C.-C., et al., *The integration of block copolymer directed assembly with 193 immersion lithography.* Journal of Vacuum Science & Technology B, 2010. **28**(6): p. C6B30-C6B34.
5. Ruiz, R., et al., *Density Multiplication and Improved Lithography by Directed Block Copolymer Assembly.* Science, 2008. **321**: p. 936-939.
6. Hinsberg, W., et al., *Self-assembling materials for lithographic patterning: overview, status, and moving forward.* Proceedings of SPIE - The International Society for Optical Engineering, 2010. **7637**: p. 76370G-76370G.
7. Cheng, J.Y., et al., *Dense self-assembly on sparse chemical patterns: Rectifying and multiplying lithographic patterns using block copolymers.* Advanced Materials, 2008. **20**(16): p. 3155-3158.
8. Bencher, C., et al., *Self-Assembly Patterning for sub-15nm Half-Pitch: A Transition from Lab to Fab*. 2011, Proceedings of SPIE.
9. Rincon Delgadillo, P., et al., *Defect source analysis of directed self-assembly process (DSA of DSA)*. 2013, Proc. of SPIE. p. 86800L-5.
10. Bencher, C., *Directed self-assembly defectivity assesment*, J. Zhou, et al., Editors. 2012: Proc. SPIE. p. 83230N-1.

11. Bates, F.S. and G.H. Fredrickson, *Block copolymers - Designer soft materials.* Physics Today, 1999. **52**(2): p. 32-38.

12. Matsen, M.W. and M. Schick, *Stable and Unstable Phases of a Diblock Copolymer Melt.* Physical Review Letters, 1994. **72**(16): p. 2660-2663.

13. Khandpur, A.K., et al., *Polyisoprene-polystyrene diblock copolymer phase diagram near the order-disorder transition.* Macromolecules, 1995. **28**(26): p. 8796-8806.

14. Heier, J., et al., *Thin diblock copolymer films on chemically heterogeneous surfaces.* Macromolecules, 1997. **30**(21): p. 6610-6614.

15. Xu, T., C.J. Hawker, and T.P. Russell, *Interfacial interaction dependence of microdomain orientation in diblock copolymer thin films.* Macromolecules, 2005. **38**(7): p. 2802-2805.

16. Huang, E., et al., *Neutrality conditions for block copolymer systems on random copolymer brush surfaces.* Macromolecules, 1999. **32**(16): p. 5299-5303.

17. Russell, T.P., et al., *Characteristics of the Surface-Induced Orientation for Symmetric Diblock Ps/Pmma Copolymers.* Macromolecules, 1989. **22**(12): p. 4600-4606.

18. Mansky, P., et al., *Controlling polymer-surface interactions with random copolymer brushes.* Science, 1997. **275**(5305): p. 1458-1460.

19. Wu, S., *SURFACE AND INTERFACIAL TENSIONS OF POLYMER MELTS .2. POLY(METHYL METHACRYLATE), POLY(NORMAL-BUTYL METHACRYLATE), AND POLYSTYRENE.* Journal of Physical Chemistry, 1970. **74**(3): p. 632-&.

20. Han, E., et al., *Effect of Composition of Substrate-Modifying Random Copolymers on the Orientation of Symmetric and Asymmetric Diblock Copolymer Domains.* Macromolecules, 2008. **41**(23): p. 9090-9097.

21. Segalman, R.A., *Patterning with block copolymer thin films.* Materials Science & Engineering R-Reports, 2005. **48**(6): p. 191-226.

22. Stoykovich, M.P. and P.F. Nealey, *Block copolymers and conventional lithography.* Materials Today, 2006. **9**(9): p. 20-29.

23. Han, E., et al., *Graphoepitaxial assembly of symmetric block copolymers on weakly preferential substrates.* Adv Mater, 2010. **22**(38): p. 4325-9.

24. Ross, C.A., et al., *Si-containing block copolymers for self-assembled nanolithography.* Journal of Vacuum Science & Technology B, 2008. **26**(6): p. 2489-2494.

25. Fitzgerald, T.G., et al., *Study on the Combined Effects of Solvent Evaporation and Polymer Flow upon Block Copolymer Self-Assembly and Alignment on Topographic Patterns.* Langmuir, 2009. **25**(23): p. 13551-13560.

26. Kim, M., et al., *Interplay of surface chemical composition and film thickness on graphoepitaxial assembly of asymmetric block copolymers.* Soft Matter, 2013. **9**(26): p. 6135-6141.

27. Seino, Y., et al., *Contact hole shrink process using graphoepitaxial directed self-assembly lithography.* Journal of Micro-Nanolithography Mems and Moems, 2013. **12**(3): p. 6.

28. Kim, S.O., et al., *Epitaxial self-assembly of block copolymers on lithographically defined nanopatterned substrates.* Nature, 2003. **424**(6947): p. 411-414.

29. Yang, X.M., et al., *Guided self-assembly of symmetric diblock copolymer films on chemically nanopatterned substrates.* Macromolecules, 2000. **33**(26): p. 9575-9582.

30. Kim, S.O., et al., *Defect structure in thin films of a lamellar block copolymer self-assembled on neutral homogeneous and chemically nanopatterned surfaces.* Macromolecules, 2006. **39**(16): p. 5466-5470.

31. Edwards, E.W., et al., *Dimensions and shapes of block copolymer domains assembled on lithographically defined chemically patterned substrates.* Macromolecules, 2007. **40**(1): p. 90-96.

32. Stoykovich, M.P., et al., *Directed assembly of block copolymer blends into nonregular device-oriented structures.* Science, 2005. **308**(5727): p. 1442-1446.

33. Stoykovich, M.P., et al., *Directed self-assembly of block copolymers for nanolithography: Fabrication of isolated features and essential integrated circuit geometries.* Acs Nano, 2007. **1**(3): p. 168-175.

34. Edwards, E.W., et al., *Mechanism and kinetics of ordering in diblock copolymer thin films on chemically nanopatterned substrates.* Journal of Polymer Science Part B-Polymer Physics, 2005. **43**(23): p. 3444-3459.

35. Welander, A.M., et al., *Rapid directed assembly of block copolymer films at elevated temperatures.* Macromolecules, 2008. **41**(8): p. 2759-2761.

36. Stoykovich, M.P., et al., *Remediation of Line Edge Roughness in Chemical Nanopatterns by the Directed Assembly of Overlying Block Copolymer Films.* Macromolecules, 2010. **43**(5): p. 2334-2342.

37. Edwards, E.W., et al., *Precise control over molecular dimensions of block-copolymer domains using the interfacial energy of chemically nanopatterned substrates.* Advanced Materials, 2004. **16**(15): p. 1315-+.

38. Liu, C.C., et al., *Chemical Patterns for Directed Self-Assembly of Lamellae-Forming Block Copolymers with Density Multiplication of Features.* Macromolecules, 2013. **46**(4): p. 1415-1424.

39. Chi-Chun, L., et al., *Integration of block copolymer directed assembly with 193 immersion lithography.* Journal of Vacuum Science & Technology B (Microelectronics and Nanometer Structures), 2010. **28**(6).

40. Liu, C.-C., et al., *Fabrication of Lithographically Defined Chemically Patterned Polymer Brushes and Mats.* Macromolecules, 2011. **44**(7): p. 1876-1885.

41. Detcheverry, F.A., et al., *Interpolation in the Directed Assembly of Block Copolymers on Nanopatterned Substrates: Simulation and Experiments.* Macromolecules, 2010. **43**(7): p. 3446-3454.

42. Harrison, C., et al., *Dynamics of pattern coarsening in a two-dimensional smectic system.* Physical Review E, 2002. **66**(1): p. 27.

43. Nagpal, U., et al., *Free Energy of Defects in Ordered Assemblies of Block Copolymer Domains.* Acs Macro Letters, 2012. **1**(3): p. 418-422.

44. Takahashi, H., et al., *Defectivity in Laterally Confined Lamella-Forming Diblock Copolymers: Thermodynamic and Kinetic Aspects.* Macromolecules, 2012. **45**(15): p. 6253-6265.

Chapter 2

Implementation of a chemo-epitaxy flow for directed self-assembly on 300mm wafers processing equipment*

*This chapter has been published in Journal of Micro/Nanolithography, MEMS, and MOEMS, p. 031302-1:031302-5, 2012 [1]

2.1 Abstract

In this chapter, the implementation of a chemo-epitaxy method to direct the self assembly (DSA) of block copolymers (BCP) on 300mm wafers is described in detail. Some of the challenges to be addressed during the present study include edge bead removal control of the layers forming the exposure stack and uniformity of the deposited films across the wafer. With the fine tuning of the process conditions, this flow provides chemically nano-patterned substrates with well-defined geometry and chemistry. After a film of BCP is annealed on the chemical patterns, high degrees of perfection are achieved. In the present work, a BCP with natural periodicity of 25nm was assembled on 100nm pitch pre-patterns, obtaining 4X feature multiplication. Top-down SEM images show a wide process window with depth of focus >200nm and exposure latitude >40% for lines and spaces of 12.5nm half pitch. This work will provide a platform for the study of the origin of DSA generated defects, that will be discussed in Chapters 4 through 6, and their relationship to process conditions and materials that are amenable to use by the semiconductor industry.

2.2 Introduction

Directed self-assembly (DSA) of block copolymers (BCP) has emerged as a promising candidate to succeed the current optical lithographic technology at the 16nm half pitch node and below, by 2015.[2] BCPs possess the ability to micro-phase separate into well-ordered, periodic structures with dimensions of 5-50nm.[3, 4] Recent work has shown that DSA of BCPs can be applied to repair imperfections on the original pre-patterns,[5] improve line-

width rougness[6] and line-edge roughness,[7, 8] and enhance the resolution of currently available patterning methods.[6, 8] A key advantage of this patterning approach is in the potential integration with existing lithographic techniques and processing equipment.[9-11] Also, the simplicity of the process conditions and the potential lower cost, compared to other technologies that are currently being explored to provide sub-lithographic features, has attracted the attention of the industry.

As was already discussed in Chapter 1, several techniques have been developed to direct the assembly of BCPs in thin films, the main ones considered for industrial implementation being grapho-epitaxy and chemo-epitaxy.[12, 13] The first method utilizes topographic features to control the orientation and position of BCPs,[14] while the latter consists of areas of distinct surface energies that attract blocks of a similar nature.[4] For the chemo-epitaxy process, the critical parameters to obtain good registration of lamellae forming BCP with the underlying substrate have been widely studied at the laboratory scale for two regimes, when the patterned pitch (L_s) equals the natural periodicity of the BCP (L_0)[15-17] and, when L_s is a multiple of L_0.[5, 18] The chemistry and geometry of the chemical patterns, defined by the materials' composition and the dimensions of the different regions, respectively, will determine the generation of structures with the lowest total free energy.[18] In order to understand how the thermodynamic forces control the degree of patterning perfection, the critical parameters in the fabrication of chemical patterns still need to be analyzed in the free energy landscape and compared to the resulting BCP morphologies.

One major issue for the implementation of DSA for high volume semiconductor manufacturing is in the demonstration of sufficiently high pattern fidelity in combination with low defect density.[10, 11] Work at the laboratory scale is limited by sample size and metrology capabilities, since only limited regions can be inspected.[19] The tools required for detection and quantification of defects over sufficiently large areas, are readily available in the fab. Therefore, in order to collect DSA defect information, it is necessary to translate the process from the lab to representative fab-compatible conditions on full 300mm wafers. The steps towards the integration of our DSA approach in a production fab includes optimization of the process conditions and materials, such as analysis of the annealing time-temperature relationship[20] and moving to fab-compatible solvents.[21] In this chapter, implementation of this chemo-epitaxy flow on 300mm wafer processing equipment is described. In the next stage of our work, this flow will serve as the platform for the study and optimization of defectivity in the DSA process and its relationship to

critical parameters for line/space frequency multiplication, as described throughout the following chapters.

2.3 Experimental

2.3.1 Materials

Cross-linkable poly(styrene-random-vinylbenzocylcobutene) (X-PS), hydroxyl-terminated poly(styrene-random-methyl methacrylate) (P(S-*r*-MMA)-OH) brush, and poly(styrene-block-methyl methacrylate) (PS-*b*-PMMA) BCP with L_0 = 25nm (AZ, PME069), were synthesized by AZ Electronic Materials and used as received. Propylene glycol monomethyl ether acetate (PGMEA from Sigma Aldrich) was used as solvent for these polymers and used without further purification. Photoresist AIM5484, was purchased from JSR Micro. Organic solvents RER500 (mixture of methyl ethyl ketone and ethyl lactate) and RER600 (PGMEA) were purchased from Fujifilm and used as received. Orgasolv STR 301 (Tetramethylammonium hydroxide in dimethyl sulfoxide) was purchased from BASF and was used as received.

2.3.2 Process

The process used in this study is based on a method for the fabrication of chemically nano-patterned substrates using optimized conditions, which was previously reported by our group[21, 22]. All processing was performed at imec on a TEL CLEAN TRACK ACT™12 system. Exposures were done on an ASML XT:1900Gi scanner at 1.35NA using quadrupole illumination (XY polarized, NA= 1.35, σ_o=0.87, σ_i=0.72). An inorganic antireflective coating (ARC) film of SiN, of 15nm, was deposited via chemical vapor deposition (CVD) on 300mm Si wafers. The X-PS film, with thickness of 7-8nm, was spun and annealed for 90min at 250°C under a N_2 atmosphere. After resist coating and exposure using vendor recommended settings for post-apply bake (PAB), post-exposure bake (PEB), and development, lines and spaces of 100nm pitch and 35nm critical dimension (CD) were obtained. The sample was submitted to an O_2 and Cl_2 plasma etch step to trim the resist and remove the X-PS exposed to the plasma, followed by a wet resist strip with Orgasolv at 65°C. The P(S-r-MMA)-OH brush was spun and annealed for 5min at 250°C in a N_2 atmosphere. Non-reacted material was rinsed with RER600. The PS-*b*-PMMA BCP was coated on the chemical patterns and annealed with the same process conditions used for deposition of the random brush.

2.3.3 Characterization

Edge bead removal (EBR) of the X-PS film was evaluated using a Leica INS3300 optical microscope. After spin-casting the polymer solution on a Si wafer, the sample was baked at 100°C for 60s and then visually inspected. Film thickness and uniformity of the X-PS mat and P(S-*r*-MMA)-OH brush were measured using a KLA Tencor, SCD100 ellipsometer on 49 points across the wafer's diameter. P(S-r-MMA)-OH brush grafting uniformity was evaluated by assembling a film of P(S-*b*-PMMA) and verifying random perpendicular orientation of the domains using a scanning electron microscope (SEM). A Hitachi CG4000 SEM was used to image the BCP self-assembled structures.

2.4 Results and discussion

2.4.1 Optimization of individual steps

The implementation of the process, shown in Figure 1, in the fab, required optimizations related to sample scaling and tool capabilities. During the coating of the X-PS film (Figure 1, step a), the edge of the wafer is rinsed/cleaned in a step referred to as edge bead removal (EBR). This provides a well-defined film edge and eliminates any material residues at the film cut. The EBR process done with RER500 resulted in either flaking or bleeding of the film edge, as shown in Figure 2a. This is a critical parameter in the sample preparation, since the X-PS material forms part of the stack to be introduced in the 193nm immersion tool. A clean EBR is necessary in order to avoid contamination of the immersion fluid during exposure. Analysis of the interaction between the X-PS and the EBR solvent proved that RER600 is a more suitable solvent for the EBR process when compared to the standard organic solvent installed in the tracks at imec, RER500, as is illustrated in Figure 2b.

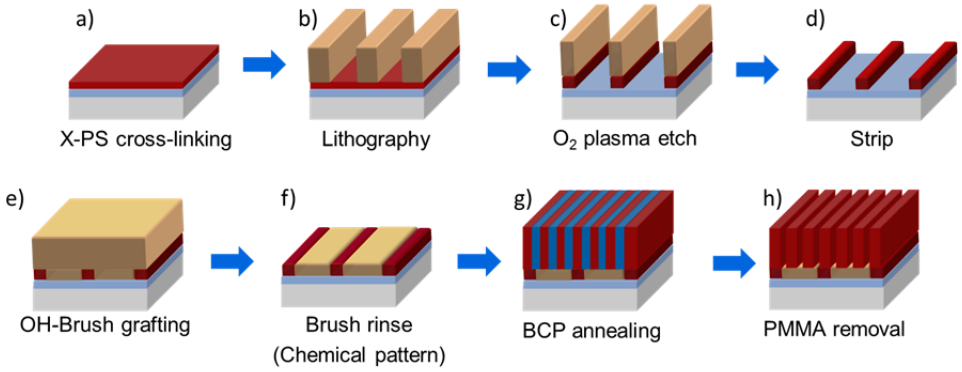

Figure 1. Process to fabricate chemically nano-patterned substrates with well-defined geometry and chemistry, and subsequent DSA of a symmetric BCP

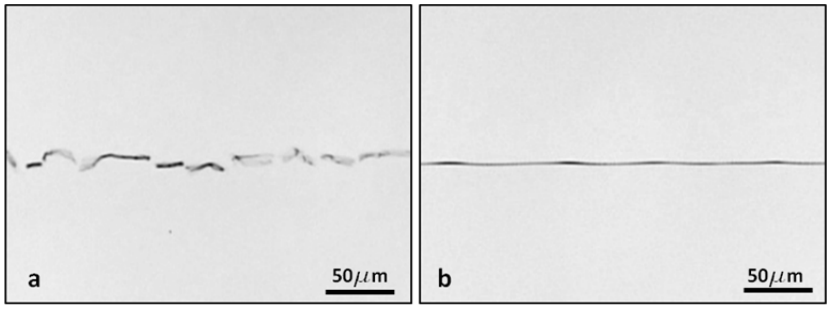

Figure 2. Optical inspection of the X-PS EBR. a) Using original imec standard solvent, RER500, resulting in flaking of the film. b) With RER600 a cleaner edge of the X-PS film was obtained.

The two critical steps of the process to achieve a geometrically well-defined chemical pattern are the exposure (Figure 1, step b) and trim etch (Figure 1, step c). A 35nm CD on reticle (at 1X) is exposed to target a 38nm CD in resist on wafer. The subsequent etch process serves two purposes. It reduces the CD of the resist patterns to a 16nm target, as shown in Figure 3b and in the same step the X-PS material exposed to the plasma is removed, leaving open X-PS stripes that will serve to guide the BCP assembly. The X-PS CD was targeted to be as close as possible to $0.6L_0$ to prevent the formation of three-dimensional structures during block copolymer assembly[23, 24]. Removal of the X-PS was verified by submitting a film of the polymer material to the optimized etching conditions, after which the initial thickness of 8nm was reduced to 0nm after the plasma etching process, according to ellipsometric thickness measurements.

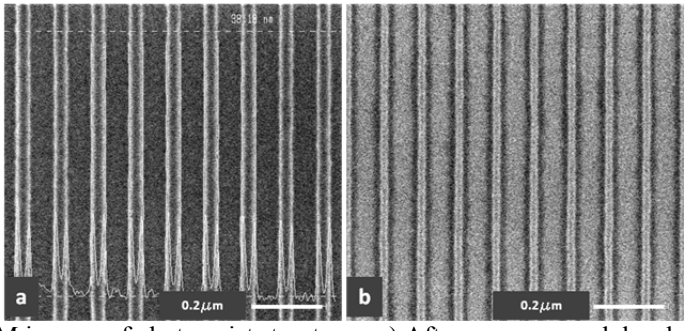

Figure 3. SEM images of photoresist structures. a) After exposure and development, CD = 38nm and b) After trim etch, CD = 16nm. The trim etch step provides structures of dimensions that cannot be resolved in the lithography step.

The chemical control of the nano-pattern is obtained through the composition of the guiding stripe and the grafted brush at the interspatial regions. It is essential to achieve uniform grafting density of the P(S-*r*-MMA)-OH brush, reflected in the thickness, across the 300mm wafer. After spin casting the brush solution, the film was annealed at 250°C for

5min under a nitrogen purge. Next, the sample was rinsed with organic solvent. Initial grafting trials revealed a thicker (~8nm) region of about 100mm of diameter, at the center of the wafer, while the edges showed a difference in thickness of about 2nm less. This difference was not present after coat and anneal, but only appears after the subsequent rinse. The initial wafer substrate preparation proved to be critical for obtaining good brush uniformity. To overcome this issue, the plasma etching process from the previous step was simulated on a blanket X-PS coated wafer, followed by the spin-casting and annealing of a 50nm brush film. After rinsing, the signature was still observed on the sample; however, the thickness difference between the center and the edge of the wafer was reduced to less than 1nm. BCP self-assembly on the grafted brush confirmed that there was no effect on the orientation of domains.

The integration of the process illustrated in Figure 1 involved additional optimization. In order to maintain the chemical contrast between the regions of the chemical patterns, i.e. the guiding stripe and the brush, it is essential to avoid any interpenetration or cross reaction of the P(S-*r*-MMA)-OH brush molecules with the X-PS guiding stripes during the grafting step (Figure 1, step e). This phenomenon was tested by annealing an X-PS film for 3min and subsequently applying, annealing and rinsing a layer of P(S-*r*-MMA)-OH brush. If neither interpenetration or cross-reaction occurs, all the brush material should be rinsed completely and a) there should be no change in the surface energy of the X-PS film, b) the assembly of the BCP should result in parallel orientation of the domains. The annealing procedure resulted to be insufficient, with the tools available in the fab, when using the conditions and materials reported previously.[21] Analysis of the post anneal X-PS was done at University of Wisconsin by pre-treating the cross-linked mat with vinyl-(polystyrene). After this step, a hydroxyl terminated brush was coated, annealed and rinsed. When a film of BCP was assembled on this surface, it presented parallel orientation. This result suggested that the vinyl-(styrene) reacted with the benzocyclobutene (BCB) groups that were not cross-linked during the X-PS anneal, and prevented the further grafting of the random brush. With the optimized processing conditions, incomplete reaction of the BCPC groups led to the formation of reactive alkenes during the random brush grafting at 250°C, which could readily react with either radicals or cations generated by the brush at high temperatures. In order to achieve complete reaction of the BCB groups, different times for the X-PS annealing process were evaluated. It was found that in order to fully degrade the BCB cross-linker, the material must be annealed at 250°C for 90min under a N_2 purge. Long annealing times are undesirable for throughput reasons. However, it does not

significantly hinder our ability to examine the fidelity of the process in terms of defects. Further material and process optimization to obtain complete cross-linking with reduced process time is ongoing.

Another challenge was encountered in the resist stripping step following the trim etch (Figure 1, step d). Following the rinse of the plasma etched resist with organic solvent, a 3nm layer remained on the substrate, probably due to cross-linking of the resist material during the etching process. Inefficient removal of the resist is a significant hindrance to the process because it can degrade the chemical contrast between the guiding stripes and the background. Therefore, a more aggressive rinsing process with Orgasolv STR 301 was necessary to completely eliminate all traces of the photo-resist. Briefly, a wafer was coated with X-PS and resist and submitted to the trim etch process. The wafer was rinsed and thickness measurements showed a 9nm layer. This additional 1nm may be due to film swelling during the rinse process. With these improved processing conditions, total removal of the resist was accomplished.

2.4.2 Integration of the process for the fabrication of well-defined chemical nanopatterns

After fine tuning the process flow as outlined above, we set out to demonstrate the performance of our well-defined chemical patterns in the fab.) Initial evaluation of the process window of the DSA of BCPs on 300mm wafers at imec was done using a focus-exposure matrix (FEM). This approach takes advantage of the multiple fields that can be exposed on a single sample by varying the focus and exposure energy simultaneously, for each exposed field, during the lithography step. Good alignment of the BCP was obtained over a wide dose range. The top down SEM images suggest a maximum exposure latitude of >40% and a depth of focus greater than 200nm, as illustrated in Figure 4. CD values after the exposure from 42-32nm result in good alignment of the BCP, as shown on Figure 5. This initial CD decreased after the trim etch, resulting in the effective width of the stripe guiding the material of 23.9-12.4nm. Even though a high degree of perfection is observed from top-down SEM images, three-dimensional structures may be formed throughout the film thickness, especially at the larger CD (or widths of the guiding stripe).[18, 23] Since it is possible that pattern profile plays a key role when transferring the PS patterns into the underlying layers, it is essential that the self-assembly process provides perpendicular structures that will be amenable for further processing.

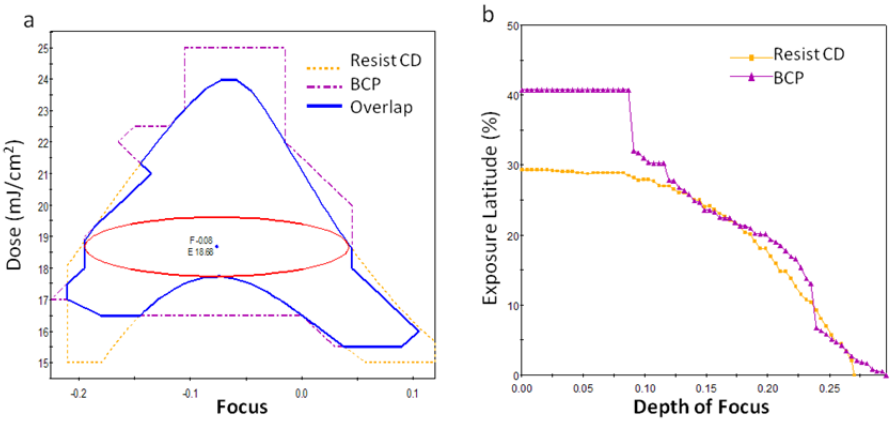

Figure 4. ±10% Process window for the photo-resist with a 38nm target and the DSA process at imec in terms of a) Dose and focus, b) Exposure Latitude. A large number of exposure conditions will result in a high degree of perfection of the BCP structures.

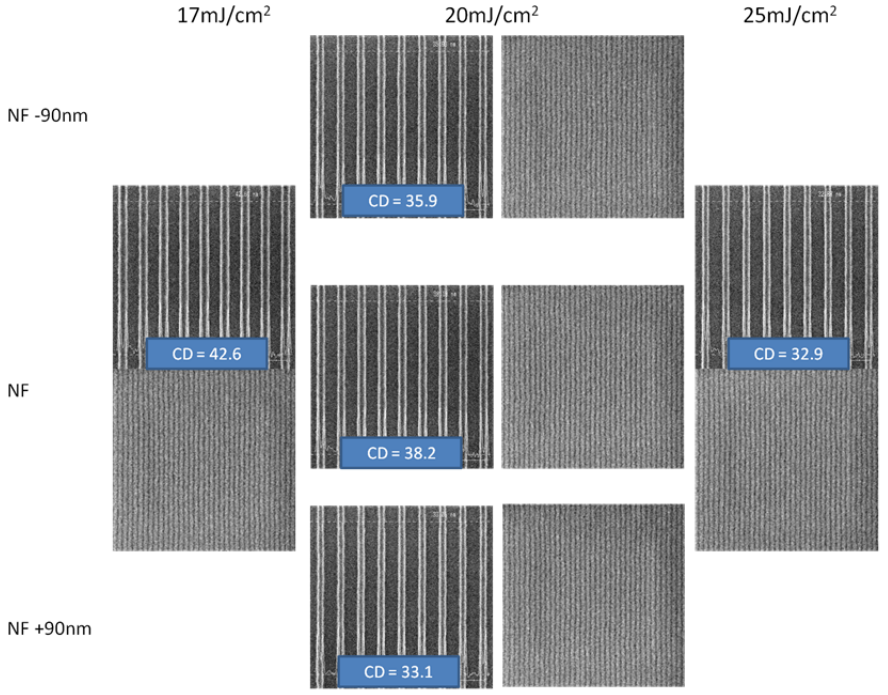

Figure 5. Top down SEM images of the photoresist and assembled BCP using the implemented LiNe flow using a 25nm pitch BCP on a 100nm pitch pre-pattern as a function of pre-pattern dose and focus settings. All images were taken with the same magnification.

2.5 Conclusions

A platform for the study of DSA of BCP and the origin of defects in the fab has been established. Initial results prove that the modifications applied to the process provide

chemically nano-patterned substrates that can guide the assembly of PS-*b*-PMMA BCP with L_0 = 25nm, i.e. 12.5nm lines and spaces, on 100nm pitch pre-patterns, over a wide range of process conditions. Evaluation of the materials and conditions used in the present implementation will be discussed in the following chapters, focusing on the determination and optimization of the defect performance and pattern fidelity of this flow. This work will elucidate the origin of defects in the proposed DSA process and its relationship with changes in the total free energy of the system, as will be discussed in Chapters 5 and 6. At the same time, it will provide a robust process window for the implementation of DSA in a manufacturing environment.

2.6 References

1. Rincon Delgadillo, P.A., et al., *Implementation of a chemo-epitaxy flow for directed self-assembly on 300mm wafer processing equipment*. 2012, Journal of Micro/Nanolithography, MEMS, and MOEMS. p. 031302-1:031302-5.
2. International Technology Roadmap for Semiconductors, 2012, *Lithography*.
3. Bates, F.S. and G.H. Fredrickson, *Block copolymers - Designer soft materials.* Physics Today, 1999. **52**(2): p. 32-38.
4. Kim, S.O., et al., *Epitaxial self-assembly of block copolymers on lithographically defined nanopatterned substrates.* Nature, 2003. **424**(6947): p. 411-414.
5. Ruiz, R., et al., *Density multiplication and improved lithography by directed block copolymer assembly.* Science, 2008. **321**(5891): p. 936-939.
6. Cheng, J.Y., et al., *Dense self-assembly on sparse chemical patterns: Rectifying and multiplying lithographic patterns using block copolymers.* Advanced Materials, 2008. **20**(16): p. 3155-3158.
7. Stoykovich, M.P., et al., *Remediation of Line Edge Roughness in Chemical Nanopatterns by the Directed Assembly of Overlying Block Copolymer Films.* Macromolecules, 2010. **43**(5): p. 2334-2342.
8. Bosse, A.W., *Effects of segregation strength and an external field on the thermal line edge and line width roughness spectra of a diblock copolymer resist.* Journal of Vacuum Science & Technology B, 2011. **29**(3): p. 7.
9. Chi-Chun, L., et al., *Integration of block copolymer directed assembly with 193 immersion lithography.* Journal of Vacuum Science & Technology B (Microelectronics and Nanometer Structures), 2010. **28**(6).
10. Bencher, C., et al., *Self-Assembly Patterning for sub-15nm Half-Pitch: A Transition from Lab to Fab*. 2011, Proceedings of SPIE.
11. Sanders, D.P., et al., *Integration of Directed Self-Assembly with 193 nm Lithography.* Journal of Photopolymer Science and Technology, 2010. **23**(1): p. 11-18.

12. Cheng, J.Y., et al., *Simple and Versatile Methods To Integrate Directed Self-Assembly with Optical Lithography Using a Polarity-Switched Photoresist.* Acs Nano, 2010. **4**(8): p. 4815-4823.

13. Gronheid, R., et al., *Frequency Multiplication of Lamellar Phase Block Co-Polymers with Grapho-Epitaxy Directed Self-Assembly - Sensitivity to Pre-pattern*. 2011: elsewhere in this issue.

14. Han, E., et al., *Graphoepitaxial assembly of symmetric block copolymers on weakly preferential substrates.* Adv Mater, 2010. **22**(38): p. 4325-9.

15. Edwards, E.W., et al., *Precise control over molecular dimensions of block-copolymer domains using the interfacial energy of chemically nanopatterned substrates.* Advanced Materials, 2004. **16**(15): p. 1315-+.

16. Edwards, E.W., et al., *Mechanism and kinetics of ordering in diblock copolymer thin films on chemically nanopatterned substrates.* Journal of Polymer Science Part B-Polymer Physics, 2005. **43**(23): p. 3444-3459.

17. Edwards, E.W., et al., *Dimensions and shapes of block copolymer domains assembled on lithographically defined chemically patterned substrates.* Macromolecules, 2007. **40**(1): p. 90-96.

18. Detcheverry, F.A., et al., *Interpolation in the Directed Assembly of Block Copolymers on Nanopatterned Substrates: Simulation and Experiments.* Macromolecules, 2010. **43**(7): p. 3446-3454.

19. Harrison, C., et al., *Dynamics of pattern coarsening in a two-dimensional smectic system.* Physical Review E, 2002. **66**(1): p. 27.

20. Welander, A.M., et al., *Rapid directed assembly of block copolymer films at elevated temperatures.* Macromolecules, 2008. **41**(8): p. 2759-2761.

21. Liu, C.-C., et al., *Towards an all-track 300mm process for directed self-assembly*. 2011, J. Vac. Sci. Technol. B.

22. Liu, C.-C., et al., *Fabrication of Lithographically Defined Chemically Patterned Polymer Brushes and Mats.* Macromolecules, 2011. **44**(7): p. 1876-1885.

23. Liu, G.L., et al., *Cross-sectional Imaging of Block Copolymer Thin Films on Chemically Patterned Surfaces.* Journal of Photopolymer Science and Technology, 2010. **23**(2): p. 149-154.

24. Liu, C.-C., et al., *Free energy minimization for directed self-assembly of block copolymers with density multiplication*. In preparation.

Chapter 3

All Track Directed Self-Assembly of Block Copolymers: Process Flow and Origin of Defects*

*This chapter has been published in Proceedings SPIE, 8323, 83230D, 2012 [1]

3.1 Abstract

Directed Self-Assembly (DSA) of block copolymers is considered to be a potential lithographic solution to achieve higher feature densities than can be obtained by current lithographic techniques. However, it is still not well-established how amenable DSA of block copolymers is to an industrial fabrication environment in terms of defectivity and processing conditions. Beyond production-related challenges, precise manipulation of the geometrical and chemical properties over the substrate is essential to achieve high pattern fidelity upon the self-assembly process. Using the chemo-epitaxy DSA approach, developed by Liu and Nealey (LiNe), offers control over the surface properties of the slightly preferential brush material as well as those of the guiding structures. This allows for a detailed assessment of the critical material parameters for defect reduction. The precise control of the environment afforded by industrial equipment allows for the selective analysis of material and process related boundary conditions and assessment of their effect on defect generation.

In this study, implementation of our feature multiplication process, described in Chapter 2, was used to investigate the origin of defects in terms of the geometry of the initial pre-patterns. Additionally, programmed defects were used to investigate the ability of the BCP to heal defects in the resist patterns and will aid to assess the capture capability of the inspection tool. Finally, the set-up of the infrastructure that will allow the study the generation of defects due to the interaction of the BCP with the boundary conditions has been accomplished at imec.

3.2 Introduction

As the lithographic industry is trying to reach the 16nm node and below, directed self-assembly (DSA) of block copolymers (BCP) has been considered as one of the potential methods to obtain feature densities that the current optical technique cannot achieve.[2-4] As it was described in Chapter 1, one of the available DSA approaches, chemo-epitaxy, consists in the generation of striped regions of alternating surface energies, on top of which a BCP film will be deposited.[5] During BCP micro-phase separation, each block will be attracted to the region of similar character.[6] The implementation of diverse chemo-epitaxy approaches on 300mm wafers, using tools that are already available in a production fab, has been recently reported [7, 8] First demonstrations confirmed good registration of the BCP with the underlying chemical pattern on full wafers over a wide range of conditions. However, in order to prove that this technique is amenable for high volume manufacturing, a thorough analysis of the formation of DSA specific defects is necessary to establish the critical parameters that dictate the assembly process. At the same time, it will be possible to define the optimal material and processing conditions that will result in a high degree of perfection, required for industrial implementation.

DSA specific defects consist of those generated from the interaction of the blocks with their boundaries i.e., BCP interface, substrate, and the free surface. Examples of these types of defects are disclinations and dislocations.[9] The composition and dimensions of the chemically nanopatterned substrate will play an essential role in the minimization of the total free energy of the system and, therefore, will determine the degree of perfection of the aligned structures.[10, 11] In terms of the geometrical aspect, the patterned pitch (L_s) must be an approximate multiple of the natural periodicity (L_0) of the BCP, i.e. $L_s \approx n\, L_0$. For the feature multiplication process, the width of the guiding stripe, W, may induce the formation of defect-like morphologies or three-dimensional structures throughout the BCP film, as shown experimentally and by theoretical calculations.[12] In order to prevent the formation of defects, it is necessary to analyze the chemical and geometrical aspects of the chemical patterns that will result in ordered domains of the BCP during assembly, as it will be discussed in Chapters 5 and 6.

Additionally, defects may be generated by external sources, such as impurities in the materials or fluctuations in the fabrication process. Reduction of contamination components can be achieved through the proper manipulation of the samples and materials. Examples of process related defects include imperfections in the pre-patterns obtained in the lithography step, such as irregular critical dimension (CD) or line edge roughness (LER). Although

BCPs possess the ability to correct some of these issues,[13] it is desirable to understand the rectification capabilities of these materials and establish the critical processing parameters that will result in defect formation.

In this Chapter, our previously reported method to direct the self-assembly of block copolymers is used to study the generation of defects. With a defined chemistry, the geometry of the chemical patterns was investigated in terms of the CD on the pre-patterns for a 3X feature multiplication factor. Moreover, programmed defects were induced in the pre-patterns to examine the sensitivity of the BCP to such irregularities and, at the same time, evaluate the set up of the required metrology to capture the defects that pertain to DSA.

3.3 Experimental

3.3.1 Materials

Cross-linkable poly(styrene) (X-PS, AZEMLBY NLD-128), hydroxyl-terminated poly(styrene-random-methyl methacrylate) (P(S-*r*-MMA)-OH, AZEMBLY NLD-127) brush, and poly(styrene-block-methyl methacrylate) (PS-*b*-PMMA, AZEMBLY PME-120) BCP with L_0 = 28nm, were manufactured by AZ Electronic Materials and used as received. ArF immersion photoresist AIM5484, was purchased from JSR Micro. Organic solvent RER600 was purchased from Fujifilm and Orgasolv STR 301 was bought from BASF. Both solvents were used as received.

3.3.2 Process

The process used in this study is based on our previously reported method for the fabrication of chemically nanopatterned substrates and optimized conditions.[14, 15] All processing was performed at imec on a TEL CLEAN TRACK ACT™12 system. For a 3X feature multiplication process, where the pattern pitch was 84nm, exposures were done on an ASML XT:1900Gi scanner at 1.35NA using quadrupole illumination (XY polarized, NA= 1.35, σ_o=0.87, σ_i=0.72). An inorganic antireflective coating (ARC) film of SiN, of 15nm, was deposited via chemical vapor deposition (CVD) on 300mm Si wafers. The X-PS film, with thickness of 7-8nm, was spun and annealed for 90min at 250°C under a N_2 atmosphere. After resist coating and exposure using vendor recommended settings for post-apply bake (PAB), post-exposure bake (PEB), and development, lines and spaces of 84nm pitch and critical dimension (CD) of about 38nm were obtained. The sample was submitted

to an O_2 and Cl_2 plasma etch step to trim the resist to target 17nm CD and remove the X-PS exposed to the plasma, followed by a wet resist strip with Orgasolv STR 301. The P(S-r-MMA)-OH brush was spun and annealed for 5min at 250°C in a N_2 atmosphere. Non-reacted material was rinsed with RER600. The PS-*b*-PMMA BCP was coated on the chemical patterns and annealed for 5min at 250°C in a N_2 atmosphere.

3.3.3 Characterization

A Hitachi CG4000 scanning electron microscopy (SEM) was used to evaluate the CD of the pre-patterns after exposure and development, as well as post oxygen plasma etch (trim step). BCP assembly was verified using the same technique. Defect inspection was done in a KLA Tencor 2835 and the location and imaging of the defects was performed with an AMAT G3 Star SEM Vision.

3.4 Results and discussion

The chemo-epitaxy process flow, described in Chapter 2, was tuned for a new BCP material. This was done to accommodate to the dimensions used on our dedicated DSA reticle, which was designed to explore in detail the origin of defects at L_0= 28nm. In the previous chapter, 4x feature multiplication was achieved using a PS-b-PMMA BCP of L_0 = 25nm on a 100nm pre-pattern pitch. In this study, chemical patterns of 84nm pitch where fabricated, which correspond to a 3x feature multiplication factor for a 28nm L_0 BCP. After exposure, pre-patterns of 38nm CD were targeted on wafer. Following BCP assembly, top-down SEM images of the focus-exposure matrix (FEM) show that for the new BCP system, maximum exposure latitude of 35% and a depth of focus >200nm are obtained, as shown in Figure 1. The fields that presented good registration with the underlying chemical pattern correspond to initial pre-pattern CDs of 35-43nm, as shown in Figure 2. After trim etch using oxygen plasma, the CD were decreased to 16-29nm. If we consider that the latter CD is equal to the width of the X-PS guiding stripe, W, then the obtained CD range corresponds to values of W/L_0 of about 0.5-1.0. These results are in remarkable agreement with the ones obtained for 4X feature density multiplication presented on Chapter 2. In the same manner, even though top-down SEM images present high degree of order in the BCP structures at the free surface, 3D morphologies may form throughout the film thickness. For this reason, analysis of the effect of this parameter on the PS profiles and the impact on pattern transfer using advanced characterization techniques, such as grazing-incidence small-angle x-ray scattering (GISAXS) is necessary.

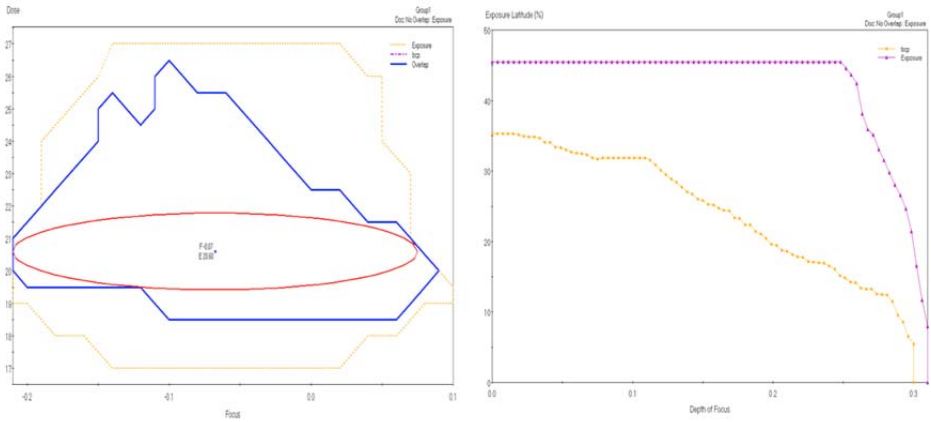

Figure 1. Process window for the photoresist with a 38nm target and the DSA process in terms of a) Dose and focus, b) Exposure latitude. A large number of dose and focus conditions during the exposure will result in well-ordered BCP domains with a high degree or perfection.

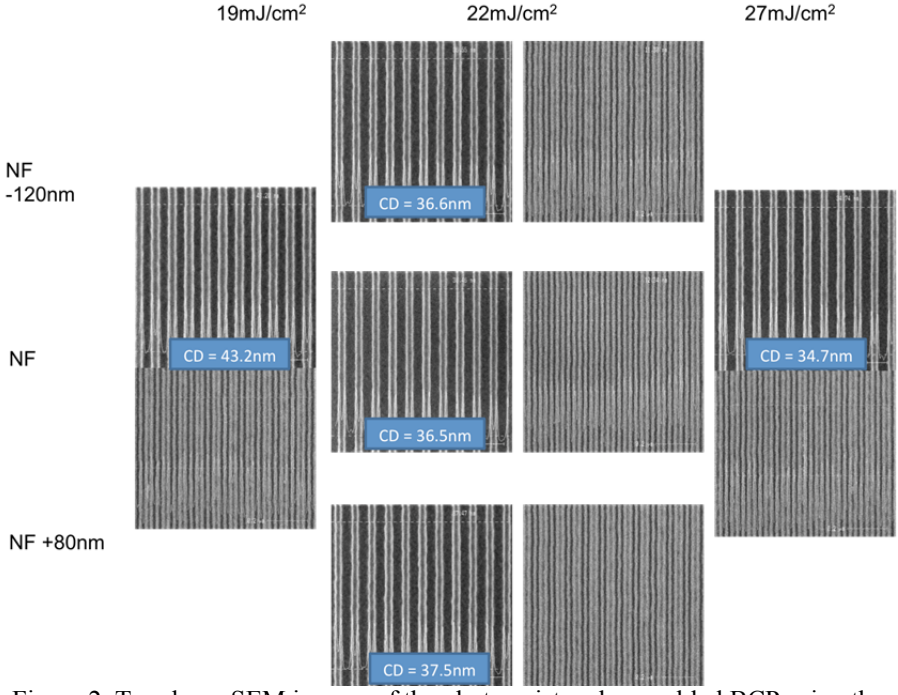

Figure 2. Top down SEM images of the photoresist and assembled BCP using the implemented LiNe flow using a 28nm pitch BCP on an 84nm pitch pre-pattern as a function of pre-pattern dose and focus settings. All images were taken with the same magnification.

Using the results from the FEM, best dose and focus were selected to expose uniform wafers for the preliminary defectivity analysis. In the first part of the study, programmed defects were used to analyze the response of the BCP to chemical patterns. In the next stage, statistical data about the formation of defects was used to verify the capability of the

inspection tool to capture the dislocations. Defect types A, B, and C, defined as stitch, gap, and CD bias respectively, with different sizes were induced in the resist structures during the lithography step, as shown in Figure 3. Due to the lack of contrast between the X-PS guiding stripe and the PS-r-PMMA random brush during SEM imaging, it was only possible to confirm that the defects were translated into the chemical patterns based on the location in the inspection blocks and BCP response. 10 repeats of each defect size in two central dies on the wafer were imaged. Figure 4 shows the size of each defect and the average response of the BCP in the two fields.

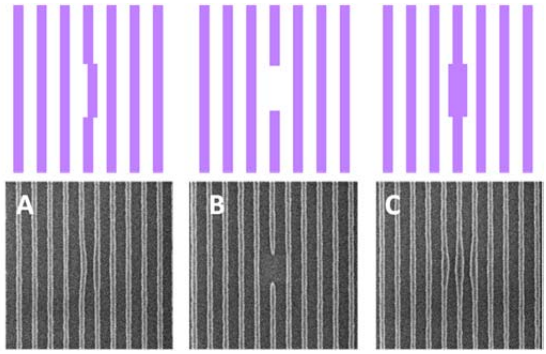

Figure 3. Programmed defects as defined for reticle design and printed on wafer. Defects A, B, and C correspond to a stitch, gap and CD bias respectively.

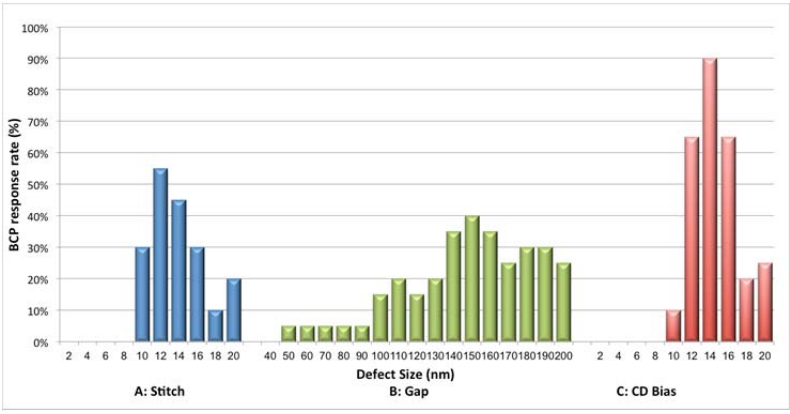

Figure 4. Average response of the BCP to each defect type and size. Two fields were inspected with 10 repeats of each defect per field.

For defect A, stitch errors of 2-20nm were printed on the resist in 2nm steps. Figure 4 suggests that the BCP responded to the programmed defects only when the stitch was 10nm or larger. An interesting observation is that the maximum number of defects is formed around 12-14nm and then decreases as the size approaches 20nm, as shown in Figure 5. However, after removing the PMMA block, undulated structures were observed at all locations for defect sizes of 10nm and above. Although these were not considered as

defects in Figure 4, they indicate that there is a response of the BCP to major flaws in the chemical patterns. Formation of 3D structures throughout the film may have occurred and could not be captured due to the two dimensional limitations of the imaging technique.

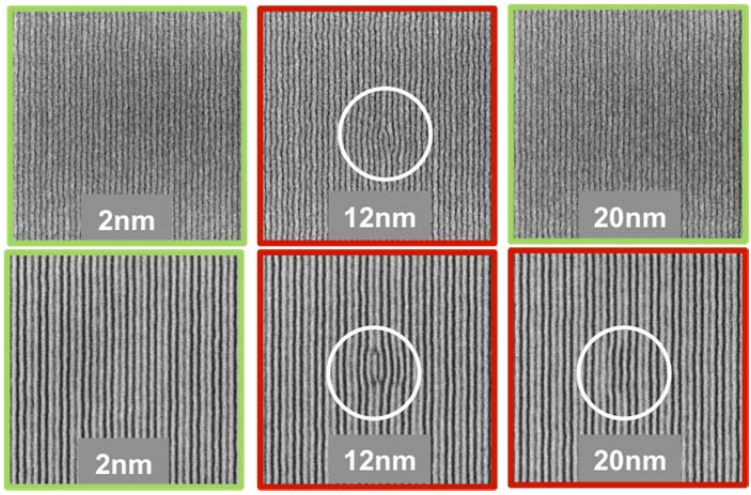

Figure 5. Top down SEM images of the response of the BCP to different sizes (amplitude) of defect A, stitch, before and after removal of the PMMA block.

Resist gaps between 40 and 200nm generated the least amount of defects compared to the other two types, suggesting that the BCP can locally heal the lack of the guiding stripe. In these interruptions, the BCP could still be directed at a 6x feature multiplication factor. For a gap size of 140-160nm more defects were generated than on gap sizes closer to 200nm. However, this phenomenon is not as evident as with defect types A and C. Additionally, at all defect locations, a lighter background (or an interruption of the dark line corresponding to the X-PS guiding stripe) was observed on the top-down SEM images, as shown by defect B at 200nm size on Figure 6. This contrast variation corresponds to the difference in the under layer between the region with and without the X-PS guiding stripe. After PMMA removal, it can be perceived that the guiding stripe is below the PS block assembled on a darker region while the blocks that are on the PS-r-PMMA brush appear to be assembled on a lighter area. Therefore, it is expected to find this “lighter” background at the locations where there was no guiding stripe.

BCP assembly was more sensitive to CD bias than to any other programmed defect, and the size that presented the largest number of defects was 14 ± 2nm. This is related to the effect of the width of the guiding stripe on the BCP assembly, as it will be shown on Chapter 5. The range where more defects are generated corresponds to a CD after trim etch of about 30nm, assuming same lateral etch at the entire length of the resist. From the FEM it has

been observed that when W becomes slightly greater than L_0, the order on the assembled structures breaks down. In the next sections of this thesis it will be shown that on large patterned areas, registration with the chemical pattern is recovered if W increases even more. Similar phenomena may be occurring in this programmed defect type. In such case, the fidelity of the details transferred from the resist structures to the chemical pattern proves to be exceptional. Additionally, 3D analysis of this defect will provide information about the correction potential of the BCP and the generation of alternative morphologies that are formed for different W values.

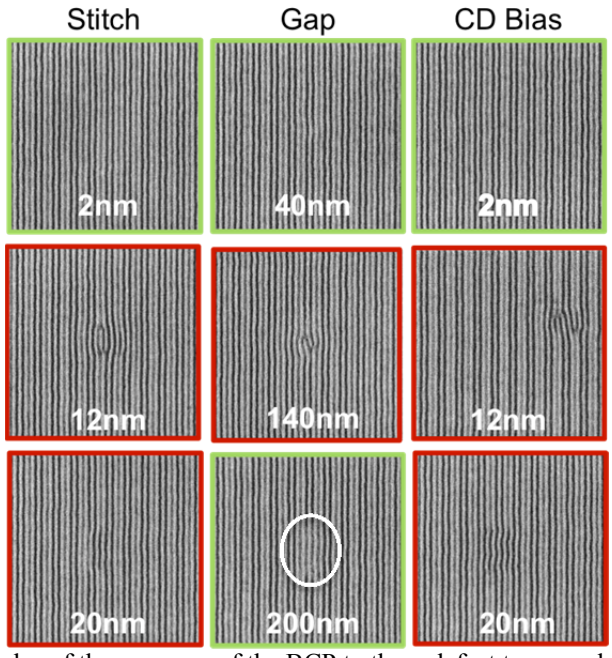

Figure 6. Examples of the response of the BCP to three defect types and sizes of defects. The smallest size did not generate any defects in the BCP, while 12nm was the more frequent defect size for defects A and C, and the largest size of defects did not produce any dislocations but induced undulation on the BCP domains.

An early stage of the metrology development consisted on the set up of a recipe that captured all the DSA specific defects using a KLA Tencor 2835 inspection tool. The goal was to certify that the smallest DSA defects were recognized and mapped. Preliminary results were obtained using manual processing of the samples (polymer solutions preparation and dispense), which caused a saturation of defects with the proposed sensitivity. Still, an initial classification of the defects was possible and 1,000 defects were randomly chosen for imaging using the SEM Vision. DSA specific defects such as disclinations and dislocations were observed, as well as a majority of defects caused by particles, such as the ones shown on Fig 7. One major break-through in this process is that

gallon size samples of the three DSA materials, i.e. X-PS, P(PS-r-PMMA)-OH brush, and BCP, were delivered at imec and installed in the TEL CLEAN TRACK ACT™12 system. Thus, the manual handling of the samples was completely eliminated and the external sources of defects are minimized, which allow a better identification of the defects of interest. With the necessary infrastructure to fabricate the samples and the information collected from the programmed defects, inspection of DSA of BCPs using 3X feature multiplication on 300mm wafers was done at imec and will be discussed in detail on Chapter 4.

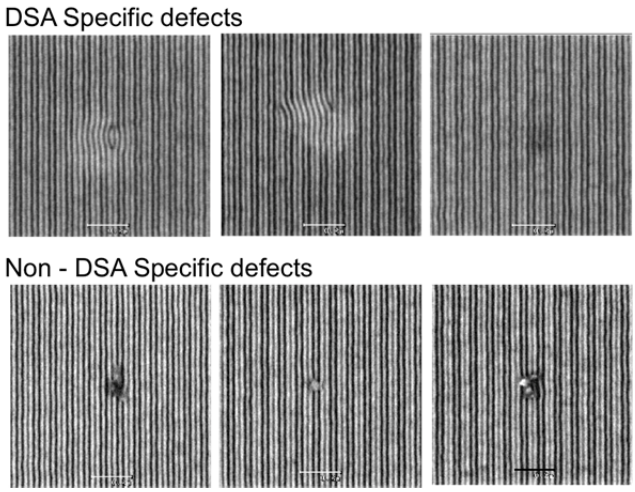

Figure 7. Top-down SEM images of DSA-specific defects, such as dislocations (center), and non-DSA specific defects, such as particles, captured during optical inspection.

3.5 Conclusions

Our previously reported chemo-epitaxy flow has been used to obtain 3x feature multiplication of a PS-b-PMMA BCP of L_0 = 28nm on an 84nm pre-pattern pitch, as well as 4x with a L_0 = 25nm on a 100nm pre-pattern, obtaining similar, large process windows. Also, the dependence on the width of the guiding stripe (with respect to L_0) was remarkable for the two systems. The use of programmed defects showed that the BCP is capable of healing minor flaws in the fabrication of the chemical patterns, particularly in the case of the resist gap. However, they also confirmed the need to study the formation of 3D morphologies through the film thickness. With the set-up developed at imec, the inspection of defects generated from the interaction of the BCP with the boundary conditions is possible. This work will explore the potential of the BCP to meet the industry's requirements in terms of defectivity and establish a robust process window for process implementation.

3.6 References

1. Rincon Delgadillo, P.A., et al., *All track directed self-assembly of block copolymers: process flow and origin of defects*. 2012: Proceedings SPIE 8323. p. 83230D.
2. International Technology Roadmap for Semiconductors, 2012, *Lithography*.
3. Cheng, J.Y., et al., *Dense self-assembly on sparse chemical patterns: Rectifying and multiplying lithographic patterns using block copolymers.* Advanced Materials, 2008. **20**(16): p. 3155-3158.
4. Ruiz, R., et al., *Density multiplication and improved lithography by directed block copolymer assembly.* Science, 2008. **321**(5891): p. 936-939.
5. Kim, S.O., et al., *Epitaxial self-assembly of block copolymers on lithographically defined nanopatterned substrates.* Nature, 2003. **424**(6947): p. 411-414.
6. Bates, F.S. and G.H. Fredrickson, *Block copolymers - Designer soft materials.* Physics Today, 1999. **52**(2): p. 32-38.
7. Bencher, C., et al., *Self-Assembly Patterning for sub-15nm Half-Pitch: A Transition from Lab to Fab*. 2011, Proceedings of SPIE.
8. Rincon Delgadillo, P.A., et al., *Implementation of a chemo-epitaxy flow for directed self-assembly on 300mm wafer processing equipment*. 2012, Journal of Micro/Nanolithography, MEMS, and MOEMS. p. 031302-1:031302-5.
9. Harrison, C., et al., *Dynamics of pattern coarsening in a two-dimensional smectic system.* Physical Review E, 2002. **66**(1): p. 27.
10. Detcheverry, F.A., et al., *Interpolation in the Directed Assembly of Block Copolymers on Nanopatterned Substrates: Simulation and Experiments.* Macromolecules, 2010. **43**(7): p. 3446-3454.
11. Liu, C.-C., et al., *Free energy minimization for directed self-assembly of block copolymers with density multiplication.* In preparation.
12. Liu, G.L., et al., *Cross-sectional Imaging of Block Copolymer Thin Films on Chemically Patterned Surfaces.* Journal of Photopolymer Science and Technology, 2010. **23**(2): p. 149-154.
13. Stoykovich, M.P., et al., *Remediation of Line Edge Roughness in Chemical Nanopatterns by the Directed Assembly of Overlying Block Copolymer Films.* Macromolecules, 2010. **43**(5): p. 2334-2342.
14. Liu, C.-C., et al., *Fabrication of Lithographically Defined Chemically Patterned Polymer Brushes and Mats.* Macromolecules, 2011. **44**(7): p. 1876-1885.
15. Liu, C.-C., et al., *Towards an all-track 300mm process for directed self-assembly*. 2011, J. Vac. Sci. Technol. B.

Chapter 4

Defect source analysis of directed self-assembly (DSA of DSA)*

*This chapter has been published in Journal of Micro/Nanolithography, MEMS, and MOEMS, **12**(3) 2013. [1]

4.1 Abstract

As design rule shrinks, it is essential that the capability to detect smaller and smaller defects should improve. There is considerable effort going on in the industry to enhance Immersion Lithography using DSA for 14 nm design node and below. While the process feasibility is demonstrated with DSA, material issues as well as process control requirements are not fully characterized. The chemical epitaxy process is currently the most-preferred process option for frequency multiplication and it involves new materials at extremely small thickness. The image contrast of the lamellar Line/Space pattern at such small layer thickness is a new challenge for optical inspection tools. In this investigation, the focus is on the capability for optical inspection systems to capture DSA unique defects such as dislocations and disclination clusters over the system and wafer noise. The study is also extended to investigate wafer level data at multiple process steps and determining contribution from each process step and materials using 'Defect Source Analysis' methodology. The added defect pareto and spatial distributions of added defects at each process step are discussed.

4.2 Introduction

Directed self-assembly (DSA) of block copolymers (BCP) has been studied in detail by academia since its initial demonstration, a decade ago.[2] More recently, the potential of this technology for enabling patterning for the semiconductor industry has been

suggested.[3] There are, however, various open questions that need to be answered in order to prepare the technology for use in manufacturing, including design decomposition for DSA[4] and pattern placement accuracy.[5, 6] In addition, the capabilities of DSA for low defectivity need to be demonstrated. Achieving high pattern fidelity is crucial for any profitable patterning solution in semiconductor processing. The ability of a thermodynamically driven process (such as DSA) to achieve the required low defect densities has been questioned. Typical random defects that could be expected in a process that uses lamellar phase BCP materials to obtain line/space patterns include dislocations and disclinations.[7] However, initial experimental studies have indicated no fundamental showstoppers.[8] In addition, simulations have indicated that the defect rate may be very low when the boundary conditions for the DSA process are properly optimized.[9]

In the previous chapters, implementation of the Liu-Nealey (LiNe) chemo-epitaxy process (Figure 1) in a 300mm wafer flow has been demonstrated.[10] A thin (~7nm) cross-linkable polystyrene (X-PS) layer is coated on an SiN substrate wafer. Subsequently ArF immersion lithography provides an 84nm pitch pre-pattern targeted at ~38nm CD. Next, a plasma etch step trims the CD to ~18nm and simultaneously etches through the uncovered X-PS layer. The resist is selectively stripped using a wet process. Next, an –OH terminated poly(styrene-*r*-methyl methacrylate) brush is coated over the X-PS pattern. During the subsequent anneal bake, the –OH group grafts to the SiN substrate. A solvent rinse is used to remove excess brush material yielding the chemical pre-pattern. A 28nm L_0 lamellar phase poly(styrene-*b*-methyl methacrylate) BCP material is coated over it and thermally annealed resulting in 28nm pitch line/space structures (3X frequency multiplication). Finally, a dry plasma process affords selective removal of the PMMA blocks from the BCP to give free standing polystyrene (PS) lines.

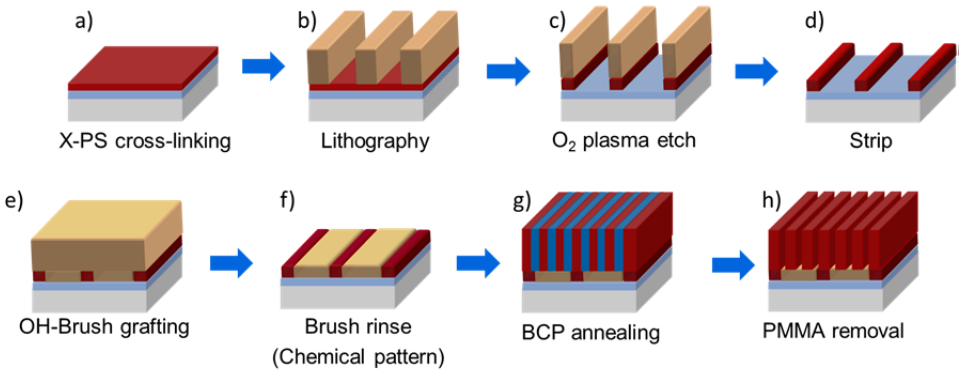

Figure 1. Schematic overview of the LiNe chemo-epitaxy process flow.

The process aims at constructing a chemical pre-pattern (after the rinse step) with an approach that allows full control over dimensional and surface chemical properties. The dimensional control is obtained by means of the trim etch step, which allows to achieve feature dimensions that are difficult to access through optical lithography on its own. The surface chemistry control is obtained by the 'brush-last' approach that avoids chemical modification of sensitive neutral layer during processing. Building on this process, its defect performance has been studied, especially focusing on dislocation defects, which are deemed the most likely DSA specific defects. Main attention in this study has been on 1) setting up the defect metrology such that a maximum sensitivity is obtained for these dislocation defects, 2) determining the defectivity performance of our current process and 3) identification of the root causes for the current defects.

4.3 Experimental

4.3.1 Materials

Cross-linkable poly(styrene) (X-PS, AZEMBLY™ NLD128), hydroxyl-terminated poly(styrene-random-methyl methacrylate) (P(S-*r*-MMA)-OH) brush (AZEMBLY™ NLD127), and poly(styrene-block-methyl methacrylate) (PS-*b*-PMMA, AZEMBLY™ PME312) BCP with Lo = 28nm, were synthesized by AZ Electronic Materials and were used as received. ArF immersion photoresist AIM5484, was purchased from JSR Micro. Organic solvent RER600 was purchased from Fujifilm and Orgasolv STR 301 was bought from BASF.

4.3.2 Process

The process used for this experiment is based on the method for the fabrication of chemical nanopatterns describen in Chapters 2 and 3. All processing was performed at imec on a TEL CLEAN TRACK ACT™12 system. For a 3X feature multiplication process, using a pre-pattern pitch of 84nm, exposures were done on an ASML XT:1950Gi scanner at 1.35NA using quadrupole illumination (XY polarized, NA= 1.35, σo=0.87, σi=0.72). An inorganic antireflective coating (ARC) film of SiN, of 14nm, was deposited via chemical vapor deposition (CVD) on 300mm Si wafers. The X-PS film, with thickness of 7-8nm, was spun and annealed at high temperature for 5min under a N2 atmosphere. After resist coating and exposure using vendor recommended settings for post-apply bake (PAB), post-exposure bake (PEB), and development, lines and spaces of 84nm pitch and critical

dimension (CD) of 38nm were obtained. O_2 and Cl_2 plasma etch was used to trim the resist to target 17nm CD and remove the X-PS exposed to the plasma. The remaining resist was stripped at room temperature with Orgasolv STR 301. The P(S-r-MMA)-OH brush was spun and annealed for 5min at 250°C in a N_2 atmosphere. Non-reacted material was rinsed with RER600. The PS-*b*- PMMA BCP was coated on the chemical patterns and annealed for 5min at 250°C in a N_2 atmosphere. Defect inspection was done in a KLA-Tencor 2835. Location and imaging of the defects were performed with a review scanning electron microscope (SEM).

4.3.3 Metrology

For defect inspection and source identification, the tool utilized in this study is a broadband brightfield optical inspection system (2835). This widely adopted tool for both R&D and production monitoring inspection applications was found to be capable for investigating the defect source analysis of the Directed Self Assembly process given the current status of maturity of this next generation lithography contender. In some cases, for new processes techniques and design rule nodes, the initial setup of the tool (wavelength, apertures, modes etc.) can be driven from the results of a proprietary off-line simulation methodology from KLA-Tencor which uses a Rigorous Coupled Wave Analysis (RCWA) method to solve the EM simulation. Directed Self Assembly, being a new generation lithography process, the critical defects of interest (such as dislocation and disclination post BCP PMMA removal step) were first studied from simulations to determine the best potential optical setup "recipe" to maximize signal. The recipe was then verified and further optimized to maximize sensitivity to all defects of interest whilst suppressing potential noise sources.

The first step while setting up inspection recipe is ensuring that the inspection is capable of detecting the defect types of interest (DOI). Inspection setup to maximize sensitivity is initially performed at the final or target inspection step post BCP PMMA removal). The KLA-Tencor state-of-the-art Brightfield inspection tools have high flexibility in inspecting different materials, structures and layouts, with the selection of specific wavelength bands, imaging modes and post processing algorithms that can be applied. A rigorous inspection setup methodology is required for new process techniques where we cannot use previous learning on a potential best inspection method. The most important aspect of recipe setup on a brightfield inspection system is to ensure the inspection tool is able to see the correct structures of interest with good contrast or resolution (however resolving pattern is not essential for defect detection). The next step is to identify potential inspection modes and compare the signal of the defects of interest to the background wafer noise. Through this

signal to noise analysis the best mode for a particular DOI / layer stack can be selected. We followed a methodology where multiple initial inspection modes were identified through simulation and then are run as 'hot scans', after defect review, best 'modes' can be selected for re-scan and a final mode selected for optimization. Finally, the optical attributes of the defects of interest and any noise or false defect types are analyzed for the application of post processing and filtering techniques to maximize signal and increase efficiency of defects capture. The best mode identified for the final inspection is then also used for all preceding inspection steps through the source analysis to provide sensitivity to the same defect types. General inspection for defect source analysis investigations can run with a higher potential nuisance rate as a greater reliance is placed upon Engineering defect review than would be typically seen with production monitor recipes. A further benefit in the early stages of defect reduction for a new process or process module they are typically specific defect types that dominate particular sub-steps leading to high defect densities of real defects, allowing easier quantification and relatively low nuisance rates typically in the 10-25% range. With this small number of defect types with high defect densities we can quickly drive down defect levels by identifying and fixing a relatively small number of issues.

4.3.4 Defect Source Analysis (DSA) methodology

Defect Source Analysis is a methodology developed by KLA-Tencor to identify the "source" of key defect types in a given semiconductor process. The premise of this methodology depends on the fact that the coordinates of defects captured in an optimized inspection by a tool such as the 2835 can be reported to a very high accuracy (better than a micron). When inspection is carried over multiple process steps, the coordinates of defects reported at each process step can be stacked to separate "added defects" from "previous layer defects." The "search radius" is a user definable parameter which can be effectively used under different process conditions to discern added defects from previous layer defects.

In the LiNe chemo-epitaxy process flow described in Fig.1, optimized inspections were set up at seven steps (SiN, X-PS, Exposure Resist, Trimming Resist, Rinse Guide pattern, chemical pattern, and PMMA removal). Given the engineering nature of this methodology, high sensitivity inspections were set up at each step and the associated slightly higher nuisance rates were acceptable. Defect classification was performed for added defects, example images were captured and paretos were created at each step. At the last step (in this case is PMMA removal) or any other intermediate step, defects found could be tied

back to their source. A step-contribution analysis could be conducted to account for and identify the possible sources of the defect types. This provided clear, undisputable, actionable data for defect reduction activities.

4.4 Results and discussion

4.4.1 Process performance

In order to investigate the contribution of each step of the process to defectivity (density and defect type) generated by materials or processing, defect source analysis of directed self-assembly was performed using the LiNe flow currently implemented at imec. To this end, a set of 7 samples was defined, as shown on Table 1. After each step of the fabrication of the chemical patterns and BCP anneal, all the samples were inspected using broadband defect inspection. Then, at each step one sample was removed from the flow to perform defect SEM review. In addition, a control sample was added to the flow (as indicated in column 1) , which was only inspected after BCP assembly. The purpose of the control wafer was to assess the impact of the inspection on the sample properties.

	Description of Wafer							
Process Step ↓	Control Wafer	DSA of DSA	Chemical Pattern Adders	Resist Strip Adders	Trim Etch Adders	Guide Pattern Exposure Adders	X-PS Adders	SiN
SiN	N	I	I	I	I	I	I	I / R
XPS	N	I	I	I	I	I	I / R	
ER (Expose Resist)	N	I	I	I	I	I / R		
TR (Trimming Resist)	N	I	I	I	I / R			
STR (Rinse Guide pattern)	N	I	I	I / R				
CP (Chemical Pattern)	N	I	I / R					
BCP (PMMA removal)	I / R	I / R						
N = No Inspection; I = Brightfield Inspection; I / R = Brightfield Inspection & Review								

Table 1. Design of the DSA of DSA experiment. Each step of the process of the LiNe flow was inspected using optical inspection.

Using defect source analysis, it is possible to differentiate between common and adder defects at several stages of the fabrication process, by comparing their position on the die/wafer (as explained in Section 2.4). For the LiNe flow, it was possible not only to

follow the progression of defects at each step, but also, to see their evolution. This allowed us to relate them to physical and chemical key parameters of directed self-assembly.

Figure 2 shows the overall defect density for each process and the break-down in its diverse contributors. For example, the SiN deposition did not have a significant impact on the final BCP defectivity, accounting for only 4 defects/cm^2 through all the sample fabrication procedure. Defect density increased to about 500 def/cm^2 after X-PS coat and anneal, and remained constant along the chemical pattern fabrication. The adder defects that were captured from the exposure, trim etch, and strip steps did not contribute to the final density after BCP anneal and PMMA removal. For the brush grafting step, 98% of the defects correspond to particles (data not shown). SEM images do not provide enough information to establish if these particles came from the brush coat or if they were deposited on the surface during the rinse of the un-reacted material. Since the sample was not inspected after brush coating, the root cause for this defect was not identified yet. Finally, after BCP coat and anneal, the defect density was about 564 cm^{-2}. These are adder defects and can be related to the BCP material or assembly process.

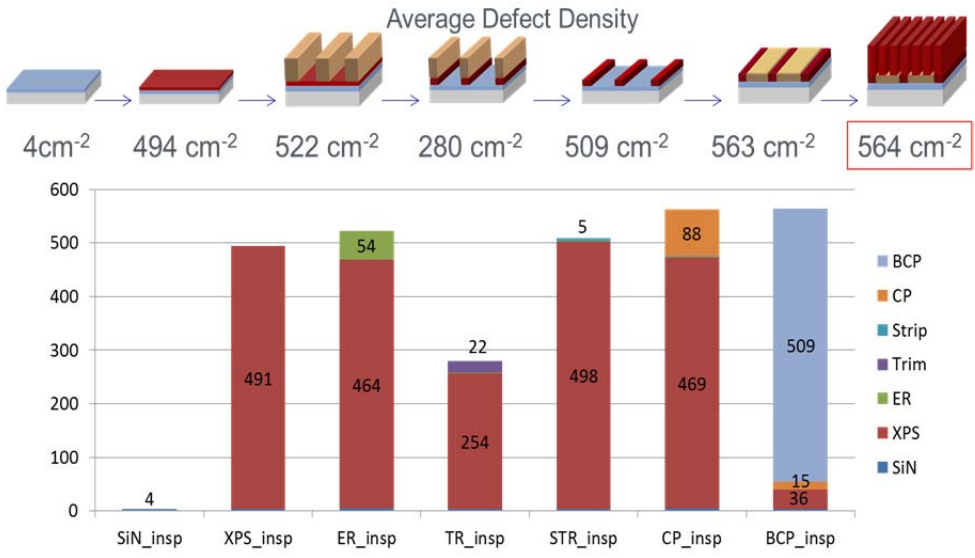

Figure 2. Evolution of defects in DSA of DSA experiment. The defects generated in the X-PS annealing step correspond propagate until the last step of the process. During the brush grafting, particles are added to the sample.

The main contributors to the final defectivity were, then, X-PS anneal, brush grafting, and BCP coat and anneal. For the X-PS, about 99% of the defects corresponded to bright spots, the majority of which (98%) had a diameter smaller than 200nm. Examples of bright spots

are shown on Figure 3. The capture rate of these defects was remarkably constant at each step of the process, except the trim etch. During this step, the SiN was exposed to the surface and the substrate presented contrast variations from the different materials (SiN, X-PS and etched resist). The sensitivity of the inspection recipe was adjusted to avoid excessive nuisance defects. However, after the photo-resist was removed in the strip step, all of the bright spots captured during the X-PS inspection were captured again. At this point, it was possible to verify that the bright spots will produce an (or multiple) interruption in the guiding stripe, as shown on Figure 3.

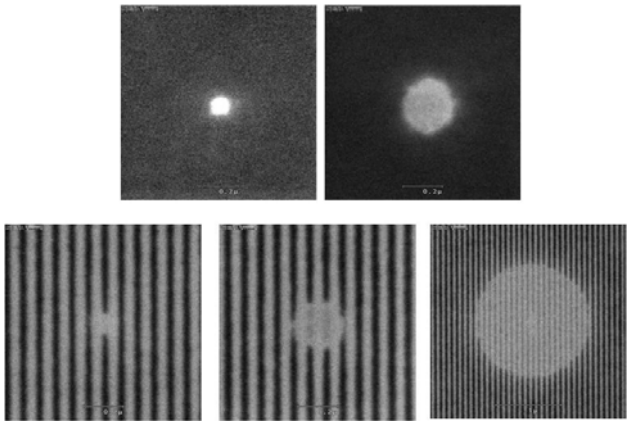

Figure 3. Sample top-down SEM images of typical white spot X-PS defects after X-PS coat and anneal (top) and after the photo-resist strip step (bottom).

The other significant common defect contributor to the BCP defectivity is in the brush grafting step. This step adds particles to chemical patterns, which persist and induce defects in the BCP patterns. Filtration optimization is required to mitigate this source of defects.

Directed self-assembly of block copolymers is a thermodynamically equilibrated process that relies on the interaction between the BCP and the surface. In order to achieve zero defectivity, the chemical patterns must provide the necessary conditions to achieve a high degree of order during block copolymer assembly. DSA of DSA has proven to be an effective method to identify the critical parameters during the fabrication of the chemically nanopatterned substrates that will result in a high degree of order of the BCP features assembled on them.

4.4.2 BCP defect root cause analysis

From the DSA of DSA experiment, it is evident that the white spot defects that are found in the X-PS guide layer are an important contributor to the defectivity that is found in the BCP. Due to the small size of the white spots and, therefore, of the missing guiding stripes,

a large number (>90%) of this type of defects are repaired by the BCP self-assembly process. As a result, the number of X-PS common defects is reduced drastically. This result is in agreement with the work presented in Chapter 3, using programmed defects, which showed that a gap in the guide stripe may be healed by the BCP in most cases.[9] However, it is possible to generate DSA-specific defects due to this issue, in particular, when the larger white spots result in too large an area where there is no guide pattern available and dislocation clusters appear (Figure 4). Note that the circular shape of the X-PS white spots is also somewhat apparent in the BCP dislocation pattern.

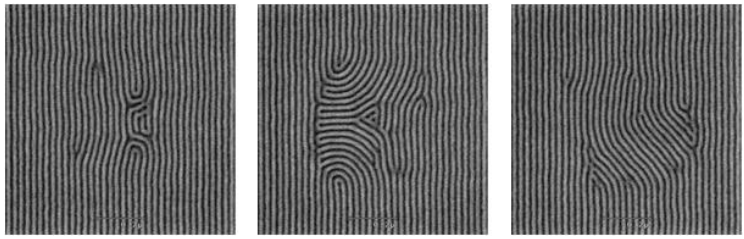

Figure 4. Sample top-down SEM images of typical common 'white spot' defects between X-PS only and full DSA process.

The root cause for the white spot defects is believed to be in dewetting of the X-PS material from the substrate. Attempts to mitigate this phenomenon are not only done by process optimization, but also by material improvements. For the processing, different coating techniques (dynamic and static) and annealing conditions (time and temperature), showed no decrease in defect density. A new X-PS material from AZ Electronic Materials has been tested and has resulted in significant reduction of the number of white spot defects. Figure 5a shows the bright spot density, where the image on the right corresponds to the new material. This sample was manually processed and the large difference in the values from die to die may be due to the coating conditions. For this reason, the dies marked in the rectangle were not considered in the reported average defect density. Further testing with this new material, including performance through the DSA flow and defectivity on fully automated samples, showed that even though the bright spots were significantly reduced, NLD166 conveyed a different type of defect. Dark defects as the ones showed on Figure 5b were captured in larger numbers than the bright spots (about two orders of magnitude) even when dispensed automatically. Therefore, this alternative guiding material did not replace NLD128.

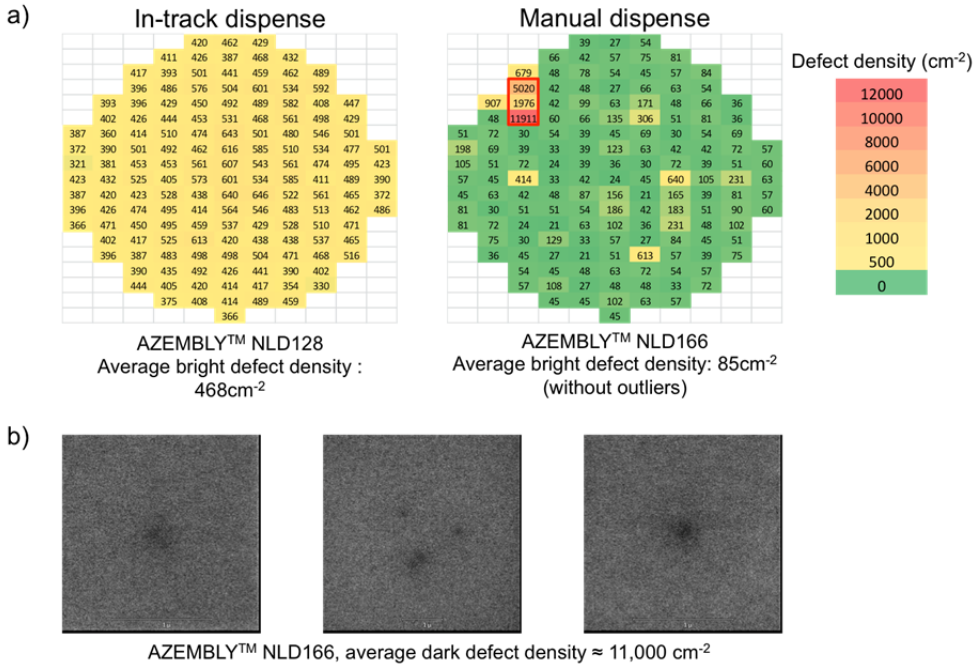

Figure 5. Defect maps of the density of white spot defects of in-line coated AZEMBLY™ NLD-128 (left) compared with manually coated AZEMBLY™ NLD-166 (right).

As it is shown on Figure 2, most defects in the BCP pattern are not common with the defects from any of the previous processing steps. More detailed analysis shows that the distribution of these defects is not homogeneous across wafer and across field. When we first consider the across wafer signature (Figure 6) a clear hot spot of defectivity is seen on the right side of the wafer. This hot spot correlates well with the post-trim etch CD signature, but not with the post-litho CD. The trim tech step has so far not been optimized for across wafer CD uniformity. This results in a lower average CD right of the center which is also where the high defect dies are found.

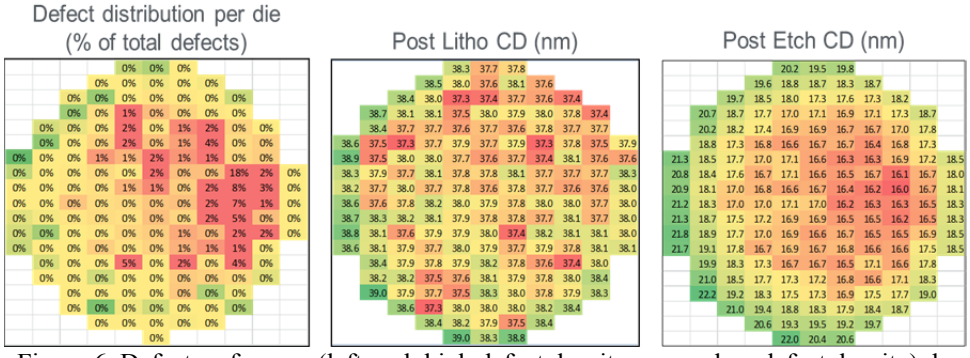

Figure 6. Defect wafer map (left; red: high defect density, green: low defect density) does not correlate with the post-litho CD across wafer (middle), but correlates well with the post-trim etch CD (right).

Interestingly, when a defect map is plotted of any of the high defect dies, there is and additional distinct signature. Most defects are present near the bottom left corner of the die (Figure 7). In contrast, defect maps of the low defect dies show an even distribution of defects across the die area. Also, for the intrafield signature there is a clear correlation with the post-trim etch CD. In this case, however, the CD signature stems from the exposure itself. A more detailed analysis of the CD of the photoresist after exposure, which consists of 15 measurements over the die, shows a difference of about 2nm (average of 163 dies) from the bottom left to the top right corner. After the trim etch process, not only the largest CD on the die shifted to the center position, as the edges tend to etch faster, but also, the difference in CD increased to about 4nm. It should be noted that this die CD signature does not automatically lead to high defect numbers. The dies comprising the hot spot on the wafer correspond to those having the smallest CD values (below 14nm) on both the left side of the die and on the sample (data not shown).

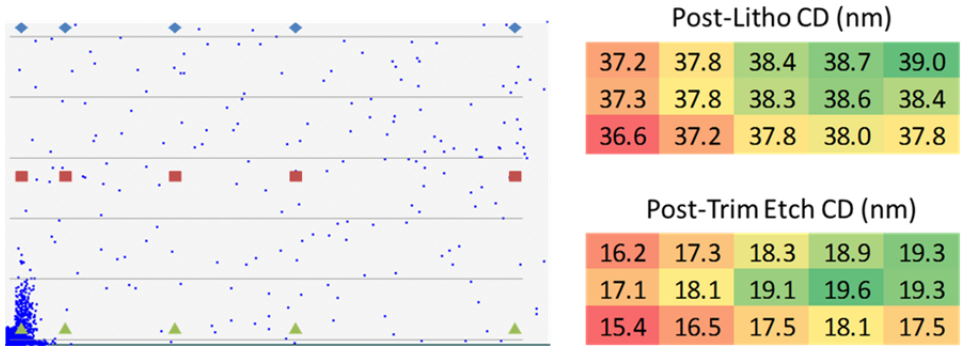

Figure 7. Typical defect map of a high defect die (left) shows a clear signature of high defectivity near the bottom left corner. The defects in this region are mainly large dislocations and correlate well with the post-litho and post-trim etch CD signature (right). The diamonds, squares, and triangles correspond to the positions where the CD measurements were taken.

The combination of the inter- and intrafield defect and CD signatures demonstrate that the root cause of these signatures is the small CD that results in insufficient guiding of the X-PS stripe, at which point dislocation clusters are formed. This is confirmed by the fact that the majority of the defects in the bottom left die corner are dislocation clusters. The remaining defects that are more evenly distributed across the die are almost exclusively particle defects (see below). It should be noted that the CD variations in the pre-pattern wafers (~6nm) are very large considering the target feature size after the trim etch(~18nm). In that respect, the defective area may be regarded as surprisingly small. Proper

optimization of the exposure and trim etch process is expected to remove the defect fingerprints and therefore the dislocation fingerprints.

When the dislocation defects from the bottom left corner of the die are removed, a significant number of defects on the BCP pattern can be captured, but none of those are dislocations or dislocation clusters (outside the X-PS common defects that were discussed earlier). The main contributor on the defect pareto now are small particles. In all cases these particles span less than one pitch in the final DSA pattern. The SEM review (Figure 8) shows some minor topography in the morphology of the defects indicating that these are particles embedded in the BCP material. Improvements in the filtration method of the material at the production site showed a dramatic decrease of 98% in the number of particles.

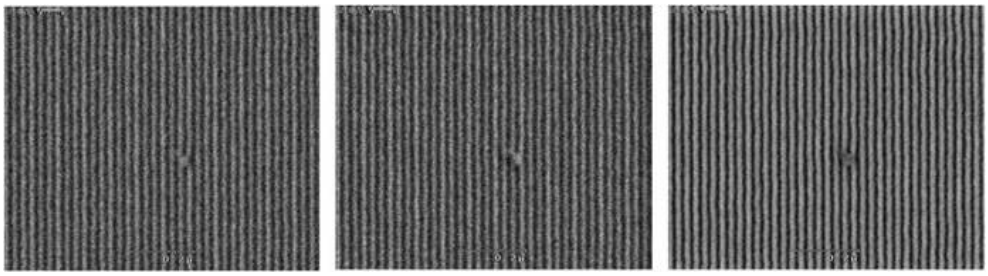

Figure 8. Sample SEM images of embedded particles in the BCP patterns.

In summary, our detailed analysis of the defect root causes has revealed no uncontrollable defect sources. When the geometrical and surface chemical properties of the pre-pattern are properly controlled and filtration strategies are further optimized, the DSA process defectivity will be driven down by several orders of magnitude.

4.5 Conclusions

The critical steps for process and material improvements required to minimize defect formation have been identified by running Defect Source Analysis in the chemo-epitaxy LiNe directed self-assembly flow. The defect source analysis technique on state-of-the-art defect inspection equipment has proven to be a powerful tool for controlling and understanding defectivity in the DSA process flow.

Root causes for the DSA-specific dislocation defects that have been found are identified as defect types that are commonly known from traditional optical lithography: pinholes, CD control in the pre-pattern and particles. In order to further improve the defect performance of this flow, optimizations of both materials and process will need to be implemented. For the cross-linkable polystyrene mat material, the bright spots (pinholes) after coat and bake need to be eliminated to prevent missing guiding stripes. For the block copolymer material, gel particles need to be eliminated since they account for the largest number of defects from the BCP layer. Further optimization to eliminate intra-die and intra-wafer CD non-uniformities generated during the exposure and etching steps, respectively, is necessary to avoid large dislocation clusters. Specifically, the across wafer uniformity of the trim etch step needs to be improved. Further transfer of the nanopatterns into the SiN and silicon substrate, discussed in Appendix A, shows good agreement with this study regarding the observed types of defects. However, the higher sensitivity achieved after eliminating the polymer materials is required to capture dislocations and additional defects of interest more efficiently.

4.6 References

1. Delgadillo, P.R., et al., *Defect source analysis of directed self-assembly process.* Journal of Micro-Nanolithography Mems and Moems, 2013. **12**(3).
2. Kim, S.O., et al., *Epitaxial self-assembly of block copolymers on lithographically defined nanopatterned substrates.* Nature, 2003. **424**(6947): p. 411-414.
3. Hinsberg, W.D., *Self-assembling materials for lithographic patterning: overview, status, and moving forward*, J. Cheng, H.-C. Kim, and D. Sanders, Editors. 2010: Proc. SPIE. p. 76370G-1.
4. Wong, P., *Block copolymer directed self-assembly enables sublithographic patterning for device fabrication*, C. Bencher, X.-Y. Bao, and L.-W. Chang, Editors. 2012: Proc. SPIE. p. 832303-1.
5. Bencher, C., *Directed self-assembly defectivity assesment*, J. Zhou, et al., Editors. 2012: Proc. SPIE. p. 83230N-1.
6. Doerk, G., *Measurement of placement error between self-assembled polymer patterns and guiding chemical prepatterns*, C.-C. Lui, et al., Editors. 2012: Proc. SPIE. p. 83230P-1.
7. Harrison, C., et al., *Dynamics of pattern coarsening in a two-dimensional smectic system.* Physical Review E, 2002. **66**(1): p. 27.
8. Bencher, C., et al., *Self-Assembly Patterning for sub-15nm Half-Pitch: A Transition from Lab to Fab*. 2011, Proceedings of SPIE.

9. Nagpal, U., et al., *Free Energy of Defects in Ordered Assemblies of Block Copolymer Domains.* Acs Macro Letters, 2012. **1**(3): p. 418-422.

10. Rincon Delgadillo, P.A., et al., *All track directed self-assembly of block copolymers: process flow and origin of defects*. 2012: Proceedings SPIE 8323. p. 83230D.

Chapter 5

Dimensions of Chemical Patterns for High-Throughput Directed Assembly of Block Copolymers with Density Multiplication

5.1 Abstract

The Liu-Nealey (LiNe) chemo-epitaxy flow for directed self-assembly (DSA) of block copolymers (BCP) has proved to be an effective method to improve the resolution of traditional lithographic techniques. This process allows for the fine-tuning of the properties of the chemically nanopatterned substrates, defined by the chemistry and geometry, which can be related to material and processing conditions. In addition, its implementation on 300mm wafers has allowed for high-throughput investigation of a wide parameter space on a single sample, using the tool automation that this sample size offers. In this work, we studied the impact of the geometry, or dimensions, of the chemical patterns, such as the chemical pattern pitch (L_s) and the width of the guiding stripe (W). Two process windows were observed and explained using a simple model of the interfacial energy between the nano-patterned substrate and the BCP. The larger range of W that resulted in a high degree of perfection of the BCP structures was $0.4L_0 < W < 0.9L_0$, which corresponds to the conditions around the interfacial energy minimum at $0.5L_0$. Our results suggest that fine control of the properties of the chemical patterns is required to achieve the defects levels posed by the semi-conductor nano-patterning industry in BCP anneal times amenable for high volume manufacturing.

5.2 Introduction

The ability of self-assembled materials to generate ordered periodic structures of 50nm and below has attracted the attention of the academia and the industry,[1] which has identified them as a next generation complimentary patterning technique.[2] Directed self-assembly (DSA) of block copolymers (BCP) offers a cost-effective solution to enhance the performance of current 193nm immersion lithography technology for obtaining dense

arrays of features with dimensions that are naturally found in these materials (5-50nm).[3-5] Additionally, previous reports have shown that DSA of BCP can improve some of the challenges of traditional lithography, such as line edge roughness (LER),[6] line width roughness (LWR), and critical dimension (CD) control. Using the tools that are available in the fab, fine control of the substrate properties is possible and the feature density of the original photoresist can be multiplied with a high degree of perfection of the aligned structures on full 300mm samples.[7, 8] Still, in order to consider the implementation of DSA of BCP for high volume manufacturing, this technique must meet the defect density requirements that the industry requires. To accomplish this, the role of multiple processing and material parameters and their relationship to the thermodynamic forces that drive the DSA of BCP must be established in order to define the conditions that will lead to minimum defect formation.

In DSA of BCP, the properties of the final polymer features, such as shape, size, orientation, and direction, depend on the complex interplay of thermodynamics and kinetics during BCP annelaing.[9-12] Specifically, the role of thermodynamic parameters in DSA of BCP has been characterized through phenomenological models for the minimization of the total free energy.[10, 13] These models are based on the fact that, for specific annealing conditions, the balance between the system with its boundaries will determine the orientation and degree of order of the resulting morphologies. These models have been developed for two chemo-epitaxy schemes: (1) 1:1 assembly, where the resist pattern pitch (L_s) equals the BCP bulk natural periodicity (L_0), ($L_s = L_0$), and (2) feature density multiplication, where L_s is an approximate integer multiple of L_0, ($L_s = \text{n } L_0$). Edwards *et. al*. were able to capture the simultaneous effect of the chemistry and geometry of the chemical patterns for case (1), in which the BCP can stretch or compress up to $0.1L_0$ to accommodate to the printed pitch, given the largest chemical contrast possible between the stripes. For case (2), the alternating regions consist of a guiding stripe (W), with preferential wetting of one of the blocks, and a background region with a slightly preferential behavior towards the opposite block.[14] In the same manner, Liu *et. al.* arrived to a simple expression of the BCP-substrate interfacial energy that quantitatively shows that the chemical composition of the backfill region must be finely tuned for different multiplication factors, as a means to minimize the BCP-substrate interfacial energy.[13] The model showed good agreement with their experimental results. Additionally, theoretical and experimental work has shown that three-dimensional structures are generated throughout the BCP film thickness when W approaches or is larger than L_0,

especially when the interaction of the blocks with the chemical pattern is strong.[15, 16] For both 1:1 assembly and density multiplication, the ability to relate fundamental thermodynamic parameters to materials and processes has provided deep insight into the conditions that are required to achieve high pattern perfection using DSA of BCP.

Experimental evaluation of the thermodynamic parameters is effectively accomplished through the chemo-epitaxy process for density multiplication proposed by Liu and Nealey *et. al.* (LiNe flow). Through a careful material design, using mats and brushes, the surface energies of the guiding stripe and background regions are finely tuned. Additionally, control of L_s and W is achieved by the combination of exposure conditions and a trim etch step. The LiNe flow has been implemented in an experimental fab, which involves not only the fabrication of chemically nanopatterned substrates with high control and reproducibility over entire 300mm wafers, but also the inspection of large areas. Although, significant progress has been made recently on the inspection of full samples using optical techniques, industrial scanning electron microscopy (SEM) has allowed the assessment of multiple material and processing conditions in a reduced amount of time. In addition, this set-up has provided initial insight into the impact of materials and processing conditions required for the fabrication of chemical patterns designed to target the minimum in the total free energy landscape, and, therefore, obtain the defect-free structures predicted by theoretical work.

In this study, we characterized the nano-patterned substrates, fabricated as described in Chapters 2 and 3, and investigated the impact of the dimensions of the chemical patterns for 3X feature density multiplication. By generating chemically nano-patterned substrates with different pitches, the impact of commensurability (L_s/L_0) was investigated. At the same time, we aimed to find the conditions for which W will guide the BCP with a high degree of perfection. For the conditions used in this work, two process windows were found as W increases, where the widest process latitude at small W ($< 1.0\ L_0$) reflect the need to adjust the CD after exposure and trim etch to avoid unfavorable guiding stripe-PMMA block interactions. These results can be explained in terms of the interfacial energy at the BCP – substrate interface, considering only perpendicular structures throughout the film. Our model effectively captures the impact of the properties of the chemical patterns on the total free energy of the system and, therefore, on BCP assembly.

5.3 Experimental

The process used in this study, referred to as the Liu-Nealey (LiNe) flow is based on our method for the fabrication of chemically nano-patterned substrates described in the previous chapters. Briefly, a cross-linkable poly(styrene) film (X-PS, AZEMBLY® NLD128, AZ Electronic Materials) was spin-coated to 8nm film thickness and annealed for 90min at 250°C under a nitrogen atmosphere on 14nm of silicon nitride. These two layers function as an antireflective coating (ARC) during the exposure step. Next, photoresist (AIM5484, JSR Micro) was coated and a focus-exposure matrix (FEM) was exposed on an ASML XT:1900Gi scanner at 1.35NA using quadrupole illumination (XY polarized, NA= 1.35, σ_o=0.87, σ_i=0.72), a dose range of 16-26mJ/cm^2 in 1 mJ/cm^2 steps, and a focus range of 360nm in 20nm steps. Illumination conditions were optimized to target 84nm pitch and 35nm critical dimension (CD). The reticle used for this work includes a large range of pre-pattern pitches and CD that can be analyzed within a single exposure condition. Additional pitch-CD combinations can be accessed by analyzing different dose and/or focus steps. However, variations in the focus will result in either positive or negative sloped profiles of the photoresist. The impact of this parameter is out of the scope for this study, therefore, only photoresist structures exposed at the best focus were considered. After exposure and development, lines and spaces of 79 to 88nm pitch were obtained (exposure conditions were not modified for each pitch). The samples were then submitted to an O_2 and Cl_2 plasma etch step in a V3A Lam Research tool, to trim the resist lines and, simultaneously, remove the X-PS exposed to the plasma. In the following step, a wet strip was used to selectively remove the photoresist from the X-PS using Orgasolv® STR 301 (BASF). A hydroxyl-terminated poly(styrene-*r*-methyl methacrylate) brush with approximately 51% polystyrene content (P(S-*r*-MMA)OH, AZEMBLY® NLD127) was spun and annealed for 5min at 250°C under nitrogen atmosphere. Excess material was removed by rinse with RER600 (Fujifilm). Poly(styrene-*b*-methyl methacrylate) BCP with L_0 = 28nm (PS-*b*-PMMA, AZEMBLY® PME312, AZ-EM), was coated on the chemical patterns and annealed with the same process conditions used for deposition of the random brush. To improve the contrast on the SEM images, the PMMA block was removed using a dry etch process.

The profile of the X-PS guiding stripes and the chemical patterns was characterized using a Tecnai F30 transmission electron microscope (TEM and HRTEM) and a Nanoscope IVa Dimension 3100 atomic force microscope (AFM) in tapping mode. Samples were analyzed after resist strip and after brush deposition. A Hitachi CG4000 CD-SEM was used to image

and measure the CD of the photoresist after exposure and trim etch, as well as the BCP self-assembled structures after PMMA removal.

5.4 Results and discussion

5.4.1 Exposure

The LiNe process followed for the fabrication of chemical patterns, shown on Figure 1.1. The pitch of the nanopatterns and the width of the guiding stripe, are defined in steps b) and c) on Figure 1.1. In the lithography step, the pitch of the pre-patterns will be given by the mask design, while the CD of the photoresist lines will depend on both the reticle design and on the energy used during exposure. In the current experiment, the impact of L_s and W was investigated simultaneously by varying the pre-pattern pitch from 80 to 87nm with 8 different CD available per pitch and per die, as indicated in Figure 1.2. Although a larger range of pre-pattern pitches was available on the reticle, the illumination conditions were not optimal for smaller pitches and the resist patterns presented poor quality. A focus-exposure matrix (FEM) was exposed and five different doses at nominal focus, shown on Figure 1.3, were analyzed after lithography, trim etch, and rinse.

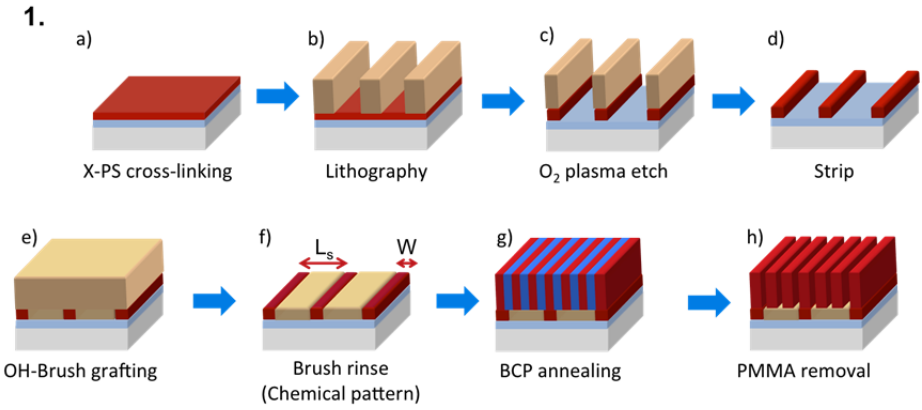

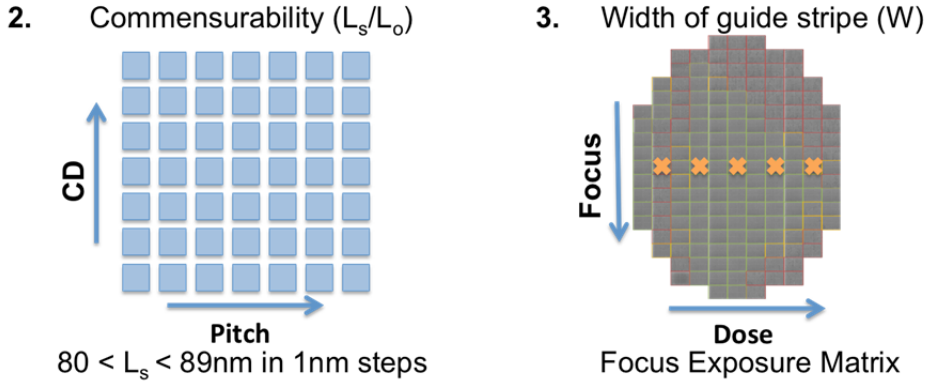

Figure 1.1 LiNe flow for the fabrication of chemical patterns for directed self-assembly of block copolymers with feature multiplication; 1.2 Schematic of the pitch and CD combinations available from the reticle design; 1.3 Design of a focus exposure matrix, where the dose is varied across and the focus increases along the sample.

5.4.2 Trim etch

Theoretical and experimental work has shown that the best assembly occurs when the width of the guiding stripe is about half the periodicity of the BCP (W=0.5L_0).[14] Therefore, for the current material AZ-PME312, W must be about 14nm. In order to access small CD values, which cannot be resolved using 193 immersion lithography and to break through the PS material for further brush grafting, a trim etch process was used. The impact of the trim etch conditions, such as the plasma chemistry and processing time, on the etching rate of the photoresist as a means to finely tune W, was initially verified using top-down SEM images after exposure and after etch. CD measurements of post-litho and post-etch conditions, corresponding to the same exposure conditions, are shown in Figure 2A and were obtained using an in-tool algorithm, for a series of Ls = 84nm lines. The etching rate of the photoresist lines with smaller CD after exposure is higher than for the wider lines. However, it is possible to tune the processing conditions in the two steps to target desired values of W. In addition, top-down SEM images provide information related to the effectiveness of the etching process to remove the X-PS material that is exposed to the plasma. Based on the contrast variations on the etched samples along the CD axis, figure 2A suggests that this process is dependent on the CD of the photoresist. After exposure, a black background, corresponding to the X-PS material, can be observed between the bright photoresist lines. After the trim etch, large CD values (left end) also present dark spaces between the lines. However, as the CD decreases, scattered bright areas appear in the background, which correspond to the SiN, around W = 28nm. At 23nm post-etch CD it is evident that large areas of SiN are open but with some X-PS residues remain after the

etching step. At the smallest CD, a clear bright background can be observed between the etched photoresist lines. The thin dark lines between the SiN and the photoresist correspond to footing of the X-PS stripe. Although, top-down SEM images provide limited information about the geometry of the guiding stripe, they provide an easy manner to evaluate the exposure and etching conditions necessary to achieve desired *W* values.

To gain more insight into the shape and dimensions of the guiding stripes and the chemical patterns, samples processed until the strip and brush rinse steps were analyzed using TEM and AFM. Large inspection blocks of 7.5x5mm^2 with L_s = 84nm, included in the sample design, were exposed at 21mJ/cm^2 and used for this purpose. The TEM image shown in Figure 2B provides detailed information about the trapezoidal profile of the PS guiding stripes, which resulted from the (partially) isotropic dry etch process. Measurements of the trapezoid are shown in Table 1. SEM measurements indicate that the CD of the photoresist after exposure and development is 36.6nm, and in the following step it is reduced to about 20.8nm. The top of the trapezoid, W_1, is comparable to the CD after trimming, and the base, W_2, is similar to the CD after exposure. Additionally, the height of the stripes was measured to be about 6nm, which is about 2nm less than the PS film thickness originally spun on the SiN. The height difference may be caused by the beam damage of the sample during analysis. AFM results from a sample processed with the same conditions confirmed the trapezoidal shape of the guiding stripes, but indicated that the height of the guiding stripes is 8nm, which corresponds to the thickness of the X-PS after spin coating and annealing as show on Figure 2C. This measurement and the TEM micrograph suggest that the photo-resist was completely removed using Orgasolv STR 301. In spite of the sloped profile of the guiding stripes, it is possible to tune the processing conditions such that a region of the X-PS material, defined by *W*, is protected by the photoresist during the trim etch and will effectively function to direct the assembly of the BCP.

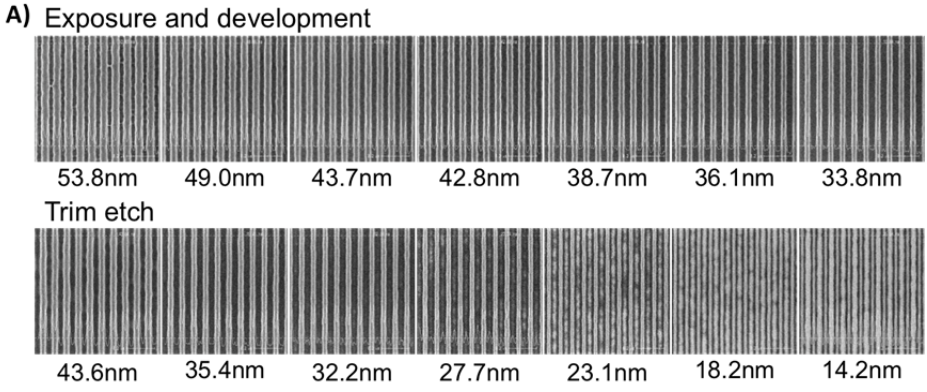

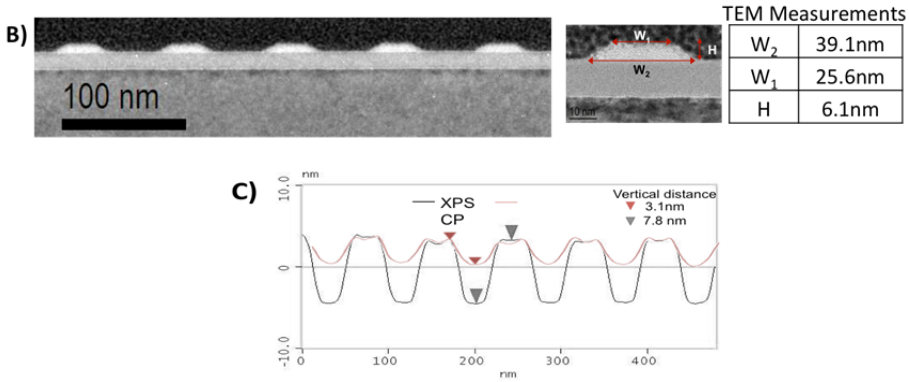

Figure 2. Characterization of the chemical patterns: A) top-down SEM images of 84nm photoresist lines after exposure and trim etch, B) TEM micrograph of a X-PS guiding stripe after photoresist strip with Orgasolv STR 301, C) Height AFM measurements of the guiding stripes (grey) and the chemical patterns (red).

5.4.3 Brush grafting

During the trim etch step, the X-PS material on the slopes of the trapezoid was exposed to the plasma and functionalized with oxygen moieties. This may allow the brush to react on these regions and on the SiN, but not on the X-PS that was protected by the photoresist, resulting in a chemical pattern of defined geometry and chemistry. Figure 3 indicates that, for a uniform wafer exposed at 21mJ/cm^2, the OH-P(S-*r*-MMA) random copolymer effectively reacts on the areas between the PS stripes and a chemical pattern is obtained. AFM analysis also shows that the area between the X-PS stripes is filled with the brush material, with a final height difference of about 3nm between the two regions as shown on Figure 2C. This is the expected value given the difference in height of the X-PS guide stripes (8nm) and the thickness of the brush coated on blanket silicon wafers (5-6nm). It is important to note, however, that the trim etch must be optimized to be more anisotropic in order to eliminate the footing on the guiding stripe and achieve a uniform grafting of the brush only to the SiN areas and improve control over *W*. Direct measurement of the width of the guiding stripe is not possible, either before of after brush grafting, due to lack of contrast with either technique used in this work. Still, comparison of the CD of the photoresist after the trim etch obtained with TEM to CD-SEM, suggests that the latter may provide an effective estimation of *W*. Therefore, for the present study, CD-SEM measurements after trim etch are used as an estimate of the top guide CD W_1. This allows to investigate the impact of geometry on the behavior of PS-*b*-PMMA with L_0 = 28nm on chemical patterns designed for 3X feature density multiplication and relate them to changes in the total free energy of the final assembled structures.

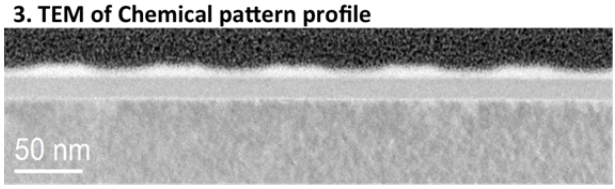

Figure 3. TEM micrograph of a X-PS guiding stripe after brush grafting.

5.4.4 BCP Self-assembly

After the fabrication of the chemical patterns for 3X feature density multiplication with dimensions in the range of interest, the combinatorial effect of L_s and W on the assembly process was investigated by coating a 36nm film of BCP on the 300mm wafer and annealing at 250°C for 5min. After micro-phase separation, the PMMA block was removed and alignment of the BCP was evaluated using top-down SEM images. From all the investigated L_s - W combinations, images corresponding to BCP assembled on chemical patterns with W = 0.5, 0.6, 0.8, 1.0, 1.14, 1.25, and 1.5 L_0 were selected. Although, in each case, the inspected area was only 0.9x0.9μm^2, the images shown in Figure 4 are representative of multiple pictures obtained for similar L_s and W conditions. The geometry of the chemically nano-patterned substrates has a clear impact on the degree of perfection of the assembled structures.

Investigation of the impact of commensurability (L_s/L_0) in the assembly process, indicates that, for the composition of the guide stripe and backfill regions used in this study, the BCP material AZ-PME312 can accommodate to a wider range of smaller pitches rather than to larger pitches, i.e. the chains present more tolerance towards compression (3.6% L_0) than stretching (1.2% L_0), assuming L_0=28nm, as shown in Figure 4. At L_s = 80nm the quality of the chemical patterns starts to decrease, since the illumination conditions during exposure were not optimized for this pitch. Therefore, any results below this value are not considered. As it is suggested by the present results, the BCP shows a limited tolerance towards stretching, therefore, if L_0 is not matched correctly with the pitch of the pre-pattern, defects may be obtained mainly at larger pitches, when using the annealing conditions described in section 5.3. According to our results, a BCP of 27.7nm will already be at the limit of the periodicity that can provide good alignment on an 84nm pitch chemical pattern. One important aspect is that the current material, AZ-PME312, is a blend. Therefore, the results may vary with different formulations. Although the study of commensurability for as a function of composition is out of the scope of the present study, it will be of significant importance, especially when establishing the specifications for material design.

When assessing the BPC behavior through W, two regimes can be observed. The first one at small values of W, starting at $W = 0.5\ L_0$, where the BCP is assembled with a high degree of perfection for 81nm < L_s < 85nm, indicated by the green squares. At W = 28nm, only randomly oriented structures were captured for all the investigated pitches. Order is recovered around W = 36nm (1.25 L_0), where almost perfectly aligned lamellae can be observed. As W approaches 1.5 L_0, random orientation is observed again.

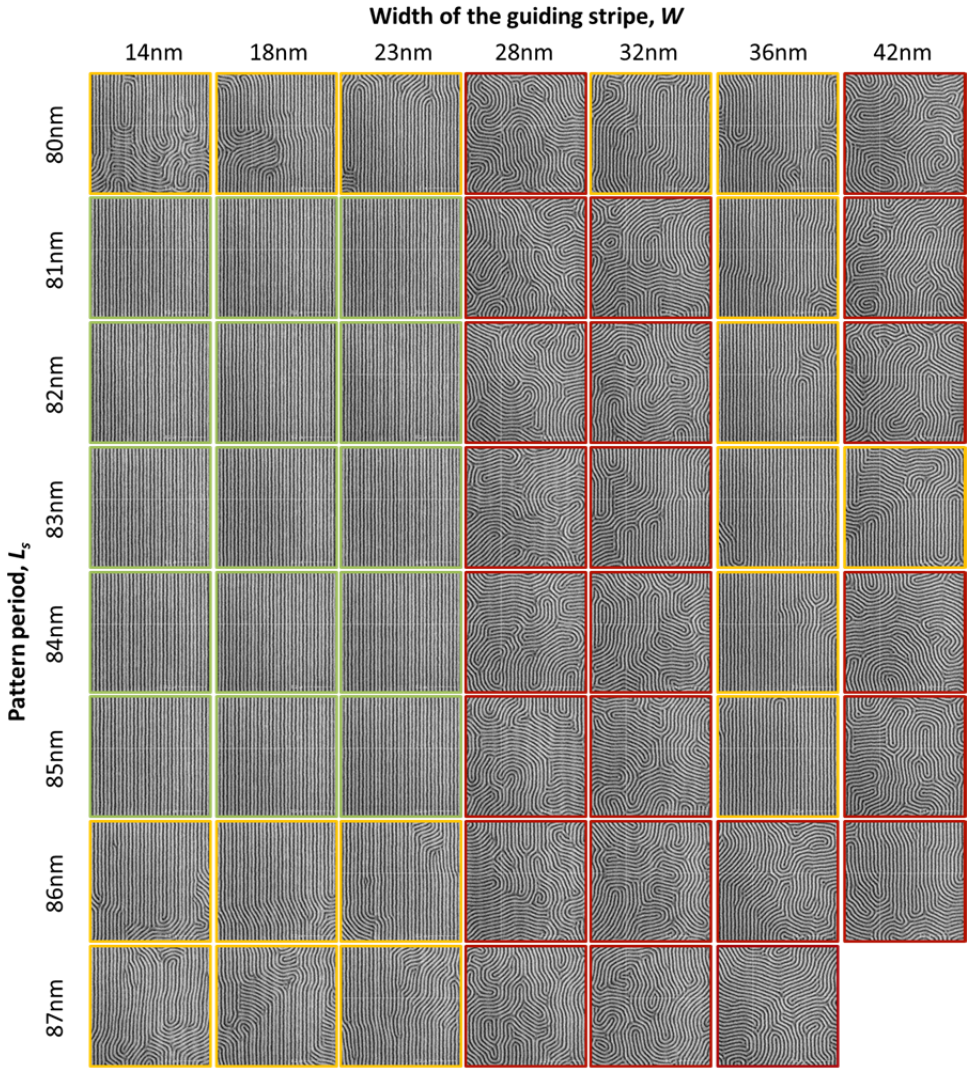

Figure 4. Top-down SEM images of assembled BCP on chemicall patterns of defined dimensions. The border indicates the degree of order.

Fine detail of the impact of the boundary conditions on DSA of BCP can be obtained when all the available experiments are considered. In order to assess the degree of order of the

final BCP structures, obtained for all the available L_s - W combinations, scores from 0-3 were assigned to each image. Fingerprint-like structures, or random orientation, were assigned a score of 0, while a high degree of perfection (absence of defects) obtained 3. Intermediate states with partial alignment were defined as 1 and 2 in increased order, as illustrated on Figure 5. The larger number of experimental conditions that can be investigated with the automated tools allows a precise definition of the dimensions that lead to a high degree of perfection or to random orientation, for the processing conditions used in this work. Assessment of the behavior of the system at various pitches supports the previous observation that the BCP shows more tolerance to be compressed rather than stretched. The pre-pattern pitch L_s = 84nm, which is also closest to commensurability, has the largest range with a continuous score of 3. In this case, the first process window of the two observed previously spans the range 12nm < W < 26nm ($0.43L_0$ < W < $0.9L_0$). It was not possible to analyze smaller W values since the photoresist lines presented poor quality (increased roughness and missing sections) after the trim etch process. Random orientation is observed when 26nm <W< 36nm (0.9 L_0 <W< 1.3 L_0). At L_s=84nm, order is partially recovered when 36nm <W< 42nm (1.3 L_0 <W< 1.5 L_0) with order corresponding to a score of 2. However, due to the low definition and large width of the lines obtained after exposure and trim etch around W=1.5 L_0, (Figure 2A, 43.6nm CD after trim etch) it is not possible to define experimentally if the process window could be larger with a more effective exposure and trim of the photoresist and break through the X-PS.

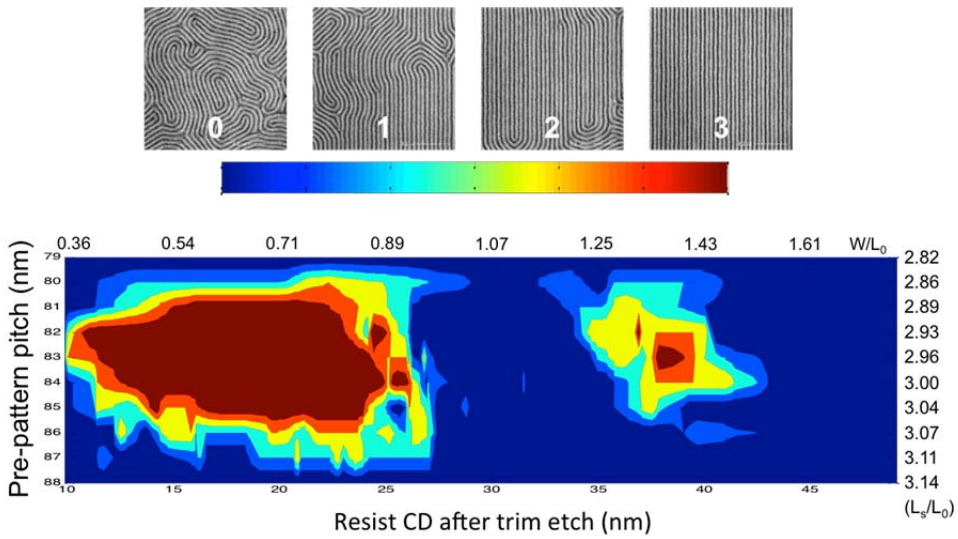

Figure 5. Scores assigned to BCP assembly at different geometry conditions. The score of 0 corresponds to random orientation, while a score of 3 represents perfectly aligned BCP lamellae.

The two process windows, corresponding to lamellae assembled with a high degree of perfection, result from the tendency of the system to minimize its total free energy as the thin film of BCP interacts with its surroundings. In order to understand to which degree the materials and the processing conditions impact this phenomenon, a simple sum of the contributors to the total free energy is considered:

$$F = F_{elastic} + F_{AB} + F_{surface} + F_{substrate} \quad (1)$$

where $F_{elastic}$ corresponds to the chains' configurational entropy, F_{AB} is the interfacial energy between the A-B blocks, $F_{surface}$ is the interfacial energy at the free surface, and $F_{substrate}$ is the interfacial energy at the BCP-substrate boundary.[10] The first two terms in Equation 1 are minimized when the BCP adopts the bulk properties, i.e. the natural periodicity L_0 and smallest possible interfacial A-B area. The $F_{surface}$ contribution to the free energy depends on the surface tension of the polymer blocks, which are fixed at specific annealing conditions. In chemo-epitaxy, the properties of the chemically nanopatterned substrate, such as the chemistry and geometry, will define $F_{substrate}$, and, in an indirect way, may impact $F_{elastic}$ and F_{AB}. Therefore, by finding the conditions in which $F_{substrate}$ is at its minimum, it can be assumed that the total free energy of the system, F, is also at its minimum, making the formation of defects less likely.

The interfacial energy between the BCP and the chemically nanopatterned substrate will depend on the strength of the interaction and the contact area between the blocks with each region of the nanopatterns in the following way:

$$\gamma_{BCP-CP} = \gamma_{S-g}\frac{A_{S-g}}{A} + \gamma_{S-b}\frac{A_{S-b}}{A} + \gamma_{M-g}\frac{A_{M-g}}{A} + \gamma_{M-b}\frac{A_{M-b}}{A} \quad (2)$$

where $\gamma_{SM\text{-}gb}$ and $A_{SM\text{-}gb}$ are the interfacial energy and interfacial area, respectively, between the poly(styrene) (S) or poly(methyl methacrylate) (M) blocks with the guiding stripe (g) or backfill brush (b), and A is the total interfacial area. Results shown in Figures 3 and 4 can be explained in terms of Equation 2, where the individual interfacial energies are estimated through known expressions[17] or obtained from experimental results[18] for the materials and processing conditions used in this study. Therefore, $\gamma_{SM\text{-}CP}$ will be a function of the change in the contact area between the components of the system, $A_{SM\text{-}gb}$, as W is varied. In this case, our goal is to use the interfacial energy to predict the behavior of the total free energy of the system and relate it to the experimental conditions that are required to obtain defect free structures. For this purpose, straight profiles of the polymer structures are assumed throughout the entire range of W, so that there is no undulation of the domains or formation of 3-dimensional morphologies due to the preferential wetting of one of the

blocks to the guiding stripe or backfill region[12, 13, 19-21] It also implies that $F_{elastic}$ and F_{A-B} are the same as in the bulk state, therefore, there is no contribution to changes in the total free energy of the system by these terms on Equation 1. Additional parameters, such as the film thickness and BCP formulation, which have been shown to impact the final assembled structures, are excluded from our simple model.[22, 23] Under these assumptions, Figure 6A shows the graphical representation of the interfacial energy of a system comprised by a chemical pattern designed for 3X feature density multiplication and a PS-*b*-PMMA BCP thin film, for $0.1< W/L_0 < 2.0$ and $\gamma_{S-g} = 0$. In addition, Figure 6B shows the increase in free energy, or the penalty that is originated from any misalignment of the lamellae with respect to the center of the guiding stripe and provide insight into the origin of experimental results.

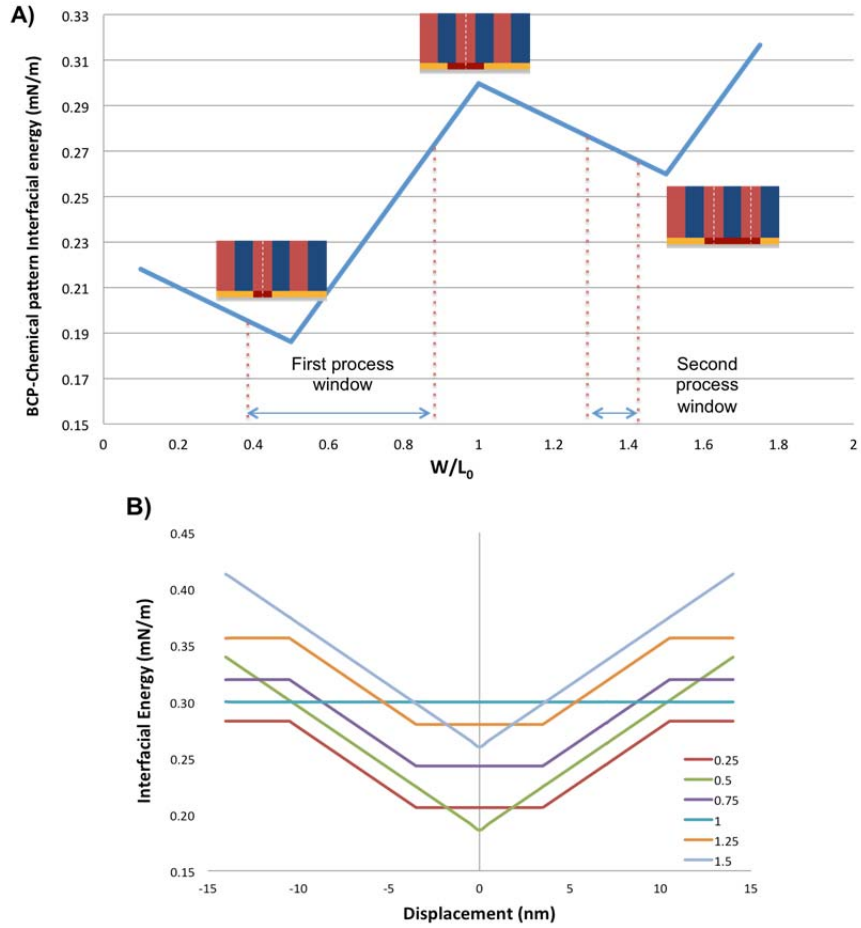

Figure 6. A) Interfacial energy between a PS-b-PMMA BCP and a chemical pattern designed for 3X density multiplication, with cross-linkable polystyrene guiding stripe and a slightly preferential backfill brush. B) Interfacial energies of the system with different displacements (misalignment) of the domains with respect to the center of the guiding stripe, when $W = 0.25, 0.5, 0.75, 1.0, 1.25$ and $1.5L_0$.

Directed self-assembly of block copolymers obtained on fully patterned wafers can be related to the fundamental parameters included in our free energy model by comparing the experimental results to Figure 6. First, the minimum and maximum points of plot 6A show good agreement with the different zones of alignment and random orientation, respectively, shown in Figure 4. The larger process window is around the interfacial energy minimum at W/L_0 =0.5, where perpendicular lamellae are assembled on a chemical pattern with dimensions that avoid unfavorable PMMA-X-PS interactions. This condition will be defined as the perfect or reference state. Although at small values of W/L_0 (<0.5) differences in the interfacial energy with the perfect state are small and good registration with the underlying chemical pattern would be expected, the experiments cannot capture this due to a) the width of the guiding stripe is too small so the BCP is practically assembled on a homogeneous substrate, or b) chemical patterns of high quality cannot be resolved at these dimensions. In the range $0.5< W/L_0 < 0.9$, good alignment of the BCP is captured from top-down SEM images while the interfacial energy, relative to that of the perfect state, is monotonically increasing. Even though multiple conditions were imaged, the inspection technique provides information of small areas and may be insufficient to capture the impact of such increase in free energy in terms of defect density. One critical aspect for the implementation of DSA for high volume manufacturing is to investigate the sensitivity of the system to such differences in free energy as a function of different materials and processing conditions, this is, the combined effect of the system's thermodynamics and kinetic pathways on defect formation. Alternative methods that provide more data statistics at high rate, such as optical inspection, are necessary to determine if the transition between the high degree of order and random orientation is gradual, following the same trend as the interfacial energy, or abrupt, as shown on Figures 3 and 4. Another limitation of the metrology is that it does not provide information of the through film profile. Even though straight lamellar profiles are assumed in our model and imaged with top-down SEM, preferential wetting of the polystyrene block to the guiding stripe may lead to 3-dimensional morphologies, reported previously.[7, 12, 13] The maximum interfacial energy occurs at W/L_0=1.0, which agrees with the random orientation that is observed at this condition for all investigated pitches. Even more, Figure 6B shows that the interfacial energy at this guide width does not change when the structures are misaligned with respect to the center of the guiding stripe. In other words, in addition to the large difference in the interfacial energy when compared to the reference state, there is no penalty for any displacement or configuration of the lamellae; therefore, there will be no driving force for the registration of the domains with the underlying chemical pattern.

Finally, the interfacial energy decreases again when $W > 1.0\ L_0$ and directed assembly is observed experimentally. The position of the second process window shown in Figures 3 and 4 is slightly shifted with respect to the minimum in the interfacial energy at $W/L_0 = 1.5$. This suggests that chemical nanopatterns with large W, cannot be resolved using the scheme used in the present study. Figure 2A shows that the photoresist lines are not well defined when CD >50nm after exposure and that they are also poorly delineated after the trim etch. Although the size of the second process window cannot be defined through experiments, the free energy model indicates that it could be slightly larger. Still, this window has a higher energy minimum than the first window, suggesting that better defect performance will be obtained at small values of W. Again, the potential formation of 3-dimensional structures through the film thickness, particularly in this range of W, should be considered for applications involving pattern transfer.

5.5 Conclusions

In summary, we have shown that the LiNe flow can be used to obtain chemically nanopattened substrates with defined geometry on 300mm wafers and that these substrates can effectively direct the assembly of BCP while increasing the resolution by a factor of 3. The dimensions of the guiding stripe and backfill regions can be finely tuned through the exposure and trim etch steps. Geometric characterization done on the guiding stripe, in addition to the agreement of the observed behavior of the BCP with phenomenological models and theoretical work, indicate that the CD values measured from top-down SEM after the trim etch are similar to the reported values of W. The study of the impact of commensurability on DSA of BCP suggests that the material has more tolerance for compression than stretching. Therefore, control in the BCP formulation is critical to obtain good alignment of the BCP at the annealing conditions relevant for industrial processing. The impact of W on DSA of BCP was investigated experimentally and through a simple phenomenological model on chemical patterns with $0.4 < W/L_0 < 1.5$. Two process windows where the BCP presented a high degree of perfection were obtained, which correspond to the two minima of the interfacial energy between the BCP and the chemical pattern. Overall, the results suggest that the interfacial energy model with perpendicular structures throughout the film effectively captures the impact of the properties of the chemical patterns on the total free energy of the system and, therefore, on BCP assembly. This model can be further utilized as a guideline to optimize materials and processing conditions required to achieve zero defects in times amenable for high volume manufacture.

5.6 References

1. Bates, F.S. and G.H. Fredrickson, *Block copolymers - Designer soft materials.* Physics Today, 1999. **52**(2): p. 32-38.
2. I. T. R. f. Semiconductors, q.L., " ed, 2009, *Lithography*. 2009.
3. Chi-Chun, L., et al., *Integration of block copolymer directed assembly with 193 immersion lithography.* Journal of Vacuum Science & Technology B (Microelectronics and Nanometer Structures), 2010. **28**(6).
4. Cheng, J.Y., et al., *Simple and Versatile Methods To Integrate Directed Self-Assembly with Optical Lithography Using a Polarity-Switched Photoresist.* Acs Nano, 2010. **4**(8): p. 4815-4823.
5. Bencher, C., et al., *Self-Assembly Patterning for sub-15nm Half-Pitch: A Transition from Lab to Fab*. 2011, Proceedings of SPIE.
6. Stoykovich, M.P., et al., *Remediation of Line Edge Roughness in Chemical Nanopatterns by the Directed Assembly of Overlying Block Copolymer Films.* Macromolecules, 2010. **43**(5): p. 2334-2342.
7. Ruiz, R., et al., *Density multiplication and improved lithography by directed block copolymer assembly.* Science, 2008. **321**(5891): p. 936-939.
8. Rincon Delgadillo, P.A., et al., *Implementation of a chemo-epitaxy flow for directed self-assembly on 300mm wafer processing equipment*. 2012, Journal of Micro/Nanolithography, MEMS, and MOEMS. p. 031302-1:031302-5.
9. Kim, S.O., et al., *Defect structure in thin films of a lamellar block copolymer self-assembled on neutral homogeneous and chemically nanopatterned surfaces.* Macromolecules, 2006. **39**(16): p. 5466-5470.
10. Edwards, E.W., et al., *Precise control over molecular dimensions of block-copolymer domains using the interfacial energy of chemically nanopatterned substrates.* Advanced Materials, 2004. **16**(15): p. 1315-+.
11. Edwards, E.W., et al., *Mechanism and kinetics of ordering in diblock copolymer thin films on chemically nanopatterned substrates.* Journal of Polymer Science Part B-Polymer Physics, 2005. **43**(23): p. 3444-3459.
12. Detcheverry, F.A., et al., *Interpolation in the Directed Assembly of Block Copolymers on Nanopatterned Substrates: Simulation and Experiments.* Macromolecules, 2010. **43**(7): p. 3446-3454.
13. Liu, C.-C. and A. Ramirez-Hernandez, *Chemical Patterns for Directed Self-Assembly of Lamellae-Forming Block Copolymers with Density Multiplication of Features*, E. Han, et al., Editors. 2013: Macromolecules. p. 1415-1424.
14. Liu, C.-C., et al., *Fabrication of Lithographically Defined Chemically Patterned Polymer Brushes and Mats.* Macromolecules, 2011. **44**(7): p. 1876-1885.
15. Liu, G.L., et al., *Cross-sectional Imaging of Block Copolymer Thin Films on Chemically Patterned Surfaces.* Journal of Photopolymer Science and Technology, 2010. **23**(2): p. 149-154.
16. Liu, G.L., et al., *Nonbulk Complex Structures in Thin Films of Symmetric Block Copolymers on Chemically Nanopatterned Surfaces.* Macromolecules, 2012. **45**(9): p. 3986-3992.

17. Wu, S., *Polymer interface and adhesion*. 1982, New York: M. Dekker. xiii, 630 p.

18. Mansky, P., et al., *Controlling polymer-surface interactions with random copolymer brushes.* Science, 1997. **275**(5305): p. 1458-1460.

19. Wang, Q., et al., *Symmetric diblock copolymer thin films confined between homogeneous and patterned surfaces: Simulations and theory.* Journal of Chemical Physics, 2000. **112**(22): p. 9996-10010.

20. Pereira, G.G. and D.R.M. Williams, *Lamellar interface distortions of thin, commensurately aligned diblock copolymer films on patterned surfaces.* Langmuir, 1999. **15**(6): p. 2125-2129.

21. Pereira, G.G. and D.R.M. Williams, *Thin films of perpendicularly oriented diblock copolymers: Lamellar distortions driven by surface-diblock interfacial tensions.* Macromolecules, 1999. **32**(5): p. 1661-1664.

22. Suh, H.S., et al., *Thickness Dependence of Neutral Parameter Windows for Perpendicularly Oriented Block Copolymer Thin Films.* Macromolecules, 2010. **43**(10): p. 4744-4751.

23. Delgadillo, P.A.R., et al., *Geometric Control of Chemically Nano-patterned Substrates for Feature Multiplication Using Directed Self-Assembly of Block Copolymers.* Journal of Photopolymer Science and Technology, 2012. **25**(1): p. 77-81.

Chapter 6

Combinatorial Effect of Composition and Dimensions of Chemically Nanopatterned Substrates on Directed Self-Assembly of Block Copolymers

6.1 Abstract

Directed Self Assembly (DSA) using block copolymers (BCP) has received considerable attention over the past few years as a potential complementary lithographic technique. The goal of this work is to understand the fundamentals of the block copolymer assembly through the interactions of the block copolymer with the underlying chemical pattern, and the evaluation of process parameters to obtain a high degree of order of the BCP morphologies. Using the flow proposed by Liu and Nealey (LiNe), implemented at imec, substrate properties, such as the geometry and chemistry, were studied and provided the first results regarding the dimensions of the nanopatterns and the energetic conditions necessary to obtain good alignment of the BCP. Characterization of the wetting properties of the X-PS guiding stripe indicated that it loses some of is strength throughout the process. Also, it was shown that for a 3X density multiplication factor, the best composition of the backfill brush is 51%PS-*r*-49%PMMA, based on both process windows, line width roughness, and line edge roughness data. With this approach, the definition of an optimized process window and materials for defect minimization can be established.

6.2 Introduction

Directed self-assembly (DSA) of block copolymers (BCP) using chemically nanopatterned substrates for lithographic applications has undergone a transition from the laboratory scale to the fab due to the increased interest of the semi-conductor and hard disk industry to assess this technology for high volume manufacturing (HVM), especially going towards the 16nm node and below.[1-3] In addition to the advantages inherent to this technique, such as improvements in line width roughness (LWR) [4], line edge roughness (LER) [5, 6] and

critical dimension (CD) control, the potential insertion of DSA of BCP to production is also driven by the enhanced resolution, reduced cost, and high throughput that this technique offers over alternative patterning methods.[7, 8] However, one of the primary remaining challenges for the implementation of block copolymer lithography in HVM is to meet the defect levels posed by the industry.

Self-assembly of BCP thin films on chemically nano-paterned substrates is an effective method to control the substrate interface as a means to obtain dense arrays of ordered structures with a high degree of perfection.[9-12] This method relies on the generation of alternating stripes of different surface energies and the preferential wetting of the blocks to each stripe. Mansky *et. al.* and others have demonstrated that the composition of random copolymers (usually of the same monomer units as the BCP system to be used) can be varied to tune the surface energies in a precise manner and can be applied on different surfaces in the form of brushes or mats, via chemical reaction or coating/annealing, respectively.[13, 14] In the case of hydroxyl terminated poly(styrene-*random*-methyl methacrylate) copolymers (P(S-*r*-MMA)-OH), the composition in which the interfacial energy between the brush and the domains of a lamellae forming P(S-*block*-MMA) BCP is roughly the same, corresponds to about 58-60%PS (40-42%PMMA). This non-preferential character of the substrate provides the energetic conditions that result in perpendicular assembly of the polymer domains through the film thickness.[15, 16] When incorporated into chemical patterns, the role of these materials remains the same, but in this case, a guiding stripe directs the features to form ordered structures. The composition of the random copolymers dictates the strength of the BCP-substrate interaction and, therefore, the registration of the polymer domains to the brush regions. Edwards *et. al.* used a series of brushes with 50%-100% polystyrene (PS) content to fabricate chemical patterns where the pre-patterned pitch (L_s) was roughly equal to the natural periodicity of the BCP (L_0).[10] In this regime, the strongest interaction of the PS block with the brush (100%PS) resulted in the minimum defect formation. The assembly process was described in terms of the composition and dimensions of the chemical patterns through a simple model of the energy provided at the substrate interface to guide the BCP structures. More recently, Liu and Nealey (LiNe) developed a chemo-epitaxy scheme to multiply the feature density with DSA of BCP.[17] In this work, L_s was an integer multiple of L_0 (L_s= n L_0). It was found that a backfill region with a slightly off-neutral surface energy was beneficial to reduce defect formation. A detailed analysis of the energetic conditions to achieve a high degree of order was presented as a function of the composition of the nanopatterns for different density

multiplication factors.[18] Fundamental understanding of the parameters that govern DSA of BCP has led to the definition of the boundary conditions required for defect minimization in times that are amenable for industrial processing.

The implementation of the LiNe flow on 300mm wafers have proven to be an excellent method to evaluate the impact of materials and processing conditions on the assembly process over large areas. The fabrication and inspection of patterned samples using automatic tools has allowed for the investigation of a vast parameter space on a single sample. On the one hand, the use of mats and brushes provides areas with specific surface energies to control the orientation and direction of the BCP morphologies. On the other hand, the precise processing achieved by industrial equipment results in a well-defined substrate that will interact with the BCP in a desired manner. With this set-up the simultaneous effect of the chemistry and geometry of chemical patterns on DSA of BCP using feature density multiplication can be investigated on a wafer-scale.

In this work, we report on the impact of different materials and processing conditions on DSA of BCP. More specifically, for substrate preparation, controlled chemistries of the backfill brush were explored for a feature multiplication factor of 3X using a BCP with a periodicity (L_0) of 28nm. Different process windows provided an insight of the optimal geometric and chemical properties of the chemical nanopatterns that are required to minimize defect formation. In summary, our work is aimed to relate process and material conditions to thermodynamic parameters that will provide fundamental information to achieve low defect levels in an effective and controlled manner.

6.3 Experimental

6.3.1 Materials

Cross-linkable poly(styrene) (X-PS) (AZEMBLY^{TM} NLD128), AZEMBLY^{TM} series of hydroxyl-terminated (P(S-*r*-MMA)-OH) brushes of controlled compositions, which are shown in Table 1, and PS-*b*-PMMA, (AZEMLBY^{TM} PME312) BCP with L_0 = 28nm, were synthesized by AZ Electronic Materials and used as received. Photoresist AIM5484 from JSR Micro was used. Organic solvents RER600 and Orgasolv STR 301 were purchased from Fujifilm and BASF, respectively, and used as received.

Table 1. Composition of the hydroxyl terminated random co-poly(styrene-methyl methacrylate) brushes grafted to the backfill region of the chemically nanopatterned substrates.

Brush	PS fraction
Brush-44	44%
Brush-46	46%
Brush-51	51%
Brush-56	56%
Brush-60	60%
Brush-63	63%
Brush-69	69%

6.3.2. Process

The implementation of the LiNe flow for the fabrication of chemically nanopatterned substrates was described in Chapters 2 and 3.[3] All the coating and annealing steps were done on a TEL CLEAN TRACK ACT™12 system. Briefly, an inorganic antireflective coating (ARC) film of SiN, of 14nm, was deposited via chemical vapor deposition (CVD) on 300mm Si wafers. An X-PS film, with thickness of 7-8nm, was spun and annealed for 5min at 315°C in N_2 environment using a TEL CLEAN TRACK ACT™12. All the coating and annealing steps were done in this system as well. Photoresist was coated and exposed on an ASML NXT:1950 scanner at 1.35NA using dipole40X illumination (XY polarization, σ_o=0.87, σ_i=0.72). The reticle used in this study includes different structures of interest, such as a series of pitches (80-89nm in 1nm steps) and critical dimensions (CD) per pitch. It also contains a large inspection block (7.5x5mm) of 84nm line/space patterns. After exposure and development, an O_2 and Cl_2 plasma etch step was used to trim the resist and remove the X-PS exposed to the plasma. This is followed by a wet resist strip at room temperature using Orgasolv STR 301 to remove the remaining photoresist from the patterned X-PS material. The P(S-*r*-MMA)-OH brushes were spun to obtain an initial thickness of ~50nm and annealed for 5min at 250°C in N_2 environment. The material that did not react with the substrate was removed by rinsing the sample with RER600. The PS-*b*-PMMA BCP was coated on the chemical patterns and annealed with the same process conditions used for deposition of the random brush. In all cases, after BCP assembly, the

poly(methyl methacrylate) (PMMA) block was removed using a dry etch process on a TEL Tactras^{TM} system to facilitate the imaging and analysis.

6.3.3 Characterization

Characterization of the materials comprising the chemical nano-patterns included static water contact angle to assess the wetting properties of the X-PS and the different backfill brushes, shown on Table 1, at different steps of the process. A Dataphysics OCAH230L contact angle measurement system was used for this purpose. In addition, ellipsometry measurements were performed using a KLA Tencor SCD100, on uniform mat and brush films deposited on (or grafted to) bare silicon wafers over 49 points across the diameter to determine thickness and uniformity.

The impact of the dimensions of the chemical patterns on BCP assembly was investigated for each brush composition. A Hitachi CG4000 scanning electron microscope (SEM) was used to image the photoresist after trim etch (and subsequent online CD measurement) and the BCP assembled structures after PMMA removal. Pre-pattern pitches ranging from 80nm to 89nm (with 1nm increments, 10 pitches in total) and 8 CD conditions per pitch were available from the reticle design. In order to collect information on a larger number of conditions, 5 different dose steps at the nominal focus were analyzed. In short, for each brush composition 8*5 = 40 guide width cases are studied at 10 pitches, resulting in a total of 400 geometry cases for each brush. Images at relatively low magnification (2.5x2.5 μm^2) were taken for this purpose. The magnification was selected to be as small as possible in order to evaluate the degree of perfection of the assembled BCP structures over a large field of view, but sufficiently large to identify defects. BCP assembly over large areas was studied on the 84nm pitch inspection blocks, which were imaged at ten locations using low magnification SEM.

6.4 Results and discussion

6.4.1 Guiding stripe

A primary characteristic of the LiNe flow is its ability to control the chemistry (and thus the interfacial energies) and the geometry through the materials and the processing conditions, respectively. The first polymer film that is coated on the substrate is the X-PS, which undergoes multiple processing steps, such as the exposure, trim etch, strip, and brush deposition. Therefore, the process impact on the chemical character of the material must be

assessed, since the latter dictates the strength of interaction of the guiding stripe with the BCP and, potentially, the probability to generate defects. Due to the dimensions of the X-PS guiding stripe and the lack of a technique to perform direct evaluation of its wetting properties, checkerboard patterns were processed in the same way as the chemical nanopatterns (except for the exposure conditions optimized for the checkerboards). These samples consist of large exposed and unexposed regions (about 3 x 3 mm), which allow performing water contact angle measurements on both regions. The checkerboards were characterized after X-PS coat and anneal, strip and brush grafting. Figure 1 shows the water contact angle data for a blanket X-PS film, as well as for the unexposed and exposed areas on the checkerboard patterns that were processed until brush grafting. A 0° angle was obtained on the exposed region after trim etch and strip.

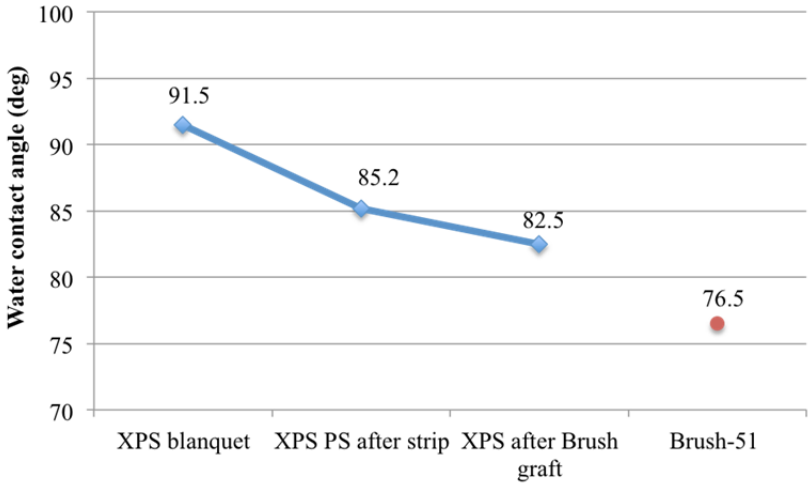

Figure 1. Water contact angle measurements of an X-PS film as coated and annealed, after resist strip, and after brush grafting , show the change in the properties of the X-PS through the different processing steps of the process. The standard backfill material, OH-(51%PS-r-49%PMMA) is shown as reference.

The X-PS film becomes more hydrophilic through each of the processing steps. In order to find the cause of the first WCA drop, the interaction of the X-PS with the Orgasolv STR 301 was investigated. A film of the polymer was coated and rinsed with the solvent. However, in the absence of a photoresist layer, Orgasolv STR at room temperature did not wet the substrate. Another possible cause is an incomplete removal of the photoresist with the available stripping chemistry, Orgasolv STR 301. During the trim etch, the Cl_2 reacts with the photoresist and forms an outer layer that protects the structures from the O_2 chemical attack.[19, 20] These byproducts, while necessary to control the etching rate of the photoresist, become difficult to remove with the standard organic solvent or

commercially available strippers (data not shown). For the present combination of photoresist and trim etch conditions, only Orgasolv STR 301 was able to remove enough material so that at the end of the process, good registration of the BCP structures with the underlying chemical pattern was observed.[3] Another explanation for the partial loss of X-PS hydrophobic character may be material modification during the plasma etch step due to diffusion of O_2 species (ions, radicals) through the photoresist. However, differentiating between the two possible mechanisms is difficult to assess experimentally. Optimization of the trim etch step is currently being investigated as a means to retain the hydrophobic character of the X-PS and increase the strength of the interaction between the guiding stripe and the poly(styrene) block assembled on it.

The second drop in WCA after the P(S-*r*-MMA)-OH coat and anneal suggests that there is partial grafting of the brush molecules to the guiding stripes. This may also be related to the incomplete removal of the photoresist or modification of the X-PS with oxygen-containing groups, which can further react with the hydroxyl end group of the random copolymer. Figure 1 shows that at the end of the process, the X-PS has a WCA of 82.5. Although the total drop of nine degrees in the contact angle does not provide enough information about the change in the material's surface energy, it indicates that the X-PS guiding stripe has lost some of its non-polar original character and a weaker interaction with the PS block is expected. Previous reports using the LiNe flow, as it is described in this study, show assembly of the BCP with a high degree of perfection [3], suggesting that the difference in interfacial energy between the X-PS and the polystyrene blocks is large enough to guide the BCP structures. Therefore, for the present work, the process described previously will remain unchanged and the difference in the surface energy of the modified guiding stripes with respect to pure X-PS lines will be considered for the analysis of the results on fully patterned samples.

6.4.2 Backfill region

The film thickness of the series of (P(S-*r*-MMA)-OH) random brushes, used to backfill the areas between the guiding stripes, was characterized using ellipsometry, which provide information about the relative grafting density and chain length of the brush molecules. Independent experiments by varying anneal time and temperature have demonstrated that the film of the standard brush-51 saturates at ~7nm at long bake times.[3, 21] This average film thickness is therefore assumed to correspond to a dense brush monolayer. Figure 2 shows a significant difference in the film thickness between the investigated brushes, for the same initial film thickness and annealing conditions. Brush-51 has the smallest film

thickness of 5.2nm, while brush-60 present the largest thickness. This difference suggests that not only the composition, but also the molecular weight, and therefore, chain length, vary between the samples of the brush series. Although more information about the materials is not available, potential differences in the topography of the chemical patterns could have an impact on the final BCP assembly. This topic is currently being investigated using molecular simulations.

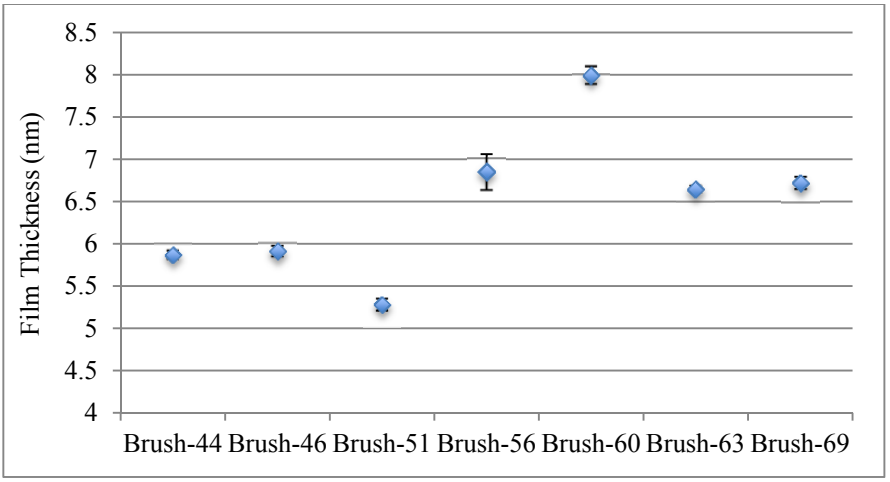

Figure 2. Monolayer film thickness after rinse of series of brushes of different compositions, as determined by ellipsometry measurements. The final film thickness of the brushes provides information on the properties of the materials, such as molecular weight.

The current characterization of brush-51 corresponds to the standard material installed in the track, which was the newest sample available with 51%PS content. Comparison with the small volume sample used for the implementation of the LiNe flow, processed manually, showed good agreement with the gallon size material. Therefore, the difference with the previously reported film thickness cannot be attributed to variations in the properties of the brush. A possible cause may lie in the characteristics of the silicon wafers. Before use, the silicon wafers are cleaned using hydrofluoric acid (HF). After this step, a native oxide film forms on the surface, which will serve to react with the hydroxyl functional end-group of the copolymer molecules. Differences in the available reactive sites due to exposure time to the environment or to residues on the substrate will result in variations in the brush grafting densities, which will be reflected in the final monolayer thickness. However, when the brushes are deposited and grafted to the chemical patterns, such differences will not occur since the substrate is submitted to an O_2 plasma etch which 'pre-conditions' the samples for further reaction with the.

Static WCA was used to compare the wetting properties of the brushes of different compositions, which provide information about the behavior of the surface energy as a function of the monomer ratio. Measurements were taken on 7-13 points on the wafer sample. As shown in Figure 2, the series of brushes present a linear increase in WCA as a function of the PS content, with values that are in agreement with previous reports.[16] For the current study, in which these materials were incorporated to chemical patterns, which are comprised of an X-PS guiding stripe, slightly PMMA preferential brushes are of interest. Using the model proposed by Liu *et. al*. [18], for a 3X density multiplication factor, a PS fraction of 0.42 will provide the minimum interfacial energy between the chemical pattern and the BCP. However, experimental results show that a higher PS content in the backfill brush is necessary to achieve a high degree of perfection of the assembled morphologies, for the same BCP annealing conditions used in this study. Therefore, the available brushes not only comprehend the range of compositions of interest (from neutral to slightly off-neutral), but also present the wetting behavior expected from these materials.

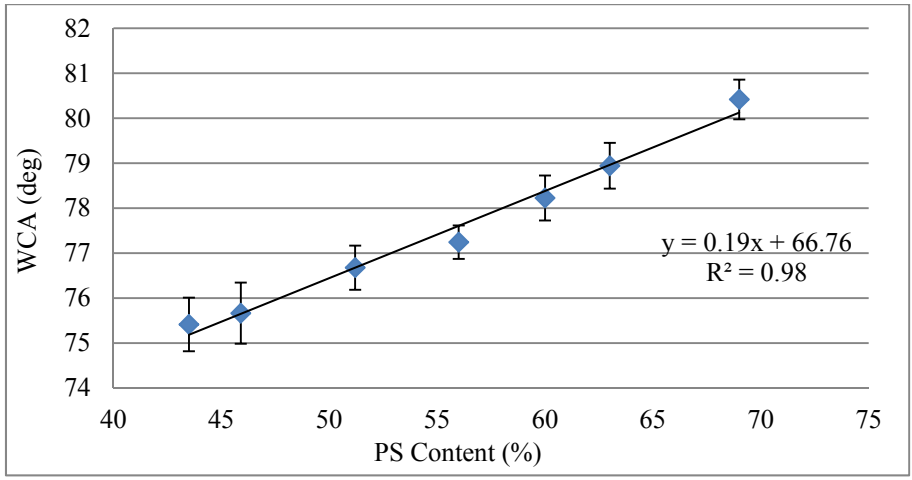

Figure 3. Water contact angle of a dense monolayer the (P(S-r-MMA)-OH) brush series grafted to silicon wafers. The linear dependence on PS content shows provides information on the behavior of the surface energy as a function of substrate composition.

Finally, the impact of brush composition on the orientation of the BCP domains, assembled on homogeneous substrates, was investigated using top-down SEM images. A 32nm BCP film was coated and annealed on the different brushes grafted to blanket wafers. As shown on Figure 4, when the BCP was annealed using standard conditions (250°C, 5min) all the samples showed randomly oriented structures, referred to as fingerprint patterns, which also suggest perpendicular structures throughout the film thickness. However, when a lower

temperature was used during BCP anneal (220°C, 20min) mixed orientation can be observed as the PS content in the brush decreases and the substrate becomes slightly preferential. At the lowest end, brush-44 showed hole and island structures characteristic of preferential substrates. In contrast, the higher PS content in the brush materials (69%PS), did not induce mixed or parallel orientation of the polymer domains. Mansky et. al. and Han et. al. tuned the interfacial energy between a BCP film with the substrate and the free surface simultaneously by the use of random brushes and by varying the annealing temperature, respectively.[22, 23] While PS has a lower surface energy than PMMA at low temperatures commonly reported for BCP annealing (160-190°C) [13, 16], the latter decreases more rapidly as temperature increases. At the standard annealing temperature used in the present study (250°C), the surface energies of the two blocks are practically equal and the free surface is neutral towards the two blocks.[24] The final orientation of the BCP domains will be determined by the tendency of the system to be in equilibrium with the boundaries. As the boundary condition at the free surface is modified from 220°C to 250°C, Figure 4 suggests that also the neutrality window changed. Finally, Han et. al. showed that for thick films of cylindrical forming BCP annealed at high temperature (230°C), even though perpendicular structures could be observed at the free surface, parallel cylinders were assembled near a slightly non-preferential substrate. In the current work, top-down SEM images do not provide information of the through-film profile of the BCP domains. Although the film thickness just above L_0, formation of 3-dimensional structures may occur on the low PS content samples due to the slightly preferential character of the surface.

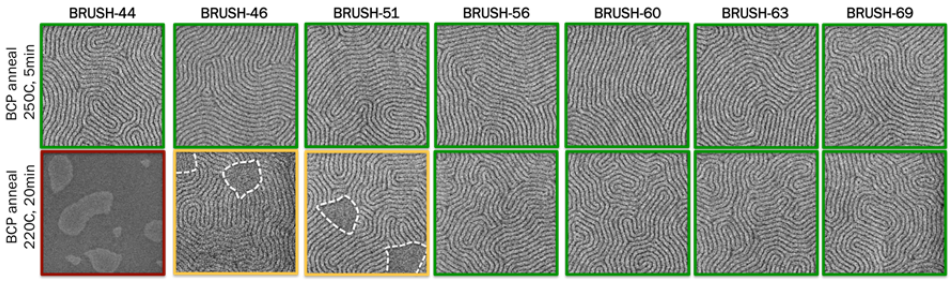

Figure 4. Top-down SEM images of a P(S-*b*-MMA) films annealed at 250°C and 220°C on random brushes of different compositions grafted to blanket silicon wafers. The green squares indicate the conditions in which perpendicular BCP domains are observed. Yellow and red frames indicate mixed orientation and hole and island (terraces), respectively.

6.4.3 Chemically nanopatterned substrates

Fabrication of chemically nanopatterned substrates using the LiNe flow is shown in figure 5. Fine-tuning of the chemistry is achieved by the cross-linkable properties of the guiding stripe, which, in principle, will prevent the interpenetration of any brush molecules during the coat and anneal of this material. In addition, the surface energy of the backfill region is controlled instep e) of Figure 5, by utilizing OH-terminated brushes of specific composition. One important aspect of this scheme is that the brush will not be submitted to any subsequent processes or materials; therefore, its chemical properties will remain unaltered for a controlled interaction with the BCP during assembly.

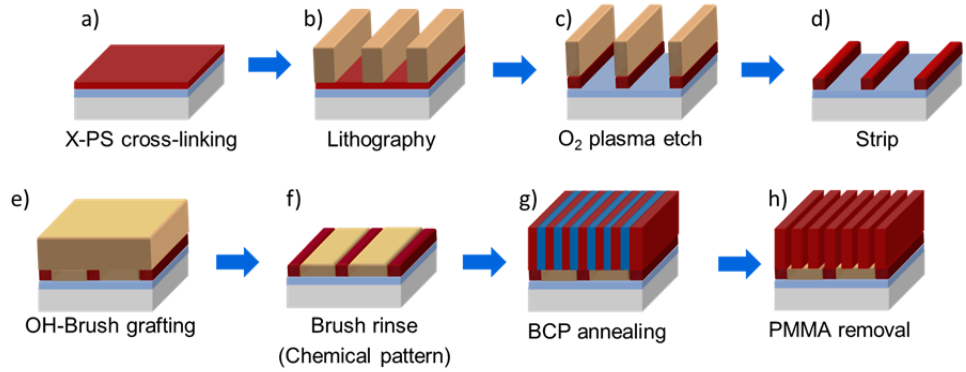

Figure 5. Liu-Nealey (LiNe) flow for the fabrication of chemically nanopatterned substrates with well-defined geometry and chemistry, and subsequent DSA of a symmetric BCP.

In this work, the response of the BCP to commensurability (L_s/L_0) and the width of the guiding stripe (W) was investigated by using a similar approach to the one described previously, in which the CD of the photoresist after the trim etch is assumed to be equivalent to W.[25] In addition, the interaction between the backfill region and the BCP ($\gamma_{SM\text{-}gb}$) was also included in the analysis by using brushes of different compositions. The degree of order of the BCP structures for each L_s, W, and $\gamma_{SM\text{-}gb}$ combination was evaluated by assigning a score to the degree of alignment, from 0 to 3 corresponding to random orientation to a high degree of order, respectively. The score was determined from top-down SEM images of 2.5x2.5μm^2 areas (1x1μm^2 are shown on Figure 6 to exemplify the scoring system). Figure 6 shows the process windows for the different brushes. For the standard backfill material, brush-51, the reproducibility of the results with previous work is remarkable. The best assembly of the BCP occurs at the target pitch of 84nm for 3X feature density multiplication factor using a 28nm BCP. In addition, the ability of the BCP to accommodate to different pitches in the range of 81nm < L_s < 86nm, with slightly higher

tolerance for compression rather than stretching was confirmed. In terms of W, two process windows are obtained. The largest window is observed at small values of the width of the guiding stripe in a range of 12.4-27.0 nm and a smaller one at 36-40nm. Similar trends are observed on the chemical patterns with low PS content in the background (44 and 46%PS). However, for these samples, the size of the second window at large W values varies significantly with each brush material. In the case of brush-44, a score of 3 is only observed when L_s = 83-84 nm and W of about 37nm. A slightly larger window can be observed as the PS content increases to 46%, in which the range of W with good alignment of the BCP increases by less than one nanometer at L_s = 83nm. The standard material, brush-51 showed the largest window around W=1.3L_0, as shown on Figure 6. Significant decrease in the number of L_s-W combinations with good alignment occurs when the PS content in the random brushes is larger than 51%. An increase in the PS content at brush-56 shows a significant impact on the size of the two process windows. This effect is magnified as the PS content increases to 60 and 63%, where only partially aligned structures were captured from top-down SEM images. The PS content in brush-69 is too high when compared to the optimal range; therefore, it was not used in this set of experiments. One thing to note is that the 60%PS brush did not present any conditions with perfect alignment, while the 63%PS material presented slightly better scores, including one image with a score of 3, around L_s = 83nm and W = 22nm.

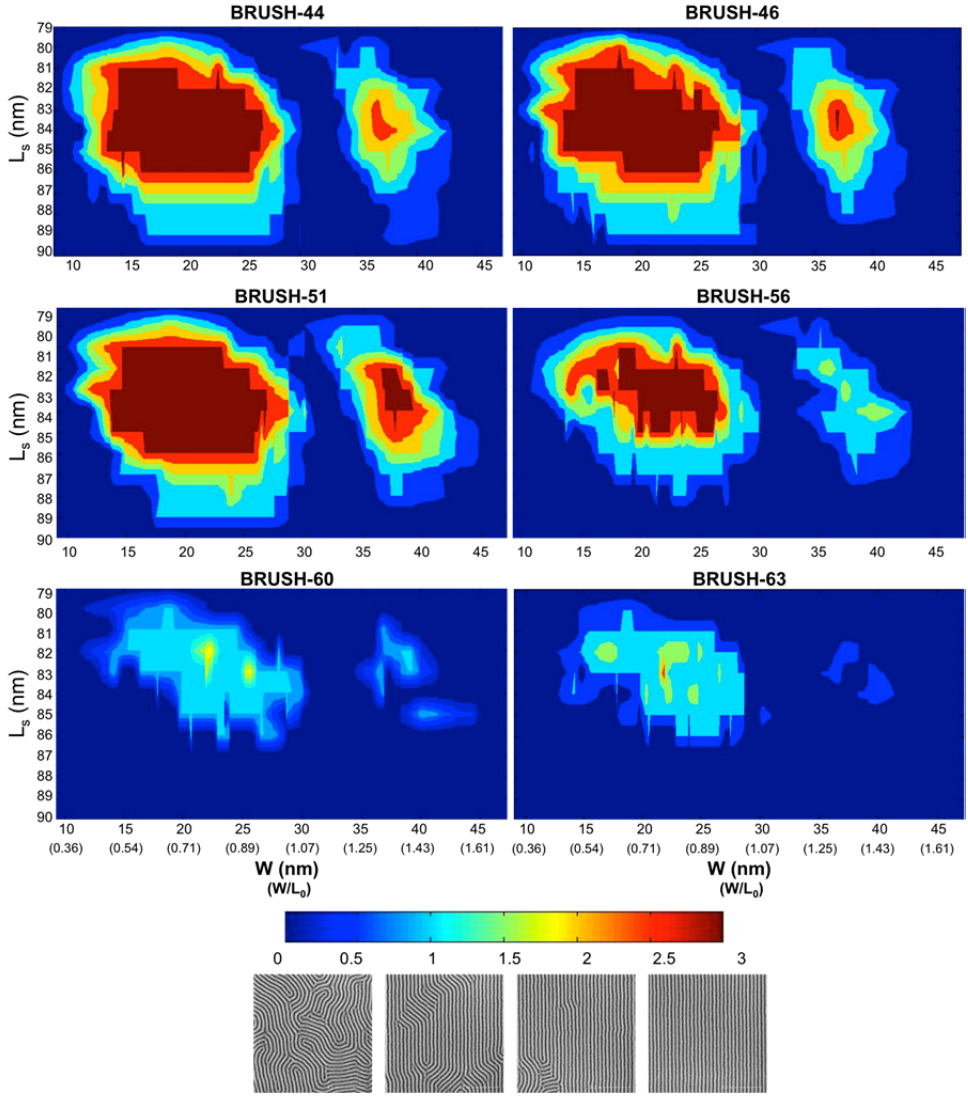

Figure 6. BCP assembly as a function of commensurability (L_s/L_0) and width of the guiding stripe (W) for various compositions of the backfill brush. The color code used to evaluate the degree of perfection of the assembled structures is based on a 0-3 score system corresponding to random orientation to good alignment, respectively, as shown by top-down SEM images.

In order to obtain information required to perform statistical analysis, the 84nm inspections blocks, included from the reticle desing, were imaged using top-down SEM at ten different locations on each exposure condition. A total area of 62.5 um^2 per die was imaged and used to evaluate the defect level through the wafer. The number of defect-free images is reported as a measure of the degree of order (out of the 10 that were collected for each condition). This method does not differentiate between random orientation and a single dislocation,

still, the transitions from disordered to ordered states can be captured, which has been used to corroborate the information obtained from Figure 6. Figure 7 shows the results for 10 dose steps, where 12.6< W <35.6nm at nominal focus for 6 brushes (full wafer maps can be found in ref. [26]). Starting with the low PS content brushes (43.5-51%), which showed similar behavior at small values of W, good registration with the chemical nanopatterns is represented by the green squares. In addition, analysis of the 10 images show that at for W≤27.3nm a similar number of defects is obtained. The defective images at W= 14.8 and 17.2 nm correspond to the locations closer to the edge of the inspections block, where it is known that W is smaller due to a non-uniform trim-etch through the patterned area. The BCP shows similar sensitivity to variations in the properties of the chemical patterns. One thing to note is that, when the second process window is analyzed, the material that resulted in the largest number of defect free images was brush-51, suggesting that this brush is optimal for a 3X feature density multiplication factor for a larger range of W values. The information collected for large PS content random copolymers (>56%PS) shows a drastic reduction of the process windows, in agreement with Figure 6. Brush-63 presents better alignment of the BCP than brush-60 when W=25-27nm. This result suggests that there is an additional mechanism for the ordering of the BCP, such as the topography generated by the height difference between the guiding stripe and the backfill region of about one nanometer (X-PS thickness of 7.2nm), which is present in brush-63, but not in brush-60. Further investigation of the impact of this parameter on DSA of BCP is necessary to define the specifications for the materials comprising the chemical patterns.

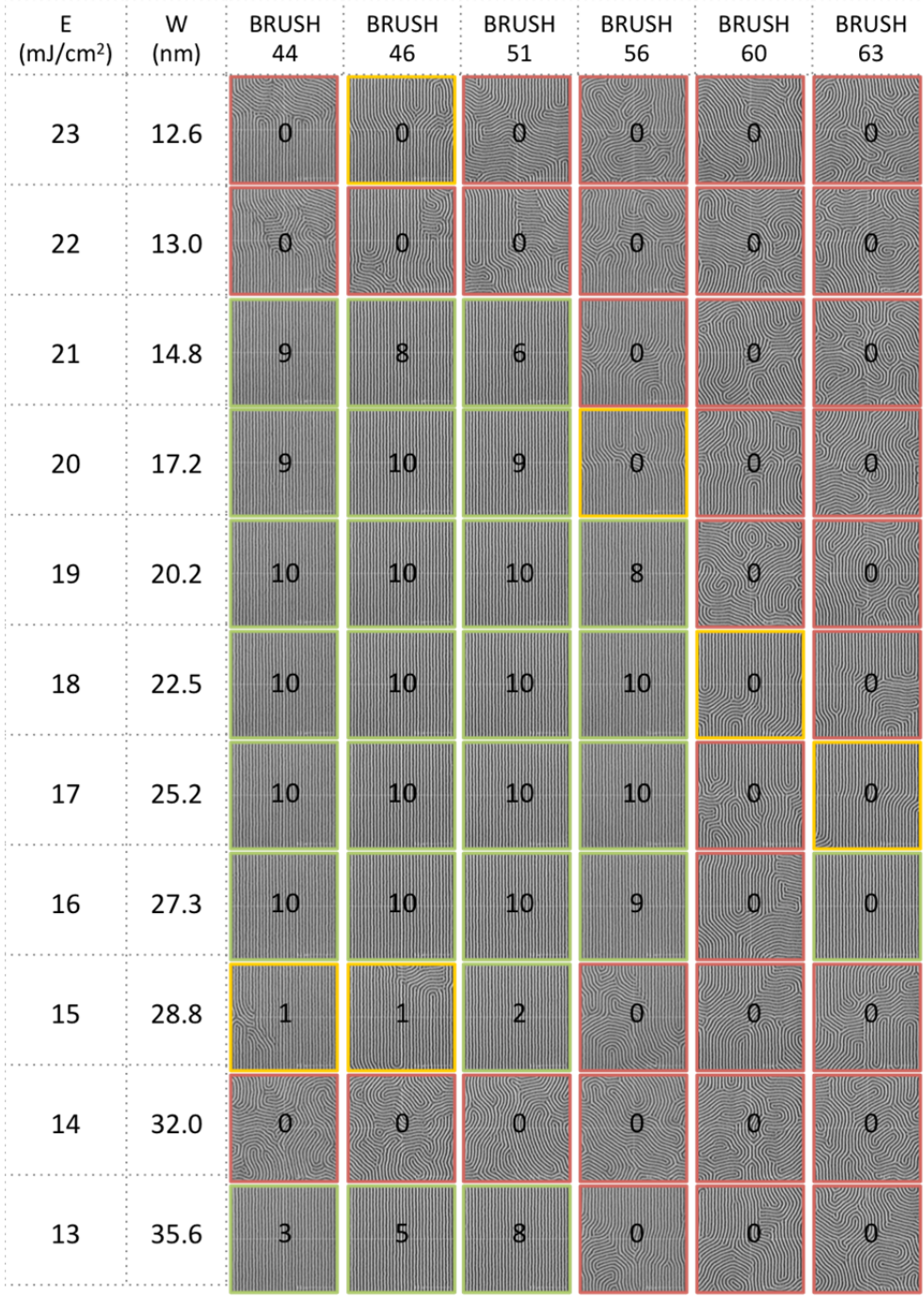

Figure 7. Top-down SEM images of the BCP assembled on chemical patterns of different *W* and composition. The numbers on each die show the number of defect-free images (out of 10).

In the previous chapter, a thorough derivation of the total free energy of the system was presented, where four main contributors related to the bulk properties and the boundaries

were identified. In addition, it was determined that for the PS-b-PMMA system, minimization of the substrate-BCP interfacial energy is the most effective way to find the minimum in the total free energy, and therefore, reduce the probability to generate defects. The interfacial energy between the BCP and the chemical nanopattern is given by the following expression:

$$\gamma_{BCP-CP} = \gamma_{S-g}\frac{A_{S-g}}{A} + \gamma_{S-b}\frac{A_{S-b}}{A} + \gamma_{M-g}\frac{A_{M-g}}{A} + \gamma_{M-b}\frac{A_{M-b}}{A} \quad (1)$$

where $\gamma_{SM\text{-}gb}$ and $A_{SM\text{-}gb}$ are the interfacial energy and interfacial area, respectively, between the poly(styrene) (S) or poly(methyl methacrylate) (M) blocks with the guiding stripe (g) or backfill brush (b), and A is the total interfacial area. The interfacial energies can be obtained from known expressions or experimental reports and the area will depend on the geometry of the chemical patterns. Figure 8, shows the difference in the interfacial energy as a function of *W* (normalized to L_0 and at constant L_s=84nm) for the different brushes, with respect to a reference state, which was defined as the condition of minimum free energy from the previous chapter (L_s= 84nm, $W = 0.5L_0$, 51%PS content in the backfill material). Three main assumptions were made for the calculation of the interfacial energy described by Equation 1. First, straight perpendicular BCP domains were hypothesized to be formed through the film thickness at all the conditions of *W,* as shown on the schematics on Figure 8 for $W/L_0 = 0.5$, 1.0, and 1.5. In this way, not only the interface is defined in a simple way, but also other contributions to the free energy, such as block-block interfacial curvature, or stretching or compression of the chains, can be excluded from the calculations. This assumption may be accurate for the chemical patterns fabricated with the current set-up of the LiNe flow, since the guiding stripe has lost part of its preferential character. This results in a weaker interaction with the polymer blocks (both favorable and unfavorable), which may be advantageous as it reduces the formation of 3-dimensional morphologies, especially at large values of *W*. Second, the position of the blocks with respect to the guiding stripe was selected to maximize favorable PS-X-PS contacts (as opposed to PMMA-X-PS). This means that a PS domain is assembled exactly on the center of the guiding stripe for $0.1 \leq W/L_0 \leq 1.0$, while for $W/L_0 \geq 1.0$, a PMMA is centered to the guiding stripe, allowing for two PS blocks to assemble simultaneously on the guiding region. Finally, based on the characterization of the wetting properties of the guiding stripe and the lack of a direct method to measure its surface energy, the X-PS was assumed to behave as a random brush. The WCA measurement was used to assign a composition of about 81%PS in the guiding material. This way, it was possible to use the harmonic

equation to obtain the interfacial energy between the modified guiding stripe and the PS and PMMA blocks.[24]

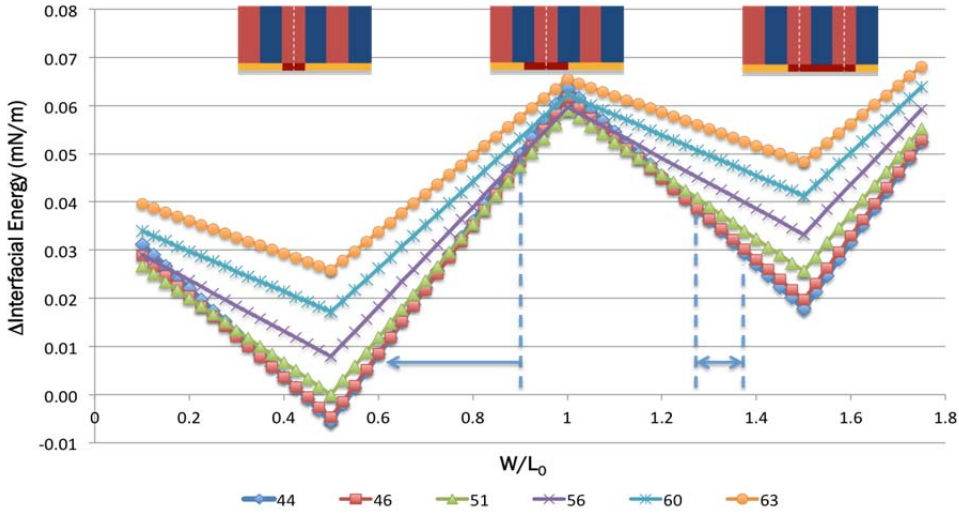

Figure 8. Difference in interfacial energy between a PS-b-PMMA BCP assembled on a chemical pattern with the reference condition (L_s= 84nm, W = 0.5L0, 51%PS content in the backfill material) and PS-*b*-PMMA BCP assembled on chemical patterns of different geometry and chemistry

Analysis of Figure 8 shows that the difference in the interfacial energy with respect to the reference point is closely related to the size of the process windows observed on Figures 6 and 7. Starting with the range of $0.4 \leq W/L_0 \leq 0.9$, the curves corresponding to brush-44, -46, and -51 practically overlap on each other. This is in good agreement with the experimental results, where good alignment of the BCP is obtained for the same *W* conditions. The difference in interfacial energy increases significantly as the PS content in the brushes increases, leading to a reduction in the size of the windows. At W/L_0=1.0, all the curves present a maximum basically at the same ΔE value, which is translated in random orientation of the BCP with every brush at this condition. Finally, at large values of W/L_0, the second minimum in the interfacial energy does not describe the experimental results, as brush-44 and brush-46 have a smaller Δinterfacial energy than brush-51 and, at the same time, poor alignment is observed at conditions where the standard brush results in a high degree of perfection. In this case, the straight profile model may not describe the real BCP structures. It has been shown by molecular simulations that depending on the strength of the guiding stripe, 3D structures and, ultimately, non-bulk morphologies may be generated through the film thickness. [18, 27, 28] A lower PS content in the backfill material would

lower the interfacial energy and stabilize the interface. However, if the backfill brush induces the preferential wetting of the PMMA block, and the guiding stripe does the same with the PS blocks, then complex structures may form on both regions on the chemical pattern and registration of the BCP domains will be less likely to occur. This is, more defects will be generated, as shown on Figure 7 (W/L_0 =1.27). For the brush materials with large PS content (≥ 56%PS), loss of registration with the underlying chemical pattern is obtained as the Δinterfacial energy value is even higher than in the case where W/L_0 = 1.0. Differences with the experimental observations may originate from the use of the harmonic equation (instead of experimental values), for the calculations of the interfacial energies and impact of film thickness, among others. However, calculation of interfacial energies, using the straight profile model, provides a good method to predict the behavior of a BCP assembled on chemical nanopatterns of different chemistries and geometries.

One last aspect of interest is the impact of brush composition on line width roughness (LWR) and line edge roughness (LER). An in-tool algorithm in the CG4000 SEM was used to measure the roughness on the samples with 44-56% PS content. Brush-60 and brush-63 could not be assessed for roughness due to the lack of conditions with good alignment, which is required for the measurements. The through dose behavior was investigated at best focus for the pre-pattern. Five doses were analyzed by taking measurements at 15 points on the 84nm pitch inspection block. Figure 9 indicates that a lower PS content in the brush increases the LWR value. The hydrophilic character of the backfill brush as the PS content decreases, promotes the preferential wetting of the PMMA block to the background region. Top-down SEM images of BCP structures that present a high degree of order show material or residues deposited between the spaces on the samples with low PS content. The lines become ‘cleaner’ as the PS content increases, i.e. as the backfill region becomes more energetically neutral and perpendicular domains are obtained through the film. These results support the observation that the preferential character of this material may have a negative impact on the profile of the domains. The dependence on *W* may be related to the preferential wetting of the X-PS guiding stripe by the PS block assembled on it. As W increases, more complex structures may be formed in order to avoid unfavorable X-PS-PMMA interactions. The trends observed for left and right LER indicate the opposite behavior. In this case, the low PS brushes show the smallest roughness values. Even though, this parameter requires further analysis to clarify its origin, the trends indicate that a larger chemical contrast between the guiding stripe and the backfill region improves the placement of the BCP domains with respect to the underlying chemical patterns. At the

same time, the impact of *W* on LER is more evident than for LWR and is also related to the placement of the blocks with respect to the guiding stripe. In this case, the quality of the chemical patterns may be better at *W*=22.5nm, or W may be shifted and this value is closer to the optimal W/L_0= 0.5, which will minimize any displacement of the domains as discussed in the previous chapter.

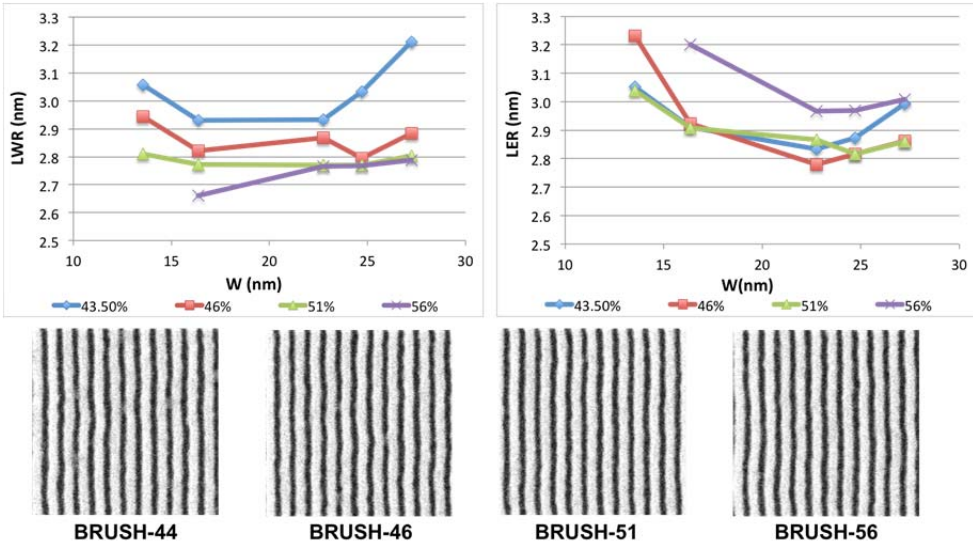

Figure 9. Line width roughness and line edge roughness for different *W* values and brush compositions. The SEM images correspond to aligned BCP structures on various brushes. Residues can be observed on brush-44 and -46, while the space between the PS lines become cleaner as the PS content increases.

6.5 Conclusions

The parameter space involved in the fabrication of chemically nanopatterned substrates, BCP materials, and processing that can be explored is extremely wide. Previous research done in the academia can be directly related and applied to investigate the critical variables of the DSA process in the fab. The implementation of a chemo-epitaxy flow allows the precise control of the properties of the chemical patterns and the thorough inspection of the samples. With this set-up, it was possible to characterize the wetting properties of the X-PS, which become weaker due to the processing conditions. Also, it was shown that for a 3X density multiplication factor, the best composition of the backfill brush is 51%PS-*r*-49%PMMA, based on process windows and LER-LWR data. The interfacial energy model was used to calculate the differences in free energy with the reference (ideal) case. With this model, the large process windows when a low PS content brush was used on the chemical nanopatterns, could be explained in an easy manner. At the same time, large

differences in the interfacial energy could also be related to random orientation observed from experiments. Through a deep understanding of the relationship between materials, process conditions and defect formation, minimum defect densities may be achieved using processing times amenable for industrial processing.

6.6 References

1. Semiconductors, I.T.R.f., *Lithography*. 2012 Update.
2. Bencher, C., et al., *Self-Assembly Patterning for sub-15nm Half-Pitch: A Transition from Lab to Fab*. 2011, Proceedings of SPIE.
3. Rincon Delgadillo, P.A., et al., *Implementation of a chemo-epitaxy flow for directed self-assembly on 300mm wafer processing equipment*. 2012, Journal of Micro/Nanolithography, MEMS, and MOEMS. p. 031302-1:031302-5.
4. Cheng, J.Y., et al., *Dense self-assembly on sparse chemical patterns: Rectifying and multiplying lithographic patterns using block copolymers.* Advanced Materials, 2008. **20**(16): p. 3155-3158.
5. Stoykovich, M.P., et al., *Remediation of Line Edge Roughness in Chemical Nanopatterns by the Directed Assembly of Overlying Block Copolymer Films.* Macromolecules, 2010. **43**(5): p. 2334-2342.
6. Bosse, A.W., *Effects of segregation strength and an external field on the thermal line edge and line width roughness spectra of a diblock copolymer resist.* Journal of Vacuum Science & Technology B, 2011. **29**(3): p. 7.
7. Sanders, D.P., et al., *Integration of Directed Self-Assembly with 193 nm Lithography.* Journal of Photopolymer Science and Technology, 2010. **23**(1): p. 11-18.
8. Chi-Chun, L., et al., *Integration of block copolymer directed assembly with 193 immersion lithography.* Journal of Vacuum Science & Technology B (Microelectronics and Nanometer Structures), 2010. **28**(6).
9. Kim, S.O., et al., *Epitaxial self-assembly of block copolymers on lithographically defined nanopatterned substrates.* Nature, 2003. **424**(6947): p. 411-414.
10. Edwards, E.W., et al., *Precise control over molecular dimensions of block-copolymer domains using the interfacial energy of chemically nanopatterned substrates.* Advanced Materials, 2004. **16**(15): p. 1315-+.
11. Stoykovich, M.P., et al., *Directed assembly of block copolymer blends into nonregular device-oriented structures.* Science, 2005. **308**(5727): p. 1442-1446.
12. Edwards, E.W., et al., *Dimensions and shapes of block copolymer domains assembled on lithographically defined chemically patterned substrates.* Macromolecules, 2007. **40**(1): p. 90-96.
13. Mansky, P., et al., *Controlling polymer-surface interactions with random copolymer brushes.* Science, 1997. **275**(5305): p. 1458-1460.

14. Ryu, D.Y., et al., *A generalized approach to the modification of solid surfaces.* Science, 2005. **308**(5719): p. 236-239.

15. Mansky, P., et al., *Ordered diblock copolymer films on random copolymer brushes.* Macromolecules, 1997. **30**(22): p. 6810-6813.

16. Han, E., et al., *Effect of Composition of Substrate-Modifying Random Copolymers on the Orientation of Symmetric and Asymmetric Diblock Copolymer Domains.* Macromolecules, 2008. **41**(23): p. 9090-9097.

17. Liu, C.-C., et al., *Fabrication of Lithographically Defined Chemically Patterned Polymer Brushes and Mats.* Macromolecules, 2011. **44**(7): p. 1876-1885.

18. Liu, C.-C. and A. Ramirez-Hernandez, *Chemical Patterns for Directed Self-Assembly of Lamellae-Forming Block Copolymers with Density Multiplication of Features*, E. Han, et al., Editors. 2013: Macromolecules. p. 1415-1424.

19. Pargon, E., et al., *Mass spectrometry studies of resist trimming processes in HBr/O-2 and Cl-2/O-2 chemistries.* Journal of Vacuum Science & Technology B, 2005. **23**(1): p. 103-112.

20. Pargon, E., et al., *Resist-pattern transformation studied by x-ray photoelectron spectroscopy after exposure to reactive plasmas. I. Methodology and examples.* Journal of Vacuum Science & Technology B, 2004. **22**(4): p. 1858-1868.

21. Liu, C.-C., et al., *Towards an all-track 300mm process for directed self-assembly*. 2011, J. Vac. Sci. Technol. B.

22. Mansky, P., et al., *Interfacial segregation in disordered block copolymers: Effect of tunable surface potentials.* Physical Review Letters, 1997. **79**(2): p. 237-240.

23. Han, E., et al., *Perpendicular Orientation of Domains in Cylinder-Forming Block Copolymer Thick Films by Controlled Interfacial Interactions.* Macromolecules, 2009. **42**(13): p. 4896-4901.

24. Wu, S., *Polymer Interface and Adhesion*. 1982, Marcel Dekker, Inc., New York.

25. Rincon-Delgadillo, P., R. Gronheid, and P. Nealey, ***Dimensions of Chemical Patterns for High-Throughput Directed Assembly of Block Copolymers with Density Multiplication*** 2014: In preparation.

26. Rincon Delgadillo, P.A., et al., *Process sensitivities in exemplary chemo-epitaxy directed self-assembly integration*. 2013: *Proc. SPIE* p. 86801H.

27. Ruiz, R., et al., *Density multiplication and improved lithography by directed block copolymer assembly.* Science, 2008. **321**(5891): p. 936-939.

28. Detcheverry, F.A., et al., *Interpolation in the Directed Assembly of Block Copolymers on Nanopatterned Substrates: Simulation and Experiments.* Macromolecules, 2010. **43**(7): p. 3446-3454.

7. Conclusions

In the last forty years, device scaling has been able to follow Moore's law. Increase in the transistor density has been accomplished mainly by advances in the optical lithography processes. In the last decade, the physical limit of 193immersion lithography was reached, and for the 32 and 22nm node, expensive techniques, such as double patterning, had to be applied. At the same time, the lack of an immediate solution to access smaller features required for the 16nm node and below, has opened the possibility for alternative methods to be considered for high volume manufacturing. In this context, directed self-assembly (DSA) of block copolymers (BCP) has emerged as a potential lithographic technique not only because of its ability to generate dense arrays of structures with a high degree of perfection, but also because it can do it in a less expensive manner, making use of tools and processes already available in the fab. The challenge that DSA has to overcome, then, lies in proving that it can meet the requirements for pattern placement accuracy, defectivity, and DSA compatible circuit design.

The aim of this doctoral thesis is to set the basis to answer the question of whether defectivity will be a limitation for the implementation of DSA of BCP in production. To that end, the chemo-epitaxy flow developed by Liu and Nealey (LiNe) was scaled-up to 300mm wafers at imec. This required modifications that were related to the process equipment and materials that are available in a fab. After each step of the process was defined, the LiNe flow scheme was the first fully automated process for DSA of BCP that provided 14 nm half-pitch lines and spaces, improving the initial 193nm immersion based pre-pattern resolution by a factor of 3. The excellent reproducibility of the results obtained in the laboratory scale over fully patterned wafers attracted the attention of the lithographic community as it was shown that DSA of BCP could provide features with desired dimensions at a low cost compared to other multi patterning schemes.

The next steps targeted two main objectives; on one hand, the development of the proper metrology to inspect large areas in reasonable times, and on the other hand to assess the impact of materials and processes on the assembly process.

Any optimization related to materials and processing condition loses its impact if it cannot be properly measured. For DSA of BCP, the ability to prove that it can achieve

0.01defects/cm^2 involves both optimization of processes and inspection techniques. Initial characterization of each step of the process was extremely valuable since it provided information about the generation and propagation of defects through the fabrication of the chemical nano-patterns. Also, DSA-specific defects, such as dislocations, were captured. It was shown that most of these defects could be related to external sources, such as particles or pinholes in the guiding material. However, in the execution of this experiment, it became evident that inspection of BCP structures on a chemical pattern conveys challenges such as its complex stack (multiple materials with different optical properties) and structures of short height and chemical composition (and optical properties) similar to the under layers, therefore, contrast for the defect inspection is limited. In order to improve the signal from the polymer structures and eliminate the effect of the chemical patterns, transferring the lines into the SiN and silicon substrate was required. Progress in this work is briefly discussed in Appendix A. Further optimizations are still ongoing at imec.

The LiNe flow provides a perfect test vehicle for the individual optimization of the properties of the chemical patterns, such as the dimensions and the chemical composition. At the same time, these 'practical' variables can be directly related to fundamental thermodynamic parameters. This allows for the rational support of each result and the use of these theoretical and experimental results as a base for further optimizations. Chapter 4 describes the characterization of the geometric properties of the nano-patterns, which include the width and shape of the preferential wetting guiding stripe and the backfill region. For future work, optimization of the trim etch step will be necessary in order to make straight sidewalls by using a more anisotropic process. This will especially be required as narrower guiding stripes will be needed for scaled versions of the LiNe flow. Chapter 5 brings together the dimensions and composition of the patterns to find the optimal processing conditions and materials for DSA of BCP using a 3X feature multiplication factor, where the current composition of the backfill brush (OH-P(51% styrene-*r*-49% methyl methacrylate)) is the preferred one for the process. The results and trends observed in this work may be used as a basis for further improvement of the quality of the nano-patterns moving forward towards zero-defectivity.

Even though the defectivity assessment is not finalized, the work presented in this thesis has shown the potential of DSA of BCP to approach the defect levels required for high volume manufacturing. The work as described in this thesis has contributed to the increasing interest and investments of the industry, including IC manufacturers, material and tool suppliers, in this technique in the last couple of years. Recently, the integration of

lines and spaces obtained by BCP lithography on device structures was demonstrated by Liu and Sayak, bringing DSA even closer to implementation. The momentum that directed self-assembly of block copolymers has gained is significant and through the collaborative work between the academia and the industry, this technique may soon be implemented into pilot production.

8. Appendix A

7.1 Optical Defect Inspection of Patterns Generated by Directed Self-Assembly of Block Copolymers

The key to directed self assembly's (DSA) insertion to high volume manufacturing lies in its ability to generate low defect patterns. The best way to demonstrate this is to investigate the formation/annihilation of defects over sufficiently large areas that allow their quantification and relation to changes in process parameters and, therefore, to total free energy of the system. However, this goal cannot be achieved without the proper metrology to capture the defects generated during block copolymer (BCP) assembly. Traditionally, non-optical techniques are utilized for imaging and collecting information of the assembly process due to the length scales that are involved in DSA of BCP. Scanning electron microscopy (SEM) and atomic force microscopy (AFM) are used in most studies, which convey the inspection of limited areas. In order to investigate the impact of fine differences in material and processing conditions on defectivity on a full-wafer scale, optical techniques are required.

The Liu-Nealey (LiNe) flow implemented at imec,[1] served as the baseline process to develop the inspection method to capture defects inherent to DSA of BCP, using KLA-Tencor's broadband brightfield optical inspection system (2835). Initial results after BCP alignment and removal of the poly(methyl methacrylate) (PMMA) block, showed the ability to capture DSA-specific defects, such as dislocations, as shown on Figure 1. However, one of the major implications of using optical inspection for DSA of BCP is that the tools do not have the resolution to 'image' the defects present on the sample. Instead, it relies on the characteristics of the nanopatterns, such as periodicity and the optical properties of the materials, to capture differences between the inspected area and a reference field. It is possible to use optical inspection methods on the line/space patterns generated with lamellae-forming BCP due to the regular features that have a high degree of perfection. Nevertheless, inspecting the polystyrene (PS) lines shown in Figure 2 presented some challenges. The height of the patterns is about 20nm. Although an initial BCP film thickness of 32nm was used, about 10nm of the film height is lost during the plasma etch process for PMMA removal. Due to the dimensions and the optical properties of the PS features, in addition to the heterogeneous stack, part of the signal obtained from the sample

inspection corresponds to the chemical patterns. The under layers can also be observed on the SEM images on Figure 1, where the bright areas underneath the dislocations correspond to pinholes in the guiding material.[2] Optical inspection proved to be an effective technique to investigate the properties of the chemical patterns, however, the capture rate of small dislocations generated due to the BCP self-assembly process could not be assessed on the polymer features.

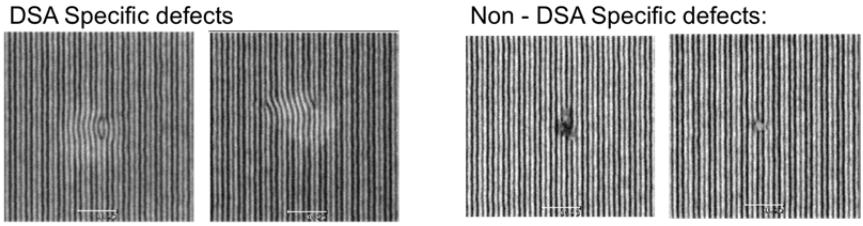

Figure 1. Types of defects captured during optical inspection of samples generated through the LiNe flow.

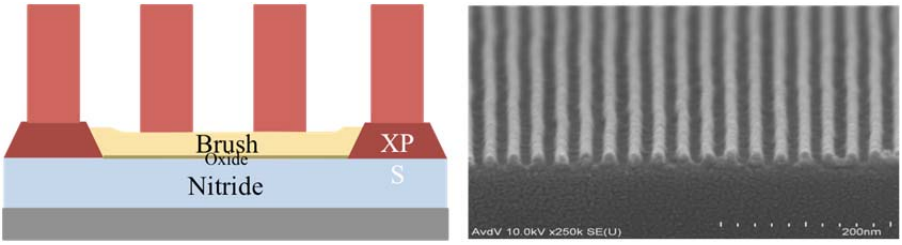

Figure 6. Schematic and SEM of PS nanopatterns (after PMMA removal).

In order to eliminate the signal from the chemical patterns and capture the defects present on the PS structures, the patterns were transferred into the SiN anti-reflective coating (ARC) and silicon substrate. A dry etch process using the TEL Tactras^{TM} etcher was developed to transfer the 28nm pitch PS lines/spaces into the substrate. Once this was achieved, the sensitivity of the optical inspection method, and therefore, the measured defect density, increased. It should be noted that in this case a reoptimization of the defect inspection recipe was done and the inspection mode was changed from brightfield (as used for inspection of the PS lines) to darkfield (for the Si/SiN line). Similar defect types compared to the ones captured at the PMMA level such as dark spots, dislocation clusters, and particles were observed after SEM review of the locations where the inspection tool detected differences with respect to the reference fields. New types of defects captured only after pattern transfer include single (belts) and multiple bridges. Dislocations pairs, which were usually detected only in the presence of particles or defects coming from the chemical

patterns, were now captured as well. A defect source analysis exercise is necessary to investigate if the origin of the dislocations is the assembly process or external sources.

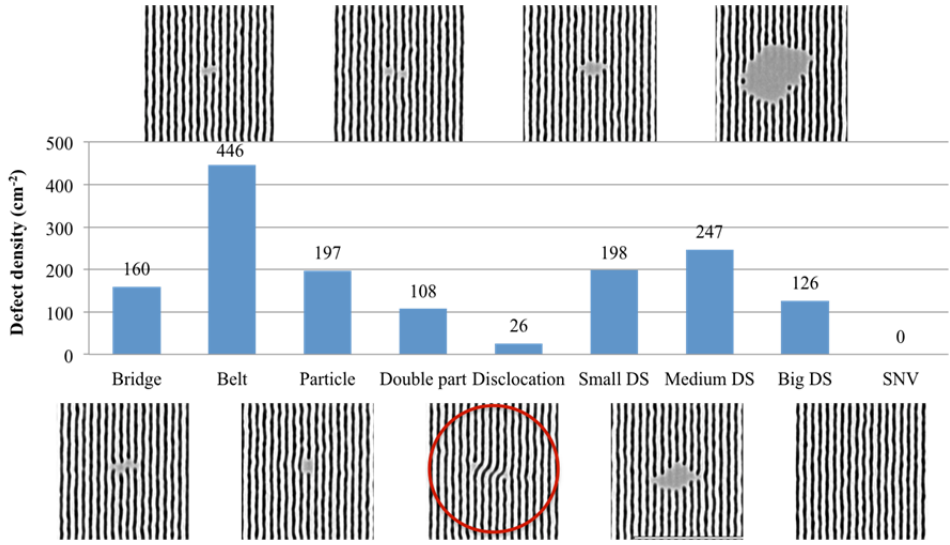

Figure 3. Normalized pareto of the defect types found in a single die.

In order to assess the capture rate of dislocation defects, programmed defects included in the inspection block were used. In the reticle design, 3 different types of defects (stich, gap and critical dimension (CD) bias) were printed in the photoresist structures and propagated to the chemical patterns. However, the BCP can heal these imperfections in most cases.[3] During optical inspection of the samples after PMMA removal, the programmed defects were captured, but after SEM review, a perfectly aligned structure was obtained. This observation supports the hypothesis that the signal came mostly from the stack. After pattern transfer, it was possible to use the programmed defects to calculate the capture rate of dislocation defects. We focused on the CD bias, since the BCP is most sensitive to this defect, especially when the amplitude of the CD is large. Information was collected from 20 repeats of the five largest defect sizes (12-20nm in 2nm steps) at five different doses on a focus-exposure matrix (FEM), as shown in Figure 4. These results are in agreement with previous observations on the maximum sensitivity of the BCP when the CD bias is 12 and 14nm, and a decrease in the dislocation formation at 16-20nm. The capture rate of the dislocations observed on the SEM images was 88%. The inspection method performed better at conditions where the defect density was relatively low, suggesting that isolated dislocations could be captured with a higher rate.

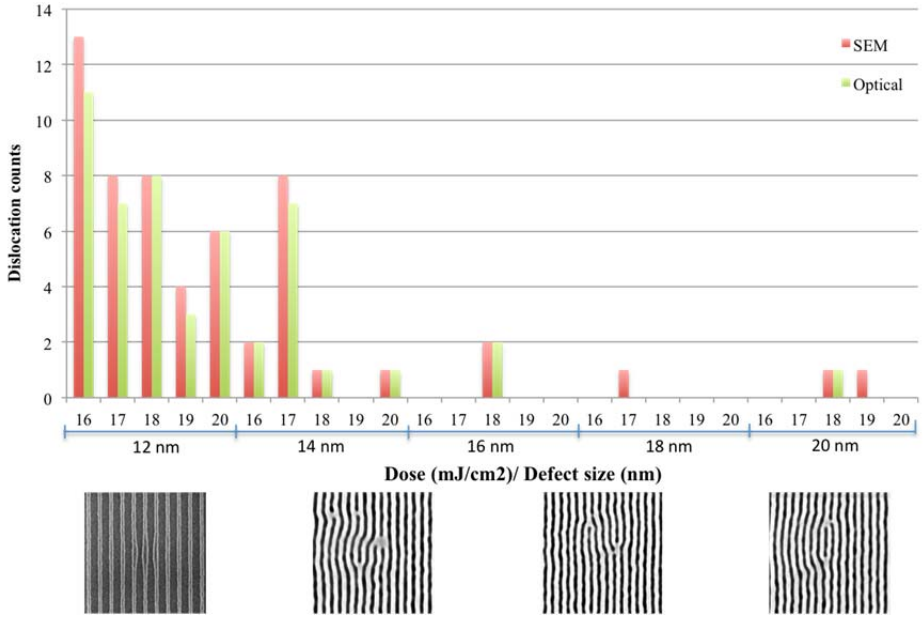

Figure 4. Dislocation counts captured by SEM and by the optical inspection. Five size of defects were imaged at 5 different doses on an FEM wafer. Examples of the defect as printed on the photoresist and the dislocations generated for this defect.

Optimizations of the etching conditions as well as post-etch improvements are currently taking place at imec. On one hand, in terms of the etching process, further tuning of the process is required to decrease the roughness on the nanopatterns observed in the SEM images of Figures 3 and 4. In addition, differences in the depth of the etched structures result in contrast variations, and therefore, in the capture rate of the defects of interest during the optical inspection. Deeper features are desirable for inspection purposes but they also increase the roughness. Therefore, the optimal point between these two parameters must be found. On the other hand, the etching chemistry requires a post-etch cleaning step of the wafers in diluted hydrofluoric acid (HF). Delay in this process, between etch and clean, results in the formation of particles on the substrate surface due to moisture in the atmosphere that can no longer be removed. Since this step cannot be performed in the same tool, optimization of the processing routes are being developed, as it became evident that times are critical for the end results.

Optical inspection is necessary for the assessment of DSA of BCP over large areas. Even more, due to the dimensions involved in this technique, the optical properties of the materials and the complex chemical patterns underneath the polymer features, pattern transfer into the substrate is required to capture the defects of interest, such as dislocations

and bridges. This new methodology involves challenges related to the processing, however, it presents new opportunities to evaluate with a great level of detail any improvements related to materials and processes that target defect minimization using DSA of BCP.

References

[1] P. A. Rincon Delgadillo, R. Gronheid, C. J. Thode, H. Wu, Y. Cao, M. Neisser, *et al.*, "Implementation of a chemo-epitaxy flow for directed self-assembly on 300mm wafer processing equipment," vol. 11, ed: Journal of Micro/Nanolithography, MEMS, and MOEMS, 2012, pp. 031302-1:031302-5.

[2] P. Rincon Delgadillo, R. Harukawa, M. Suri, S. Durant, A. Cross, V. Nagaswami, *et al.*, "Defect source analysis of directed self-assembly process (DSA of DSA)," vol. 8680, ed: Proc. SPIE, 2013.

[3] P. A. Rincon Delgadillo, R. Gronheid, C. J. Thode, H. W. Wu, Y. Cao, M. Somervell, *et al.*, "All track directed self-assembly of block copolymers: process flow and origin of defects," ed. Proceedings SPIE 8323, 2012, p. 83230D.

9. List of publications

C.C. Liu, Christopher J. Thode, **Paulina A. Rincon Delgadillo**, Gordon S. W. Craig, Paul F. Nealey, Roel Gronheid, Towards an all-track 300 mm process for directed self-assembly, *Journal of Vacuum Science & Technology B*, 29, 6, 2011, 55th International Conference on Electron, Ion, and Photon Beam Technology and Nanofabrication / Directed Assembly

Paulina A. Rincon Delgadillo, Roel Gronheid, Christopher J. Thode, Hengpeng Wu, Yi Cao, Mark Somervell, Kathleen Nafus, Paul F. Nealey, Implementation of a chemo-epitaxy flow for directed self-assembly on 300mm wafer processing equipment, Journal of Micro/Nanolithography, MEMS, and MOEMS, Vol. 11, No. 3, 2012

Roel Gronheid, **Paulina A. Rincon Delgadillo**, Ivan Pollentier, Paul F. Nealey, Todd R. Younkin, Mark H. Somervell, Joshua S. Hooge, Kathleen Nafus, Frequency multiplication of lamellar phase block copolymers with grapho-epitaxy directed self-assembly sensitivity to prepattern, Journal of Micro/Nanolithography, MEMS, and MOEMS, Vol. 11, No. 3, 2012

Paulina A. Rincon Delgadillo, Roel Gronheid, Christopher J. Thode, Hengpeng Wu, Yi Cao, Mark Somervell, Kathleen Nafus, Paul F. Nealey, All track directed self-assembly of block copolymers: process flow and origin of defects, Proceedings SPIE Advanced Lithography, 8323, 2012

Mark Somervell, Roel Gronheid, Joshua Hooge, Kathleen Nafus, **Paulina Rincon Delgadillo**, Chris Thode, Todd Younkin, Koichi Matsunaga, Ben Rathsack, Steven Scheer, Paul Nealey, Comparison of directed self-assembly integrations, Proceedings SPIE Advanced Lithography, 8323, 2012

Paulina A. Rincon Delgadillo, Roel Gronheid, Christopher J. Thode, Hengpeng Wu, Yi Cao, Guanyang Lin, Mark Somervell, Kathleen Nafus, Paul F. Nealey, Geometric Control of Chemically Nano-patterned Substrates for Feature Multiplication Using Directed Self- Assembly of Block Copolymers, Journal of Photopolymer Science and Technology, 29th International Conference of Photopolymer Sciecne and Technology, 2012

Paulina A. Rincon Delgadillo, Ryota Harukawa, Mayur Suri, Stephane Durant, Andrew Cross, Venkat R. Nagaswami, Dieter Van Den Heuvel, Roel Gronheid, Paul Nealey, Defect source analysis of directed self-assembly process (DSA of DSA), Proceedings SPIE Advanced Lithography, 8680-20, 2013

Paulina A. Rincon Delgadillo, Roel Gronheid, Guanyang Lin, Yi Cao, Ainhoa Romo, Mark Somervell, Kathleen Nafus, Paul F. Nealey, Process sensitivities in exemplary chemo-epitaxy directed self-assembly integration, Proceedings SPIE Advanced Lithography, 8680-53, 2013

Yi Cao, YoungJun Her, **Paulina Rincon Delgadillo**, Nadia Vandenbroeck, Roel Gronheid, Boon Teik Chan, Yukio Hashimoto, Ainhoa Romo, Mark Somervell, Kathleen Nafus, Paul F. Nealey, Using Process Monitor Wafers to Understand Directed Self-Assembly Defects, Proceedings SPIE Advanced Lithography, 8680-64, 2013

Todd R. Younkin, Roel Gronheid, **Paulina Rincon Delgadillo**, Boon Teik Chan, Nadia Vandenbroeck, Steven Demuynck, Ainhoa Romo-Negreira, Doni Parnell, Kathleen Nafus, Shigeru Tahara, Mark Somervell, Progress in Directed Self-Assembly Hole Shrink Applications, Proceedings SPIE Advanced Lithography, 8682-20, 2013

Roel Gronheid, Arjun Singh, Todd R. Younkin, **Paulina Rincon Delgadillo**, Paul Nealey, Boon Teik Chan, Kathleen Nafus, Ainhoa Romo Negreira, Mark Somervell, Rectification of EUV_Patterned Contact Holes Using Directed Self-Assembly, Proceedings SPIE Advanced Lithography, 8681-67, 2013

Miki Isawa, Kei Sakai, **Paulina A. Rincon Delgadillo**, Roel Gronheid, Hiroshi Yoshida, Line edge roughness measurement technique for fingerprint pattern in block copolymer thin film, Proceedings SPIE Advanced Lithography, 8682-10, 2013

Paulina Rincon Delgadillo, Gordon Craig, Roel Gronheid, Paul F. Nealey, Scale-up of a Chemo-Epitaxy Flow for Feature Multiplication Using Directed Self- Assembly of Block-Copolymers, Journal of Photopolymer Science and Technology, Vol. 26, No. 6, 2013

10. Curriculum Vitae

Paulina Alejandra Rincón Delgadillo

Current Position

- **Graduate student (Research assistant)**, PhD in Chemical and Biomolecular Engineering Department of Molecular Engineering, *University of Chicago*.
- **Graduate student,** PhD in Electrical Engineering, Department of Electrical Engineering, *Katholieke Universiteit Leuven* in collaboration with *Imec (Belgium)*

Expected graduation dual degree: June, 2014

Contact Information

Institute for Molecular Engineering

The University of Chicago

5735 South Ellis Avenue, Searle Chemical Laboratory 430
Chicago, IL 60637

princon@uchicago.edu

Education

1999-2003 **Bachelor of Science in Chemical Engineering**, *Instituto Tecnológico y de Estudios Superiores de Occidente (ITESO)*, Guadalajara, Jalisco

Thesis Project: "Correlation Comparison and Pressure Drop Calculation and Heat Transfer in Helicoidal Piping in a Turbulent Model", Professional Certificate Number: 3957456

2009-2012 **Master of Science in Chemical Engineering**, *University of Wisconsin-Madison*

Thesis Project: "Implementation of a Directed Self-Assembly Flow on 300mm Wafers for Defectivity Analysis"

Employment History

2005- 2008 **Development Engineer**, *Hilasal Mexicana SA de CV*

- Formulation and process design for towel bleaching, dyeing and printing
- Software editing for Atyc dyeing machines (dye jets)
- Testing coordination in the Development Laboratory and Dyeing and Finishing Areas
- New Products and Processes Evaluation and Implementation
- Cost Analysis and Cost Reduction
- Process Statistical Analysis
- Responsible for the Production Laboratory of Chemical preparation
- In charge of: 5 Development Lab workers and 7 Preparation workers

2003-2005 **Account Manager**, *SIG Beverages Services México, S.A. de CV (now known as Sidel México S.A. de CV)*

- Spare Part Sales for Bottling Industry machinery.
- Sales Analysis (monthly, yearly, by clients, by groups, etc.)
- Buying-Selling Spare Parts Special Projects

Scientific Presentations

Sept. 5th, 2011 Semiconductor Research Corporation Review, *University of Wisconsin-Madison*

October 27th, 2011 Program Technical Week, LITHOGRAPHY PROGRAM WORKSHOP (DSA Update), *Imec*, *Leuven, Belgium*

February 14th, 2012 SPIE Advance Lithography, All track directed self-assembly of block copolymers: process flow and origin of defects, *San Jose, California*

April 19th, 2012	Program Technical Week, LITHOGRAPHY PROGRAM WORKSHOP (DSA Update), *Imec, Leuven, Belgium*
June 28th, 2012	*29th* Photopolymer Science and Technology Conference, Geometric control of Chemical Patterns for Feature Multiplication Using Directed Self-Assembly of Block copolymers, *Chiba University, Chiba, Japan*
July 4th, 2012	International Advanced Nanopatterning Materials and Processes Workshop, Geometric control of Chemical Patterns for Feature Multiplication Using Directed Self-Assembly of Block copolymers, *Waseda University,* Tokyo, Japan
Sept. 12-14th, 2012	Fujifilm Advanced Lithography Workshop, Determination of Critical Parameters for Directed Self-Assembly of Block Copolymers, *Milan – Dresden*
Sep.t 19th, 2012	38th International Conference on Micro and Nano Engineering, Determination of Critical Parameters for Directed Self-Assembly of Block Copolymers, *Toulouse*, France
Sept. 24th, 2012	Semiconductor Research Corporation Review, *University of Chicago*
October 25th, 2012	Program Technical Week, Process improvements on UW DSA flow and defect performance, *Imec, Leuven, Belgium*
February 27th, 2013	SPIE Advance Lithography, Defect source analysis of directed self-assembly process (DSA of DSA), *San Jose, California*
February 28th, 2013	SPIE Advance Lithography, Process sensitivities in exemplary chemo-epitaxy directed self-assembly integration, *San Jose, California*
April 18th, 2013	Program Technical Week, Impact of BCP thickness and anneal conditions on pattern fidelity in the UW flow, *Imec, Leuven, Belgium*
April 18th, 2013	Program Technical Week, Improving defect performance of the UW DSA flow, *Imec, Leuven, Belgium*

Sept. 25th, 2013	Semiconductor Research Corporation Review, *University of Chicago*
October 18th, 2013	Program Technical Week, Defect monitor (post-PMMA removal) of 28nm pitch LiNe flow, *Imec, Leuven, Belgium*
October 18th, 2013	Program Technical Week, Post-Si etch defect metrology improvement and process, *Imec, Leuven, Belgium*
February25th, 2014	SPIE Advance Lithography, Kinetics of Defect Annihilation in Directed Self-Assembly of Block Copolymers Using Feature Multiplication, *San Jose, California*

Languages: English, Spanish (native speaker)